EXPERIMENTAL AND ANALYTICAL INVESTIGATION

OF MASONRY INFILL AND CONFINED

MASONRY WALL ASSEMBLIES

by

Maxim Gordon Johnson

A thesis submitted in partial fulfillment
of the requirements for the degree

of

Master of Science

in

Civil Engineering

MONTANA STATE UNIVERSITY
Bozeman, Montana

May 2017

ACKNOWLEDGEMENTS

I would like to express my gratitude to my advisor, Dr. Damon Fick, who aided me in my coursework and research during my time at Montana State University. I would also like to recognize the other members of my committee, Dr. Jerry Stephens, Dr. Mike Berry, and Mr. Anders Larsson for the contributions to my research and education.

An additional note of gratitude is extended to the various other professors and grad students who helped with my research along the way. A specific thanks to Mr. Kinsey Skillen for doing the preliminary research and constructing the test specimens. Thank you to Dr. Ladean McKittrick and Mr. Tony Lebaron for teaching me how to run the ARAMIS program for the strain analysis portion of this thesis. Lastly, I would like to extend a thank you to Mr. John Owolabi for helping me develop the LabVIEW program that was used for data acquisition.

TABLE OF CONTENTS

1. INTRODUCTION ... 1

Background ... 1
Research Objective ... 1
Organization ... 2

2. LITERATURE REVIEW ... 3

Introduction ... 3
Plain Masonry Walls ... 3
Masonry Infill Walls ... 6
Confined Masonry Walls ... 15
Damage Indices ... 21
Summary ... 24

3. EXPERIMENTAL PROGRAM ... 26

Introduction ... 26
Test Specimens ... 26
Plain Masonry Construction ... 26
Masonry Infill Construction ... 28
Confined Masonry Construction ... 29
Materials ... 31
Mortar ... 31
Concrete ... 32
Steel Reinforcement ... 33
Masonry Test Prisms ... 33
Construction ... 35
Experimental Setup ... 38
Instrumentation ... 41
Data Acquisition ... 41
Load Cells ... 42

TABLE OF CONTENTS — CONTINUED

Potentiometers ... 42
Digital Image Correlation ... 42
Experimental Procedure ... 44

4. ANALYSIS AND DISCUSSION ... 46

Results ... 46
Plain Masonry Specimen ... 46
Masonry Infill Specimen ... 48
Confined Masonry Specimen ... 54
Discussion ... 58
Plain Masonry ... 59
Masonry Infill ... 59
Confined Masonry ... 63
Displacement Capacity ... 66
Strain Analysis with Digital Image Correlation ... 69
Compressive Strut ... 73

5. A PROJECTION TO THE EARTHQUAKE ENVIRONMENT ... 76

Analytical Modeling ... 76
2D Frame Members ... 76
Hinges ... 78
Modeling a Structure Damaged by Strong Ground Motions ... 82
2015 Nepal Earthquake ... 82
Building of Interest ... 83

6. SUMMARY AND CONCLUSIONS ... 89

REFERENCES CITED ... 92

APPENDICES ... 96

TABLE OF CONTENTS — CONTINUED

APPENDIX A: Damage Indices Continued 97
APPENDIX B: ARAMIS Tutorial 119

LIST OF TABLES

Table Page

1. Masonry Bed Joint Shear Strengths (Atkinson, Amadei et al. 1989) 5

2. Material Properties of Mortar Used in Masonry Panels 31

3. Mix Design Used for Confined Masonry Concrete Confining Frame.............. 32

4. Material Properties of Concrete Used in Confinement.................................... 33

5. Material Properties of Reinforcing Steel Used in Confining Frame................. 33

6. Same-Day Test Prism Results.. 34

7. Measured Transverse Displacements for Masonry Infill Specimen 52

8. Measured Transverse Displacement for Confined Masonry Specimen............ 56

9. Specimen Comparison 58

10. Shear Stress of 12 in. x 12 in. Masonry Test Prisms 59

11. Variables Used in Concrete Shear Strength Equations................................... 62

12. Masonry Infill Wall Specimen Comparison 63

13. Calculated Shear Strengths of Masonry Infill Wall Specimens...................... 63

14. Calculated Shear Strength of Confined Masonry Wall.................................. 65

15. Displacement Capacity Associated with Each Specimen............................... 67

16. Values Used for Calculation of Compressive Strut Using FEMA 273 74

17. Actual Versus Calculated Compressive Strut Results 75

18. Properties of Tie-Members Used in Analytical Model.................................. 76

19. Masonry Strut Hinge Properties Used in SAP2000....................................... 79

20. Wall Dimensions Observed in Building Versus Model Dimensions.............. 83

LIST OF TABLES — CONTINUED

Table Page

21. Nepalese Building Model Results 86

22. Damage Levels used in Surveying 99

23. Severe Damage and Priority Indices Less than 0.4% 105

24. Damage Rating and Priority Index from Earthquakes Surveyed 107

25. Seismic Properties from Each Earthquake 111

LIST OF FIGURES

Figure Page

1. Model of masonry infill lateral force resisting system (Murty, Brzev et al. 2006) 7

2. Modeling of the diagonal compressive strut formed in the masonry panel when subjected to shear forces (Farshidnia 2009)........ 9

3. Three-story masonry infill test structure (left) before testing, (right) after testing (Pujol and Fick 2010) 12

4. Crack maps from loading test of three-story masonry infill structure (Pujol and Fick 2010) 12

5. Building collapse due to strong beam-weak column design in 2001 Bhuj, India earthquake (Murty, Brzev et al. 2006) 13

6. Multi-story collapse due to strong beam-weak column design in 1999 Turkey earthquake (Murty, Brzev et al. 2006) 14

7. Structural failures found in 1999 Turkey earthquake. (a) Joint failure due to insufficient reinforcement (b) Strong beam – weak column failure (Sezen, Whittaker et al. 2003)........ 15

8. Damage sustained to the first floor of a three-story confined masonry building after Chile’s 2010, 8.8 Mw earthquake (Brzev, Astroza et al. 2010) 17

9. Inadequate reinforcement detailing causing (a) buckling of longitudinal column reinforcement, and (b) shear cracks forming at connection of tie-column and tie-beam (Brzev, Astroza et al. 2010)........ 18

10. Opening confinement configurations: (a) confined on all sides with continuous lintel band, (b) tie-columns extending from bottom to top of tie-beam, and (c) lintel only (Singhal and Rai 2014) 19

11. Percentage of severely damaged buildings versus Priority Index for 2010, 7.0 Mw Haiti earthquake (O’Brien, Eberhard et al. 2011)........ 24

12. Plan view of the plain masonry specimen as a (a) reference drawing and (b) post construction........ 27

LIST OF FIGURES — CONTINUED

Figure Page

13. Standard clay masonry units used in all masonry panels 27

14. Plan view of the masonry infill wall as a (a) reference image and (b) post construction 28

15. (a) Concrete frame for masonry infill wall and (b) separation between concrete frame and masonry panel 29

16. Plan view of confined masonry wall as a (a) reference image and (b) mid-construction 30

17. Shear keys present in confined masonry wall 31

18. Typical mortar prisms 32

19. Masonry test prisms for same-day wall testing. (a) In MTS machine preparing for the application of diagonal compression and (b) prism exhibiting the diagonal shear crack upon failure 35

20. Platform construction for wall specimens. (a) creating holes for tension rods to pass through underneath the specimens and (b) completed platform 35

21. (a) Visqueen pulled tight over the surface of the specimen platform to provide a frictionless surface (b) completed formwork for the masonry infill specimen 36

22. Reinforcement layout for concrete beams and columns used on both confined masonry and masonry infill walls 37

23. Reinforcement used in confinement for both (a) masonry infill wall and (b) confined masonry wall 37

24. Instrumentation set up for walls (a) without concrete confinement and (b) with confinement 38

25. (a) Hydro-Stone bond between corner of specimen and loading shoe (b) loading shoe taken off following the test showing that a uniform bearing surface was attained 39

LIST OF FIGURES — CONTINUED

Figure Page

26. Test apparatus used to apply direct shear to wall from profile view (top) and section view (bottom) 40

27. Loading apparatus from (a) a profile view, and (b) looking on the plane of loading 41

28. Digital image correlation data acquisition preparation for (a) the masonry infill, and (b) confined masonry walls 43

29. Ready to test (a) masonry infill and (b) confined masonry walls with completed DIC preparation and potentiometer and loading apparatus 44

30. Plain masonry load-displacement response for potentiometer oriented parallel to loading plane accompanied with pictures of the failed specimen 47

31. Shear crack widths observed after testing of the plain masonry specimen (a) along center of masonry panel and (b) along diagonal planes respectively 48

32. Masonry infill load-displacement response for potentiometer placed parallel to loading plane accompanied with pictures of the failed specimen 49

33. Crack distribution in masonry infill specimen after failure of the (a) loaded corner and (b) the opposing corner 49

34. Gaps between the masonry panel and concrete frame of the masonry infill wall prior to testing (a) located at the bottom of the frame and (b) the top of the frame 51

35. Masonry infill load-displacement response for transverse potentiometers 52

36. Triangular crack distribution of effective shear width observed in the failed masonry infill panel from (a) a profile view and (b) focus on the loaded corner 53

LIST OF FIGURES — CONTINUED

Figure Page

37. Damage to the concrete confining frame in the masonry infill panel in the form of (a) shear failure of the tie-beam and crushing resulting from failure in the joint and (b) flexural failure of tie-column confining masonry panel 54

38. Confined masonry load-displacement response for potentiometer placed parallel to loading plane accompanied with pictures of the failed specimen 55

39. Confined masonry load-displacement response for the three transverse potentiometers 56

40. Uniform effective shear crack within confined masonry wall shown (a) from a profile view and (b) extending through the concrete tie-members 57

41. Damage observed within (a) in the shear keys located within the tie-columns of the confining concrete, (b) the concrete tie-beam at the loaded corner, (c) and the center of the masonry panel 58

42. Separation of concrete and masonry components (a) before loading and (b) after loading 60

43. Concrete confinement shear failures at peak compression load in masonry infill wall at (a) the loaded corner and (b) the opposite corner 61

44. Stiffness comparison of masonry infill and confined masonry specimens 64

45. Shear failure in the concrete frame shown in (a) the bottom corner of the wall with (b) a measurement of the amount of damage observed 66

46. Overlay of load-displacement curves showing the displacement capacity and failure load of each specimen 68

47. Damage observed at load associated with displacement capacity in (a) the masonry infill wall and (b) the confined masonry wall 68

48. Load-displacement response for the masonry infill wall with markers indicating the location of each data point 71

LIST OF FIGURES — CONTINUED

Figure Page

49. Strain correlation data for the masonry infill specimen measured (a) prior to peak load, (b) at peak load, and (c) at displacement capacity 71

50. Strain correlation data for the masonry infill specimen measured (a) prior to peak load, (b) at peak load, and (c) at displacement capacity 72

51. Load-displacement response for the confined masonry wall with markers indicating the location of each data point 72

52. Compressive strut formation in (a) the masonry infill specimen and (b) the confined masonry specimen 75

53. 2D frame model configuration used for both masonry infill and confined masonry walls 77

54. SAP analysis showing (a) hinge formation in model specimens and (b) axial load present in members 80

55. Actual versus modeled load-displacement behavior of masonry infill specimen.. 81

56. Actual versus modeled load-displacement behavior of confined masonry.. 81

57. Priority index versus percentage of buildings severely damaged in 135 sampled structures from the 2015, 7.8 Mw Nepal earthquake 83

58. Gongabu Bus Park Building 2A floor plan showing lateral resisting elements on the eastern wall of interest 84

59. Four-story building SAP2000 model results showing (a) undeformed model, (b) hinge formation in masonry infill model, and (c) hinge formation in confined masonry model.. 85

60. Masonry damage observed on the eastern wall of the Gongabu Bus Park Building 2A 86

61. Damage to reinforced concrete elements confined the masonry on the eastern wall of the Gongabu Bus Park Building.................................. 87

LIST OF FIGURES — CONTINUED

Figure Page

62. Masonry infill cracks in a full-scale building test showing crack formation at a 0.25% drift ratio........ 87

63. Priority index versus percentage of buildings severely damaged in 46 structures surveyed from the 1992, 6.7 Mw Erzincan earthquake (DataHub 2015) 100

64. Priority index value versus percentage of buildings severely damaged in 181 structures sampled from the 1999, 7.4 Mw Maramara, and 7.2 Mw Duzce earthquakes (Donmez and Pujol 2005)........ 101

65. Priority index versus percentage of buildings severely damaged for 21 structures having identical floor plans but different lateral force resisting systems in the 1999, 7.2 Mw Duzce, 7.4 Mw Marma, and 2003 6.4 Mw Bingol (adapted from Gur et al. (2009))........ 102

66. Priority index versus percentage of buildings severely damaged in 116 sampled structures from the 2008, 8.0 Mw Wenchuan, Sichuan earthquake. (Data adapted from Zhou et al. (2013))........ 103

67. Priority index versus percentage of buildings severely damaged in 160 structures sampled from the 2010, 7.0 Mw Haiti earthquake (O'Brien, Eberhard et al. 2011) 104

68. Priority index versus percentage of buildings severely damaged in 27 sampled structures from the 2007, 8.0 Mw Pisco Peru earthquake 108

69. Priority index versus percentage of buildings severely damaged in 57 sampled structures from the 2003, 6.7 Mw Bingol earthquake 109

70. Average priority index associated with each story for each of the seven surveyed earthquakes (DataHub 2015)........ 110

71. Severe failure caused by poor detailing. (a) insufficient joint reinforcement at beam-column connections, (b) poor quality concrete in structural elements (Lizundia, Shrestha et al. 2016)........ 112

72. Severely damaged masonry infill building in Peru following the 8.0 Mw earthquake (DataHub 2015) 114

LIST OF FIGURES — CONTINUED

Figure Page

73. Severely damaged structural elements found in the building; (a) Masonry infill panels that have been crushed or have fallen out completely, (b) Severely damaged concrete captive column (DataHub 2015) 114

74. School building in Bingol, Turkey that suffered collapse in the 6.4 Mw earthquake (DataHub 2015) 116

75. Severely damaged structural elements found in the collapsed school building; (a) masonry exhibiting large shear cracks and crushing, (b) concrete beam-column connection failure as a result of poor detailing (DataHub 2015) 117

ABSTRACT

Masonry has the benefit of strength and ease of construction but lacks the ability to resist lateral forces due to its brittle nature. However, with the addition of concrete confining frames to plain masonry walls, additional strength and ductility can be attained. Two such confinement systems include masonry infill and confined masonry walls. Currently, masonry infill assemblies are the most common form of lateral force resisting systems in countries where access to more traditional concrete and steel materials is limited. However, recent studies have stated that confined masonry provides improved performance because of the bond between the concrete and brick. This thesis presents an investigation of the behavior of both types of concrete confinement methods and identifies advantages of each system with regards to strength, ductility, and performance during strong ground motion events. To accomplish this objective, 1/3-scale specimens were constructed and tested in direct shear to determine the load-displacement response for both masonry infill and confined masonry walls and compared with results of each type of concrete confinement technique as compared to a plain masonry specimen. The masonry infill wall strength was 35% larger and deflected ten times more than the plain masonry wall at peak load. The confined masonry showed 80% more strength capacity; however, only deflected 2.5 times more than the plain masonry wall at peak load. The test results were incorporated into analytical models that approximated the load displacement response observed during the tests. The models were used to perform a nonlinear push-over analysis on a reduced scale 5-story building damaged by the Nepal earthquake. The first story walls of the confined masonry model failed at a base shear that was 27% larger than the masonry infill model. First story drifts were 64% larger in the masonry infill model. This supports the general observation that each wall has merit in a specific design scenario. Masonry infill walls may be preferred in for designs where energy dissipation may be critical. On the strength side, confined masonry walls may be preferred where strength is preferred over ductility.

INTRODUCTION

Background

For thousands of years, masonry has served as one of the most frequently used building materials. In order to enhance the seismic performance of masonry buildings, concrete confining frames can be used to provide additional strength and ductility to the brittle material. Two types of concrete frame assemblies are used: masonry infill and confined masonry. Currently, masonry infill is the most popular form of masonry reinforcement in countries that utilize the lateral force resisting system; however, many believe that the confined masonry wall provides for a more efficient use of materials while providing superior strength. Because of the poor performance of masonry infill buildings during earthquakes, much of the recent literature recommends using confined masonry wall assemblies. While these systems have demonstrated increased shear strength, their increased stiffness leaves them vulnerable to higher base shear forces during earthquakes. The question that this investigation attempts to address is which masonry wall assembly provides the best combination of strength and ductility during a seismic event.

Research Objective

The goal of the research was to perform a comprehensive comparison of masonry infill and confined masonry wall assemblies. This comparison included consideration of the favorable and unfavorable characteristics of each system to draw conclusions about the suitability of each system for different building types and strong ground motions.

Work began with a review of previous experimental studies related to the performance masonry infill and confined masonry systems. In an experimental program designed to test each wall specimen in direct shear, 1/3-scale specimens of plain masonry, masonry infill, and confined masonry walls were tested to determine their load-displacement responses. The results from the experimental program were incorporated into analytical models that can be subjected to seismic accelerations. In addition to testing and modeling, an investigation to determine the observed performance of masonry infill systems during the 2015 strong ground motion event in Nepal was conducted. The results of this investigation were compared to the modeled behavior of each wall to determine if any conclusions could be made about the seismic vulnerability of masonry infill and confined masonry wall assemblies.

Organization

Chapter 2 provides a literature review of previous research on the construction and behavior of both masonry infill and confined masonry walls. Chapter 3 discusses the testing set up and experimental program. The chapter also describes how each wall was constructed as well as the material properties of the components used. Analysis of the walls is presented within Chapter 4. Using the results from this analysis, a projection to expected performance in an earthquake environment is provided in Chapter 5. Chapter 6 summarizes the conclusions that can be drawn from the work completed in this thesis.

LITERATURE REVIEW

Introduction

To enhance the seismic performance of masonry buildings in developing countries, the Earthquake Engineering Research Institute (EERI) produced a Seismic Design Guide (Meli, Brzev et al. 2011). This report provides seismic design provisions and recommendations for the construction and design of confined masonry wall assemblies. In addition, the report also documents the construction methods and behavior of masonry infill walls. Masonry infill (MI) construction involves constructing a concrete frame followed by constructing a masonry wall on the interior of the frame. Confined masonry (CM) construction includes casting the concrete frame after the masonry wall is built, which forms a bond between the masonry units and concrete members. Both methods of construction provide additional capacity compared to a plain masonry (PM) wall. This literature review summarizes the characteristics of each wall assembly and recent investigations related to their performance when subjected to strong ground motion, prefaced by a description of the behavior of plain masonry walls.

Plain Masonry Walls

Plain masonry walls are included in this investigation to better understand the boundary effects of both masonry infill and confined masonry walls discussed later in this chapter. Understanding the behavior and mechanics of plain masonry that constitutes the interior of both infilled and confined systems furthers the understanding of both.

Research conducted by Atkinson, Amadei et al. (1989) investigated the range of strength of unreinforced brick masonry subjected to shear for different clay units, mortar types, and thicknesses. It was found that by applying a compression load to the corners of the specimens, also known as direct shear, the wall's behavior, strength, and deformation could be estimated with repeatable results (Atkinson, Amadei et al. 1989). Through applying cyclic load through a direct shear apparatus, both the peak and residual shear strength were reported. Several different types of masonry were tested, including brick specimens from the 1987 Whittier, California earthquake. It was found through several iterations of the study that the peak strength of the masonry bed joints occurred during the first cycle of loading, followed by residual shear strength for the rest of the cycles (Atkinson, Amadei et al. 1989). A normal load was applied to the specimens and held constant. Peak and residual shear strengths were well represented by the Mohr-Coulomb criterion. Atkinson, Amadei et al. (1989) compared their test results with other investigations of clay brick assemblies, as shown in Table 1. The average reported shear strength of bed joints from their tests was 0.383 MPa (56 psi).

Table 1: Masonry Bed Joint Shear Strengths (Atkinson, Amadei et al. 1989)

Source (1)	Unit (2)	Mortar[a] (3)	c (MPa) (4)	tan ϕ (5)	Normal stress range (MPa) (6)
This study	Old clay units (13 mm)	1:2:9	0.127 0.023 (R)	0.695 0.678 (R)	0–4
This study	Old clay units (7 mm)	1:2:9	0.213 0.038 (R)	0.640 0.6931 (R)	0–4
This study	New clay units	1:1.5:4.5	0.811 0.037 (R)	0.745 0.747 (R)	0–4
Hegemier et al. (1978)	Concrete block	Type S	0.25	0.89	0–2.75
Stöckl and Hofmann (1986)	Clay brick (MZ 20)	1:0.68:15 1:0:9.7	0.95 1.45	0.7 0.56	0–2.4
Pook et al. (1986)	Concrete block	Type S	0.76	0.7	0–1.6
Nuss et al. (1978)	New clay units	1:2:9 1:0.5:4.5 1:0.25:3	1.10 4.73 4.86	0.77 0.75 0.76	0.7–6.3 3.1–18.3 1.4–22.0
Pieper (In Mayes and Clough 1975a)	Clay	1:2:8	0.20	0.84	0–1.2
Drysdale et al. (1979)	Clay brick	1:0.5:4	0.57	0.90	0–14
Kariotis et al. (1985)	Old brick (in situ tests)	Sand-lime	0.330	1.15	0–0.150

[a](Cement:lime:sand) by volume.
Note: All c and tan ϕ values represent peak levels unless designated with an (R).

Atkinson (1989) found the specimens taken from the Whittier earthquake exhibited lower shear strength than the masonry units made in the lab, which could imply lesser quality of materials and workmanship associated with masonry structures in the impacted area.

Adequate ductility is necessary in a seismic design so that the structure can dissipate the energy being added to the system. Therefore, it is important to understand what level of ductility can be achieved from unreinforced masonry walls. Priestley (1981) noted that most masonry walls are designed to the minimum compressive strength of f'_m to eliminate the need of additional prism tests to justify higher values. However, the required ductility for plastic hinge formation and seismic dissipation may not be available at these lower compressive strengths. Priestley (1981), determined that a plain masonry wall must meet a minimum required ductility, defined as followed.

$$\mu = \frac{\Delta_u}{\Delta_y} \geq \frac{4}{S} \qquad \text{Equation 1}$$

where:

Δ_u = displacement corresponding to ultimate strain of 0.0025

Δ_y = displacement of masonry wall at yield

S = structural type factor used in the New Zealand Masonry Design Code that increases the design lateral force

The ductility of plain masonry walls is largely dependent on the ultimate compression strain. It was found that at lower strains, such as 0.0015, vertical splitting occurred in several of the tested specimens (Priestley 1981). After maximum load is reached, masonry block experiences severe spalling and crushing while exhibiting a rapid decrease in load carrying capacity (Priestley and Elder 1983).

Masonry Infill Walls

Masonry infill construction utilizes a reinforced concrete frame with masonry brick constructed as infill between the concrete beams and columns. Masonry infill walls rely on the frame for increased strength and displacement capacities. This requires proper detailing of the columns, beams, and their connections to act as moment frames and gravity supporting members. In most cases, the infill wall is not tightly placed into the frame along the sides and top, which results in gaps between the masonry brick and concrete frame. Despite the small gaps that result during construction, the masonry wall is still able to act as a diagonal strut when the frame is displaced laterally. The configuration of a masonry infill wall system is shown in Figure 1.

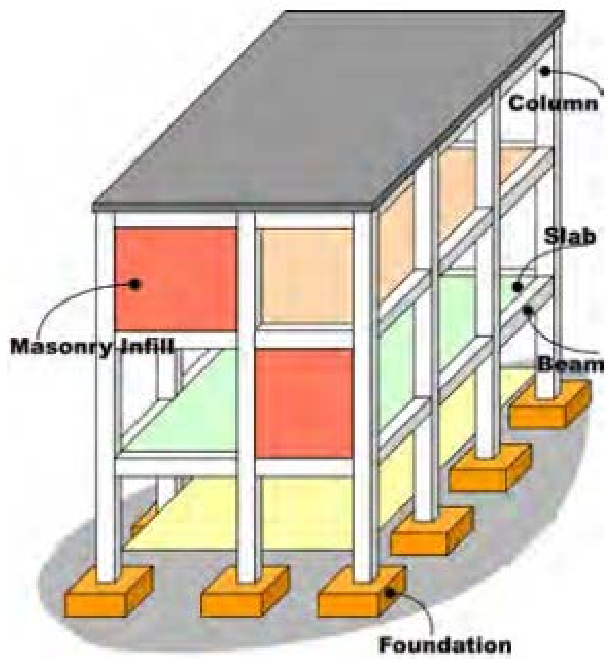

Figure 1: Model of masonry infill lateral force resisting system (Murty, Brzev et al. 2006)

The behavior of masonry infill walls has been well-researched and several modes of failure have been observed in both the masonry panels and the reinforced concrete frame. When the wall is subjected to lateral loads, shear forces develop and can result in horizontal sliding along the mortar joints. Because the mortar joints between masonry blocks are usually the weakest component of the system, stepped cracks in the masonry panel can occur as the walls are loaded in shear. This shear force applied to the masonry infill wall can cause compressive and tensile stresses in the central zone of the infill. Resulting compression within the wall can crush the masonry at the corner and toe of the wall and, if severe enough, form a diagonal strut with cracks parallel to the strut reaching from corner to corner (Farshidnia 2009).

Reports by the Federal Emergency Management Agency (Council, Agency et al. 1997, FEMA-306 1998) consider the infill to be the primary source of lateral force resistance. To model the resultant compressive strut, FEMA 273 (2009) and FEMA 306 (1998) include the following equation to compute the effective width of the compressive strut by the equation below, (Farshidnia 2009). Dimensional components associated with the equation are shown in Figure 2.

$$w = 0.175(\lambda_1 H)^{-0.4} D \qquad \text{Equation 2}$$

where:

λ_1 = coefficient derived by Mainstone (1971)= $\left(\frac{E_m t_{inf} \sin 2\theta}{4 E_{fe} I_{col} H_m}\right)^{0.25}$

Θ = inclination of the diagonal strut, radians = $\arctan\left(\frac{L_m}{H_m}\right)$

E_m = Expected modulus of elasticity of infill material, psi

E_{fe} = Expected modulus of elasticity of frame material, psi

I_{col} = Moment of inertia of column, in.^{4}

L_m = Length of infill panel, in.

H_m = Height of infill panel, in.

t_{inf} = Thickness of infill panel and equivalent strut, in.

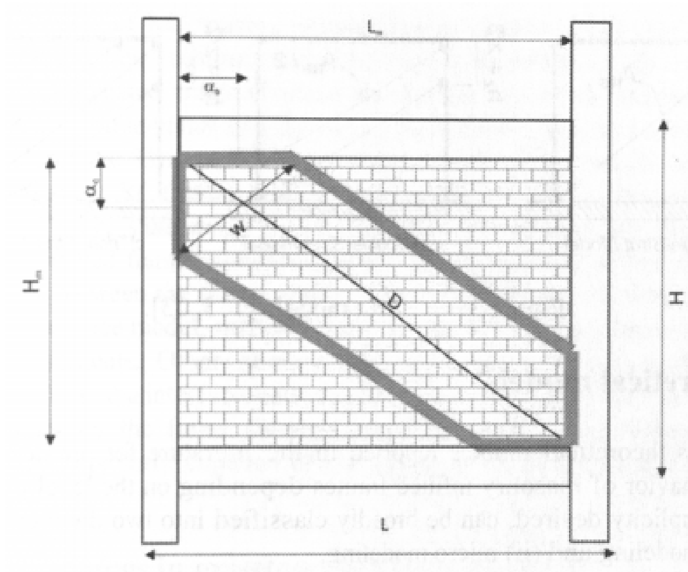

Figure 2: Modeling of the diagonal compressive strut formed in the masonry panel when subjected to shear forces (Farshidnia 2009)

Failure of the reinforced concrete frame must also be considered. Varying gravity loads in the boundary columns due to overturning seismic effects can influence the shear strength of the columns. Further, the reactions of the diagonal strut formed in the masonry infill wall can increase the magnitude of the shear forces acting at the beam-column joints. Prior to failure, this behavior can cause large bending moments in the beams resulting in wide diagonal cracks in the masonry infill (Farshidnia 2009). These effects compound at ground-level stories that may be taller with larger openings. Design and detail of the reinforced concrete frame is essential to the acceptable performance of masonry infill walls during earthquakes.

Despite the potential positive contributions the masonry wall has to an infill assembly, researchers have also found negative effects from their presence in buildings. Some have suggested that masonry infill walls have led to building collapse and that their presence may affect the response of the frames detrimentally (Murty, Brzev et al. 2006). Researchers at the EERI suggest that masonry infill walls without a seismic intensive design are inadequate and should be avoided (Murty, Brzev et al. 2006). As previously stated, masonry infill walls act as diagonal struts and increase the stiffness of the wall. However, compared to a reinforced concrete frame without infill, the addition of infill can produce a wall of 20 times greater stiffness than the frame alone (Murty, Brzev et al. 2006). This increased stiffness, combined with an irregular configuration of infill, can cause large load concentrations that result in torsionally irregular buildings (Murty, Brzev et al. 2006).

Work done by the Pacific Earthquake Engineering Research Center found that masonry infill walls have a large role in the strength and ductility of reinforced concrete frame structures and “should be considered for both analysis and design” (Hashemi 2007). The addition of infills creates a significantly stiffer wall and was also found to reduce the natural period of the structure and increase the damping coefficient (Hashemi 2007). These changes to the building’s dynamic properties influence the demand and displacement that may occur in certain structural elements. At a lower level, the addition of infills can change the distribution of load through the structure. Because the infills significantly increase the stiffness of the reinforced concrete frames, they attract a much larger share of inertial forces caused by earthquakes (Hashemi 2007).

Dolsek and Fajfar (2001) captured professional consensus of system performance stating that the infill walls can have a beneficial effect on the structural response, provided that they are placed regularly throughout the structure. This observation was also made by Sezen, Whittaker et al. (2003) after reviewing building practices in Turkey before and after the 1999, 7.6 Mw Maramara earthquake. The erratic configuration of walls seen in the first floor of damaged buildings created stiffness discontinuities that concentrated drift demand at the base level. One four-story building had the bottom two stories fail completely where it was noted that the long masonry infill walls on the upper two stories probably had significant elastic strength and stiffness, likely much greater than that of the reinforced concrete moment resisting frame (Sezen, Whittaker et al. 2003). The brittle fracture of lower story masonry infill walls prior to flexural yielding of the columns would have overloaded the non-ductile lower story columns in shear resulting in gravity load failure of the building (Sezen, Whittaker et al. 2003). These specific cases suggest that irregular placement of masonry infills can produce discontinuities of stiffness that contribute to the building collapse. The location of the infill walls should be considered along with the stiffness of the building in each direction (Sezen, Whittaker et al. 2003). These observation also supports the findings by Dolšek and Fajfar (2001) that noted improved performance of buildings with uniformly distributed infill walls.

To investigate the stiffness and strength increases achieved through the use of masonry infill walls, Pujol and Fick (2010) tested a three-story structure with masonry infill walls spanning each story and constructed in both frames. The test structure is shown in Figure 3. The walls were found to increase the base shear strength by 100% and the lateral stiffness by 500%. It was also noted that the structure was still able to resist lateral loads after 18 cycles of increasing amplitude up to 1.5% of the structures height

(Pujol and Fick 2010). The crack patterns in the three-story test structure as shown in Figure 4.

(a)

(b)

Figure 3: Three-story masonry infill test structure (left) before testing, (right) after testing (Pujol and Fick 2010)

The concentration of damage in the second floor implies that the load being applied to the test structure is not being distributed uniformly, and that the second floor gathers the majority of the load with little relief from the first and third floors. This type of behavior can be unfavorable if more stories are added to the structure.

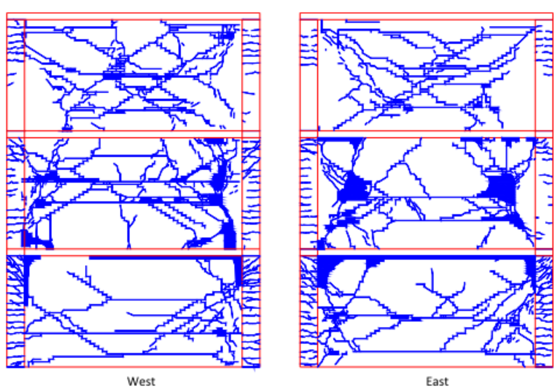

Figure 4: Crack maps from loading test of three-story masonry infill structure (Pujol and Fick 2010)

One way to improve seismic resistance in masonry infill structures is to design for strong column – weak beam behavior. The intended failure occurs first in the beams which are detailed to act as ductile members. These detailing requirements are necessary for the dissipation of seismic energy and to minimize damage and possibility of collapse. Reports from various global earthquakes including the 1999 Ducze earthquake in Turkey, 2001 Bhuj earthquake in India, and the 2003 Boumerdes earthquake in Algeria revealed that buildings that were not proportioned consistent with this design methodology suffered severe damage and collapsed in some cases (Murty, Brzev et al. 2006). Collapses due to strong beam - weak column behavior are shown in Figure 5 and Figure 6.

Figure 5: Building collapse due to strong beam-weak column design in 2001 Bhuj, India earthquake (Murty, Brzev et al. 2006)

Figure 6: Multi-story collapse due to strong beam-weak column design in 1999 Turkey earthquake (Murty, Brzev et al. 2006)

Observations from the reconnaissance conducted by Sezen, Whittaker et al. revealed that most of the severe damage was due to poor detailing and construction. Non-ductile reinforcement detailing was found in columns where concrete had spalled off; lap splices were unconfined and several splices were made in plastic hinge zones (Sezen, Whittaker et al. 2003). In addition, no transverse ties were present in joint regions, leading to brittle shear failure in several buildings. This is shown in Figure 7. Strong beam – weak column behavior was also observed in the collapse of several buildings. Non-ductile behavior of beams, often in conjunction with poor joint reinforcement detailing, led to full separation of beams from the columns is also shown in Figure 7. Sezen and Whittaker conclude that poor quality of construction and the presence of non-uniform infill walls in the epicentral region were large factors in the area's poor seismic performance (Sezen, Whittaker et al. 2003).

(a) (b)

Figure 7: Structural failures found in 1999 Turkey earthquake. (a) Joint failure due to insufficient reinforcement (b) Strong beam – weak column failure (Sezen, Whittaker et al. 2003)

Research related to the effectiveness of reinforced concrete frames with masonry infill as a lateral force resisting system is divided. There is consensus, however, that if masonry infill can be designed by a professional with consideration of seismic detailing, it does have merit as a suitable lateral force resisting system. The challenge is that masonry infill construction is most common in areas where buildings are erected without in-depth designs, and building codes are not strict as to the detailing and construction requirements.

Confined Masonry Walls

Confined masonry construction consists of horizontal and vertical reinforced concrete elements confining the masonry brick wall panel. During construction, the masonry walls are built first, followed by the casting of concrete tie-beams and tie-columns around the perimeter of the wall. Casting the concrete against the surface of the masonry wall panels, allows a bond stress to develop at the contact plane. To further increase the bond stresses, shear keys can be constructed in the masonry wall assemblies.

The tie-beams of the confined masonry assembly do not act as traditional beams since they bear on the masonry, but instead integrally share lateral loads with the masonry panel. Together, these structural elements prevent the brick wall from sudden brittle failure and improve the stability and strength of the wall against in-plane lateral loads (Meli, Brzev et al. 2011). The composite action developed between the wall and the tie-columns enable a shear wall mechanism where the tie-column members act as boundary elements (Sezen, Whittaker et al. 2003).

Unlike masonry infill walls, the performance of confined masonry walls subjected to earthquake loads has been found by researchers to be a function of "wall densities". The "wall density" is defined as the ratio of the cross-sectional area of the walls in a principal plan direction to the total floor area of the building. Brzev, Astroza et al. 2010 found that confined masonry buildings performed exceptionally well during the February 27, 2010 Chile earthquake with a majority of the one to two-story buildings having negligible damage. A few confined masonry buildings, however, suffered moderate to severe damage, including complete collapse. These buildings, such as the building in shown in Figure 8, were found to have wall densities of approximately 1% compared with recommended wall densities for low-rise buildings of 2-3% (Brzev, Astroza et al. 2010).

Figure 8: Damage sustained to the first floor of a three-story confined masonry building after Chile's 2010, 8.8 Mw earthquake (Brzev, Astroza et al. 2010)

Detailing of reinforcement in the concrete confining elements was also found to be a main source of deficiency in the confined masonry walls within damaged buildings in Chile, where inadequate confinement by tie-column reinforcement was noted. The increased spacing of tie column reinforcement resulted in buckling of the column longitudinal bars (see Figure 9). The current Chilean code requires an end spacing of 4 in. (Brzev, Astroza et al. 2010); however, this reduced spacing was not found within any of the damaged buildings because at the time of construction it was not required by the Chilean building code.

(a)

(b)

Figure 9: Inadequate reinforcement detailing causing (a) buckling of longitudinal column reinforcement, and (b) shear cracks forming at connection of tie-column and tie-beam (Brzev, Astroza et al. 2010)

Confining elements encase the masonry panel about its perimeter, contributing to the formation of compressive struts, which resist the seismic loads placed on the structure. However, if the confining elements do not also surround openings and perforations in the masonry wall, the compressive struts are interrupted. Singhal and Rai (2014) conducted an experimental investigation to determine the best method to confine openings during lateral, cyclic loading. Within their study, openings were confined using three different configurations, most notably, tie-beam confinement running horizontally the entire length of the wall, vertically the entire height of the wall, and only in the lintel. It was found that if horizontal confinement was extended throughout the full length of the wall, only minor, evenly distributed cracks formed at a drift ratio of over 2%, as shown in Figure 10. The most severely damaged buildings in Chile did not have this level of confinement around window and door openings, and thus crushing of masonry at the toe and heel of the wall dominated wall behavior, even at lower drift levels. This type of behavior can be seen in the results of the study of both a window opening with only lintel confinement and confinement that extended top to bottom of the wall adjacent to the window opening. Damage sustained by these two walls is shown in Figure 10. Overall, it was observed that openings with confinement performed 40% better when subjected to in-plane loads (Singhal and Rai 2014).

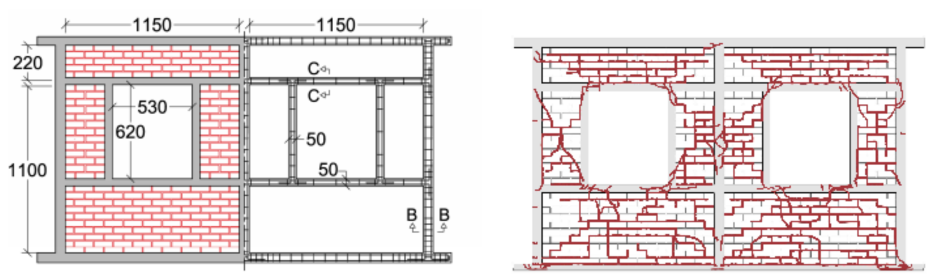

(a)

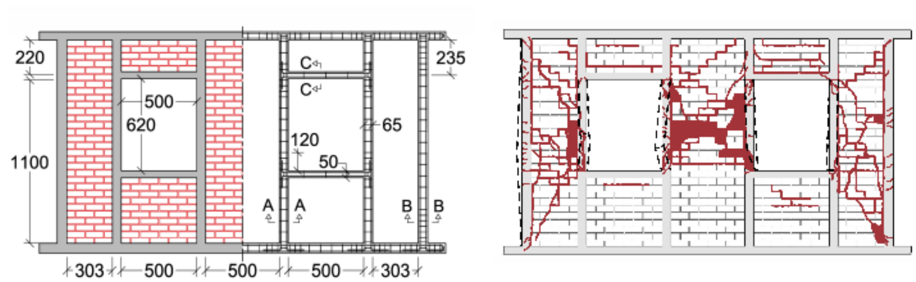

(b)

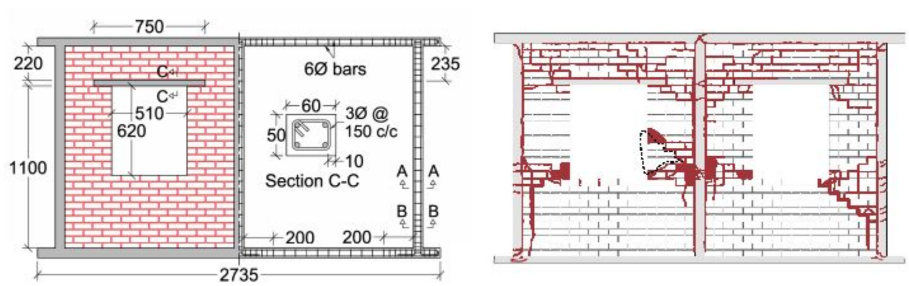

(c)

Figure 10: Opening confinement configurations: (a) confined on all sides with continuous lintel band, (b) tie-columns extending from bottom to top of tie-beam, and (c) lintel only (Singhal and Rai 2014)

Additional tests completed by Singhal and Rai (2014) provided a comparison of laterally induced failures in three different configurations of confined masonry walls and masonry infill walls. All reinforced concrete confining members were built with the same reinforcement. The confined masonry walls were constructed with course toothing, fine toothing and without toothing. The purpose of the test was to evaluate the in-plane performance of the wall configurations, and assess the role of toothing at the confining plane contacting the wall. The test results show that the toothing is highly beneficial and helped delay the failure (Singhal and Rai 2014). The performance of walls with toothing at alternate brick courses were superior in in-plane strength when compared to the non-toothed wall panels. The confined masonry walls maintained structural integrity even when severely damaged and performed much better than the masonry infill frames. With the addition of toothing, the confined masonry walls acted as a shear wall with concrete boundary elements (Singhal and Rai 2014). Non-toothed elements resisted force with a diagonal strut, with failure being controlled by the diagonal tension failure of the wall (Matošević, Sigmund et al. 2015). The confined masonry wall configuration was able to withstand 13% greater lateral loading, while dissipating twice the amount of energy, and displacing 20% less at peak lateral load. There was no report about toothing configurations in confined masonry walls in the Chile earthquake.

With respect to plain masonry wall configurations, "it was observed that confinement increased the lateral load carrying capacity by 70-90%" (Matošević, Sigmund et al. 2015). These results provide insight into the beneficial role of toothing in confined masonry walls.

Similar to the performance of masonry infill buildings, the quality associated with confined masonry construction influences their performance. The Chilean buildings that suffered the most damage were found to be made of construction materials with low strengths (Brzev, Astroza et al. 2010). It was also observed in several buildings that the masonry brick had been handmade. There was no information as to the strength of the brick found in the field; however, it is noted that the Chilean building code specifies the range of minimum clay brick strengths as 725 psi (handmade block) to 1600 psi (machine-made block) (Brzev, Astroza et al. 2010). The handmade brick likely did not provide enough masonry panel strength to resist the high lateral loads from the 8.8 Mw earthquake. Joint failures were also frequently seen along the mortar beds which were found to be as wide as 1-1/8 in. thick, which is three times wider than the 3/8 in. recommended thickness (Brzev, Astroza et al. 2010). The quality of construction and materials has a large influence on the degradation of confined masonry walls in a seismic event.

Overall confined masonry as a lateral force resisting system performed very well in response to the 2010 earthquake. In the sample size of several hundred confined masonry buildings only about 1% experienced damage.

Damage Indices

There have been several studies with the purpose of linking low wall and column densities to higher building damage in masonry infill buildings, often with the results expressed in terms of a relative damage index. One of the most common indices was developed by Hassan and Sozen (1997) and combines a wall index (WI) and a column index (CI). These indices were developed by the inspection and observation of damage levels in 46 low-rise buildings affected by the Erzincan Earthquake on March 12, 1992. Buildings surveyed spanned from one to five stories in height. None of the buildings in this sample suffered total collapse. Summing the two indices captures the contributions of both elements in resisting damage during an earthquake in seismically at-risk areas and is referred to as the Priority Index (PI) (Hassan and Sozen 1997).

The wall index is defined as the effective cross sectional area of the walls in any given direction (A_{wt}) to the total floor area above the base (A_{ft}), and is similar to the wall density described by Brzev et al (2010). The wall index is written as a percentage, with a lower index representing a higher risk for damage during an earthquake.

$$WI = \frac{A_{wt}}{A_{ft}} \times 100 \qquad \text{Equation 3}$$

where:

A_{wt} $= A_{cw} + \frac{A_{mw}}{10}$

A_{cw} = total cross-sectional area of reinforced concrete walls in one horizontal direction

A_{mw} = cross-sectional area of masonry infill in one horizontal direction at base

A_{ft} = total floor area above the base in a building

The second parameter is the column index and is defined as the effective cross-sectional area of columns at the building's base divided by the total floor area above base. Similar to the wall index, a lower column index indicates higher expected damage in the event of an earthquake.

$$\mathrm{CI} = \frac{\mathrm{A_{ce}}}{\mathrm{A_{ft}}} \times 100$$ Equation 4

where:

$\mathrm{A_{ce}}$ = $\frac{\mathrm{A_{col}}}{2}$ = effective cross-sectional area of columns at base

$\mathrm{A_{col}}$ = total cross-sectional area of columns at the base

Combining the wall and column indices to create a priority index (PI) simplifies the building assessment to one value where the lowest values represent structures with the highest likelihood of severe damage or collapse during an earthquake. The PI has been evaluated in other studies, including one that assessed the vulnerability of buildings after the 2010 Haiti earthquake (O'Brien, Eberhard et al. 2011). Similar to the results observed in the 1992 Erzincan earthquake, a trend of increased damage with lowering PI values was observed. It was found that 77% of buildings with priority indices within the range of 0.00-0.09% suffered severe damage in the earthquake. Research also shows less than 35% of buildings with indices greater than 0.40% experienced severe damage (Donmez and Pujol 2005). The trend reported by O'Brien et al. (2011) is shown in Figure 11.

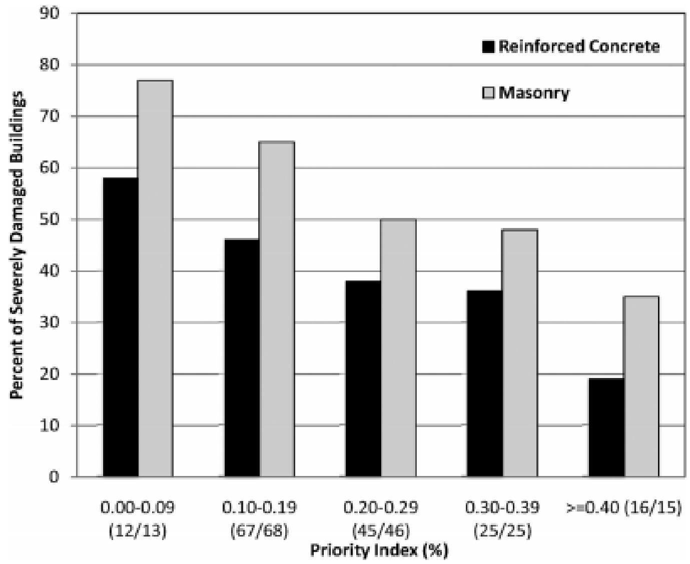

Figure 11: Percentage of severely damaged buildings versus Priority Index for 2010, 7.0 Mw Haiti earthquake (O'Brien, Eberhard et al. 2011)

The trend of severe damage increasing as the priority index decreases has also been noted in six other seismic events, including the 2015 strong ground motion event in Nepal which will be studied in more detail in a later chapter. More detail on these seismic events, where priority index records were collected and documented, and the trends that were identified can be found in Appendix A.

Summary

The current study expands on the previous research described above by experimentally measuring the shear strength of 1/3-scale plain masonry, masonry infill and confined masonry specimens loaded in diagonal compression. The experimental results are used to characterize the equivalent lateral load displacement response of the masonry infill and confined masonry wall specimens. An analytical model was created to compare the response of both wall types to observed damage levels of buildings during the 2015 Nepal earthquake. Calculated drift levels are compared with observed damage levels and calculated priorities indices.

EXPERIMENTAL PROGRAM

Introduction

Three 4 ft. x 4 ft. masonry wall assemblies were tested in diagonal compression to investigate the shear strength of each type of wall. Plain masonry, masonry infill, and confined masonry lateral force resisting assemblies were tested. Companion tests included 12 in. x 12 in. masonry prisms and 4 in. x 8 in. concrete cylinders. All masonry panels were constructed by professional masons. The test specimens, material properties, construction, and experimental setup are described below.

Test Specimens

Plain Masonry Construction

Plain masonry (PM) wall specimens were constructed with 8 in. x 3-5/8 in. x 2-1/4 in. modular blocks held together by a 3/8 in. mortar bed. The bricks were selected to represent the traditional modular brick size and finish of standard face brick (see Figure 13). The wall is 4 ft. x 4 ft. in dimension. Masonry cores were fully grouted. The plain masonry wall is shown in Figure 12.

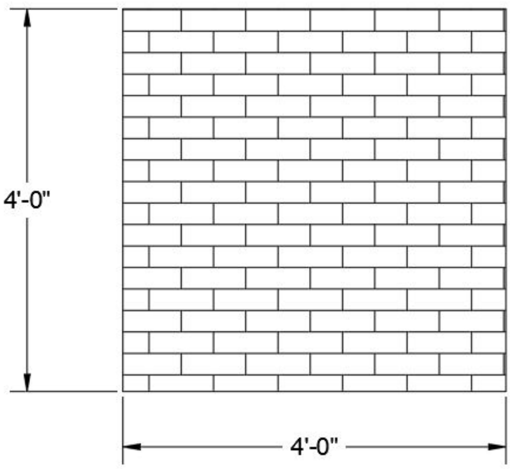

(a) (b)

Figure 12: Plan view of the plain masonry specimen as a (a) reference drawing and (b) post construction

Figure 13: Standard clay masonry units used in all masonry panels

<u>Masonry Infill Construction</u>

Masonry infill (MI) construction utilizes a reinforced concrete frame with masonry brick infill placed after the frame is cast. The 4 in. wide by 6 in. deep reinforced concrete frame was cast in a horizontal position on the laboratory floor. The width of the reinforced concrete was chosen to approximately match the modular brick size of 3-5/8 in. Reinforcement for the confinement was placed per the EERI masonry infill design guide (Murty, Brzev et al. 2006), satisfying minimum clear cover, spacing, and development lengths. The masonry infill wall assembly can be seen in Figure 14. Casting of concrete was followed by the infill of the masonry units. Small gaps, averaging 0.07 in., existed between the concrete frame and the masonry wall assembly and in most cases were not tightly spaced into the frame. The concrete frame as well as the gaps observed in the constructed specimen can be seen in Figure 15.

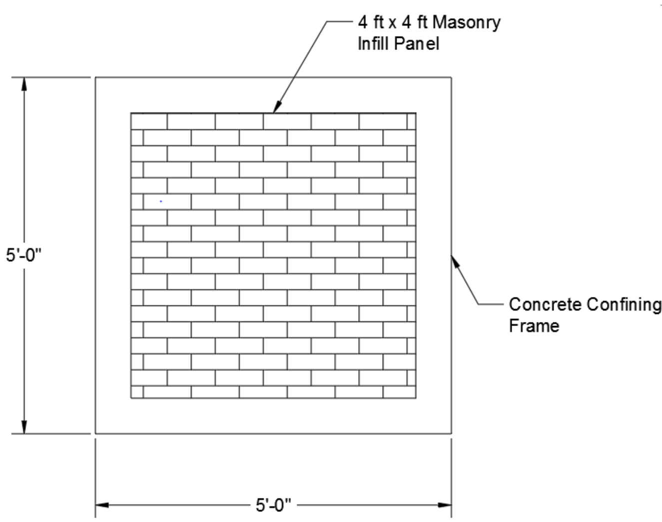

(a)

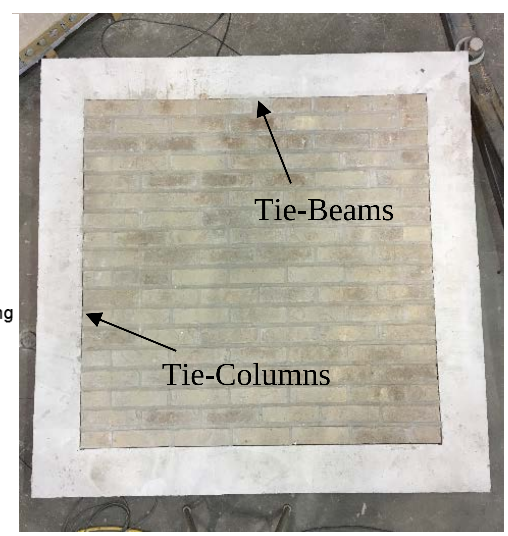

(b)

Figure 14: Plan view of the masonry infill wall as a (a) reference image and (b) post construction

(a) (b)

Figure 15: (a) Concrete frame for masonry infill wall and (b) separation between concrete frame and masonry panel

Confined Masonry Construction

Confined masonry (CM) construction consists of casting reinforced concrete tie-beams and tie-columns around a masonry wall panel. The confined masonry assembly can be seen in Figure 16.To improve the composite behavior between the concrete and masonry, recessions in the masonry, one-half a brick in length, are constructed in every other course of the panel. While casting the frame, concrete will fill these shear keys and bond to the masonry bricks. Similar to the MI wall, the tie-beams and columns were 4 in. wide by 6 in. deep in dimension.

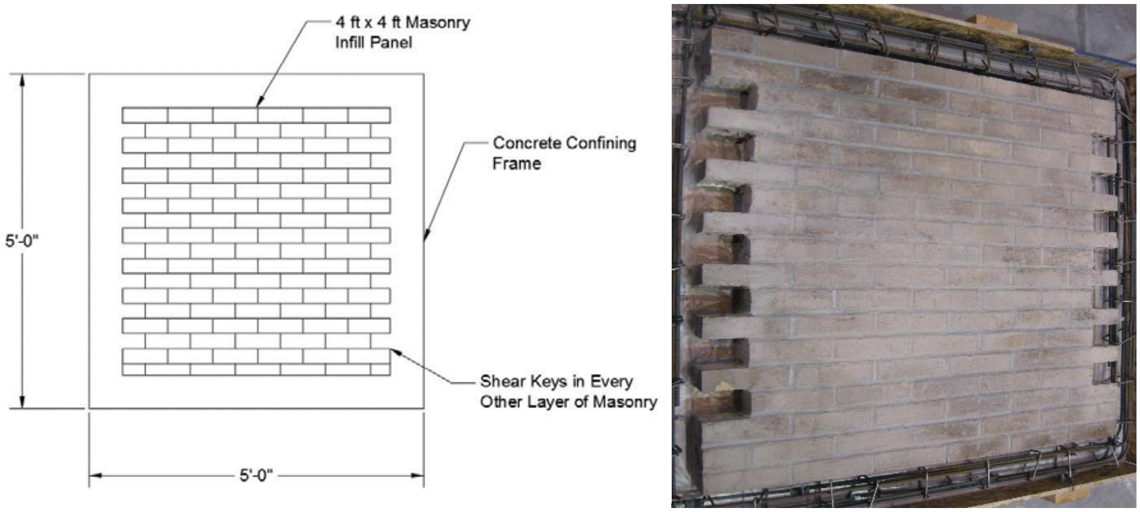

(a) (b)

Figure 16: Plan view of confined masonry wall as a (a) reference image and (b) mid-construction

For the confined masonry wall, the masonry panel was constructed first and laid onto a platform. After the masonry panel is constructed, the concrete is cast around the perimeter. Shear keys form in the brick recessions and provide an interaction between the concrete and masonry and help resist a portion of the shear placed onto the wall. Unlike the masonry infill wall, the materials in the confined masonry configuration interact through a bond developed during the curing of the concrete. The masonry shear keys can be seen in Figure 17 and are shown prior to casting the concrete frame.

Figure 17: Shear keys present in confined masonry wall

Materials

Mortar

Each masonry panel was constructed using a Type S, Quickrete mortar. Mortar beds were approximately 3/8 in. thick for each masonry course. Three mortar cubes were made for each wall assembly, which can be seen in Figure 18. Mortar compression test results performed according to ASTM C109M at 28 days are shown in Table 2.

Table 2: Material Properties of Mortar Used in Masonry Panels

Specimen	28-Day Compression Strength (psi)
PM	2439
MI	2292
CM	2396

Figure 18: Typical mortar prisms

Concrete

Concrete used for the reinforced concrete frames was a 4,000 psi mix design. Separate batches were prepared for both masonry infill and confined masonry walls. The final proportions used for specimens can be seen in Table 3, respectively.

Table 3: Mix Design Used for Confined Masonry Concrete Confining Frame

Volume (ft^3)	Water (lb)	Cement (lb)	Coarse (lb)	Fine (lb)	w/c
2.72	77.18	126.10	299.34	246.90	0.61

Compressive strengths of the concretes were determined at 28 days using the methods specified in ASTM C39. Average measured peak strengths of the two concrete batches used for the frames are reported in Table 4.

Table 4: Material Properties of Concrete Used in Confinement

Configuration	Average 28-Day Strength (psi)	Average Strength on Test Day (psi)	Percentage Increase in Strength
MI	4268	4466	4%
CM	5667	5235	-8%

Steel Reinforcement

No. 3 Grade 60 reinforcement was used for the concrete frames confining the masonry infill and confined masonry specimens. Transverse reinforcement was 1/4 in. diameter smooth bars. Strength of the No. 3 reinforcement was determined using a Baldwin tension-testing machine. Average, rounded material properties of three specimens are shown in Table 5. The arrangement of rebar within the concrete frame is described in the following Construction section.

Table 5: Material Properties of Reinforcing Steel Used in Confining Frame

Specimen	Material Property			
MI CM	Yield Strength	f_y	70,000	psi
	Ultimate Strength	f_u	110,000	psi
	Young's Modulus	E_{st}	29,000,000	psi

Masonry Test Prisms

Three 12 in. x 12 in. x 3.5 in. masonry prisms were tested the same day as the wall specimens according to ASTM E519M. The load rate was 0.0020 k/in^2/s. Specimens were loaded to half of their ultimate load in the first minute and ultimate load was reached before two minutes.

Maximum shear stresses were calculated using the following equations from ASTM E519M.

$$S_s = \frac{0.707P}{A_n}$$ Equation 5

where:

S_S = shear stress on net area, psi

P = applied load, kf

A_n = net area of the specimen, in.^{2}, calculated as followed:

$$A_n = \left(\frac{w + h}{2}\right) tn$$ Equation 6

where:

w = width of specimen, in.

h = height of specimen, in.

t = total thickness of specimen, in.

n = percent of the gross area of the unit that is solid, expressed as a decimal

Ultimate loads and shear stresses according to ASTM E519M are shown in Table 6. A figure of the test-ready masonry prism can be seen in Figure 19.

Table 6: Same-Day Test Prism Results

Configuration	Ultimate Load (k)	Max Shear Stress (psi)
PM	7.9	133.0
MI	10.3	173.4
CM	9.7	163.3
Average	9.3	156.6

(a)

(b)

Figure 19: Masonry test prisms for same-day wall testing. (a) In MTS machine preparing for the application of diagonal compression and (b) prism exhibiting the diagonal shear crack upon failure

Construction

The walls were constructed on 3/4 in. OSB board supported by 2 in. x 6 in. wood supports. The supports were notched so the bottom two 1-1/2 in. diameter loading rods could pass underneath the specimen (rods are described in more detail in experimental setup). Photos of the test specimen's support platforms are shown in Figure 20.

(a)

(b)

Figure 20: Platform construction for wall specimens. (a) creating holes for tension rods to pass through underneath the specimens and (b) completed platform

To minimize friction between the plywood and the concrete and masonry, each platform had a sheet of Visqueen polyethylene sheeting stretched taut across the plywood surface as shown in Figure 21. Concrete formwork was added to the plywood platform for the masonry infill and confined masonry specimens. For the plain masonry specimen, temporary sides were constructed to help with the masonry alignment. The completed formwork for one of the specimens can be seen in Figure 21.

Each of the masonry panels were 4 ft. x 4 ft. The specimens with confinement included a 4 in. wide by 6 in. deep reinforced concrete tie-columns on each side and similarly reinforced tie-beams above and below.

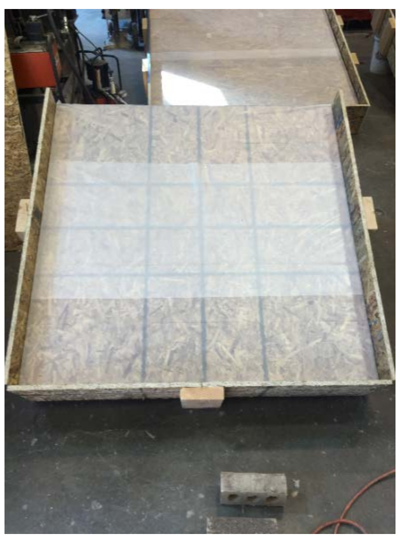

(a)

(b)

Figure 21: (a) Visqueen pulled tight over the surface of the specimen platform to provide a frictionless surface (b) completed formwork for the masonry infill specimen

The rebar layout for each frame is shown in Figure 22. Completed rebar placement for the masonry infill walls is shown in Figure 23. As a note, shear keys in the confined masonry wall received no additional reinforcement.

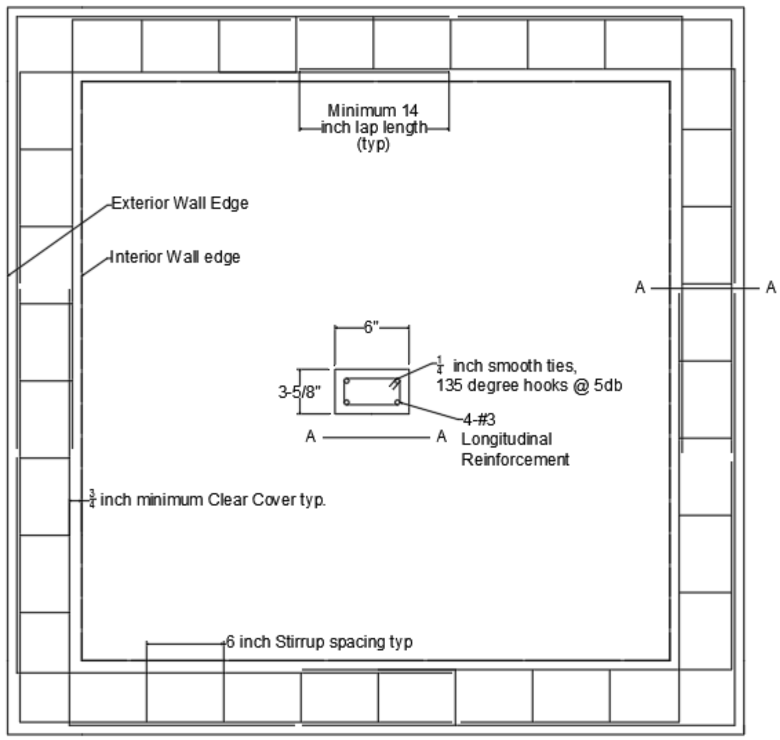

Figure 22: Reinforcement layout for concrete beams and columns used on both confined masonry and masonry infill walls

(a) (b)

Figure 23: Reinforcement used in confinement for both (a) masonry infill wall and (b) confined masonry wall

Experimental Setup

The three wall masonry wall assemblies were tested in accordance with ASTM E519M, the Standard Test Method for Diagonal Tension (Shear) in Masonry Assemblages. Load was applied to the wall assemblies through corner fixture that was designed and constructed per this specification. A self-reacting load frame consisting of diagonal tension rods was used with a hydraulic cylinder to apply load directly to opposing corners of the wall.

A single potentiometer measured longitudinal displacements of the wall specimens. Potentiometers were also placed at quarter points in the diagonal direction to measure transverse displacement of the wall in response to the applied load. A diagram of the configuration of the potentiometers placed on the walls can be seen in Figure 24.

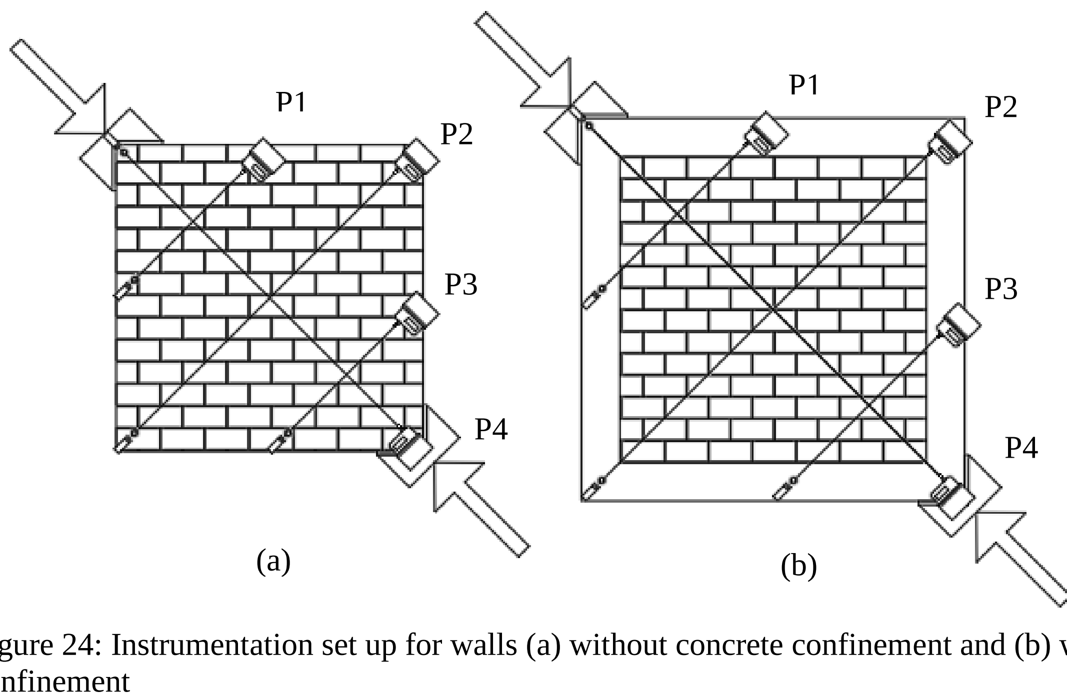

Figure 24: Instrumentation set up for walls (a) without concrete confinement and (b) with confinement

The load shoes were positioned with a layer of USG Hydro-Stone gypsum cement (10,000 psi) between the surfaces of the load shoe and the specimen. The Hydro-Stone was placed to provide a uniform bearing surface. The connection between the Hydro-Stone and fixture to the corner of the specimen is shown in Figure 25. After testing, the contact area was inspected to confirm a uniform bearing surface was achieved (see Figure 25)

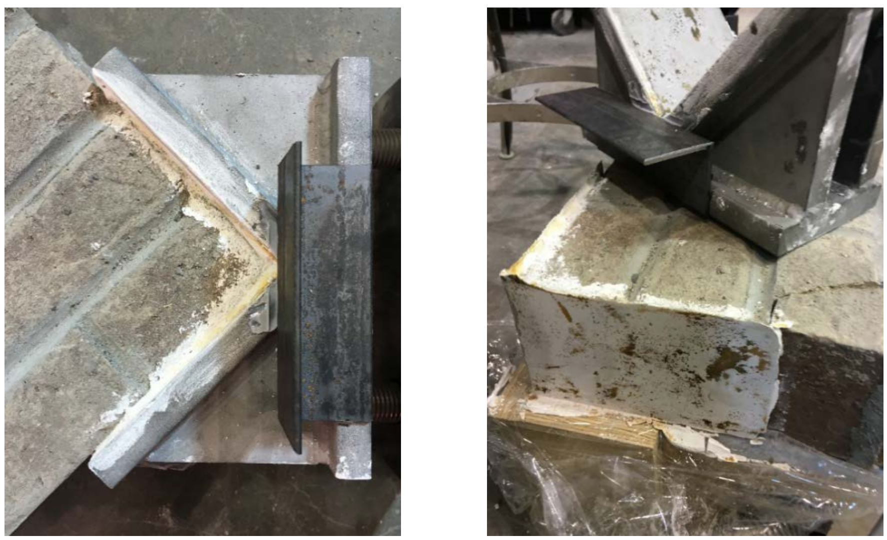

(a) (b)

Figure 25: (a) Hydro-Stone bond between corner of specimen and loading shoe (b) loading shoe taken off following the test showing that a uniform bearing surface was attained

Four, 1-1/4 in. diameter steel tension rods, two below and two above the panel were placed for the testing apparatus. The two bottom tension rods were led through the notches made in the supporting platform and connected to bearing plates placed on each corner of the specimen. The hydraulic ram was placed on one corner of the specimen and the bearing plates were adjusted to ensure that the loading was concentric. Bolts were installed snug-tight to each tension rod against the back of the bearing plate. A diagram of the loading apparatus is shown in Figure 26. The instrumentation and loading apparatus configuration can be seen in Figure 27.

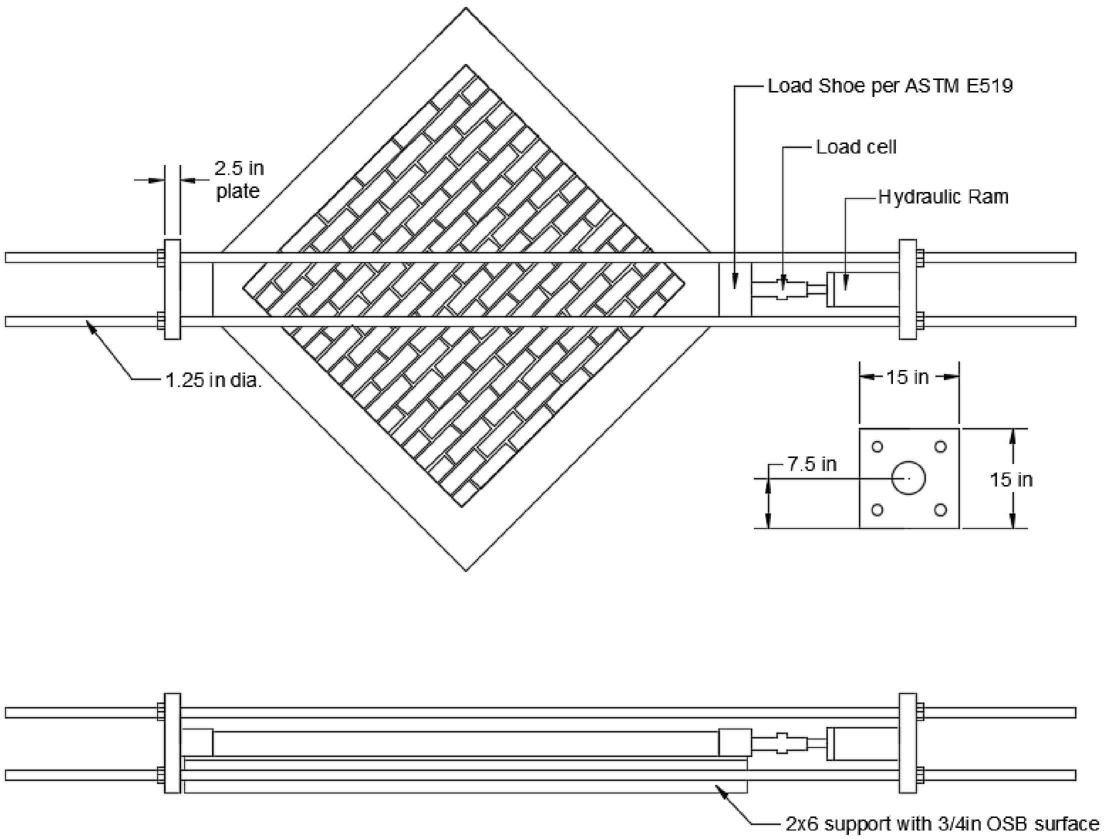

Figure 26: Test apparatus used to apply direct shear to wall from profile view (top) and section view (bottom)

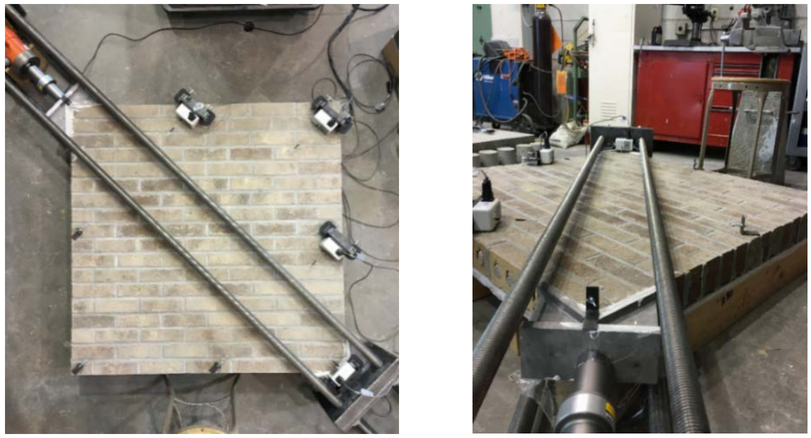

(a) (b)

Figure 27: Loading apparatus from (a) a profile view, and (b) looking on the plane of loading

Instrumentation

The diagonal compression tests used three different types of instrumentation. Load cells, potentiometers, and a digital image correlation system were used to collect a diverse range of data. A brief description of each instrument, calibration procedures, and the data acquisition used are described below.

Data Acquisition

A National Instruments data acquisition system was used to collect data during calibration procedures and the experiments. Displacements from four potentiometers was recorded as load output was measured separately. The software LabVIEW was used to convert the measured instrument voltage to engineering units using the calibration factors that were calculated using the procedures described below.

Load Cells

The load cell used for testing was calibrated by measuring the voltage output while incremental loads were applied with a 110-kip MTS testing machine. Several data points were collected to find the slope of the best-fit line on a voltage versus load plot for the calibration factor. This conversion factor (24.9 lb./volt) was applied in the LabVIEW software used during the specimen tests.

Potentiometers

Calibration of the four displacement potentiometers was completed by recording voltage output when the displacement wire was pulled to a known length and plotting voltage versus displacement. The slope associated with the output voltages was used as the calibration factors applied in LabVIEW. The potentiometer number corresponds with the number permanently written on each instrument. The inverse of the slope observed is equal to the conversion factor. Conversion factors are given in units of in./volt. Steel angles five inches in width were epoxied to the wall to hold the potentiometers in place. Potentiometers were tightly clamped to the angles to prevent any movement.

Digital Image Correlation

Because of the more ductile failure mechanisms expected for the masonry infill and confined masonry walls, it was determined that additional acquisition of deformation data would be desirable. Thus, in addition to potentiometers measuring longitudinal and transverse displacement, a digital image correlation (DIC) system was used to monitor the strain response of the entire area of the wall.

The MI and CM walls were painted white and overlaid with quarter inch black dots painted using a peg board template and spray paint. This technology requires an array of reference points to be placed on the surface of the test item. Changes in position of this array can be correlated as strain is digitally documented as load is applied. Specimens prepared for the DIC measurements before overlaying the black dots can be seen in Figure 28.

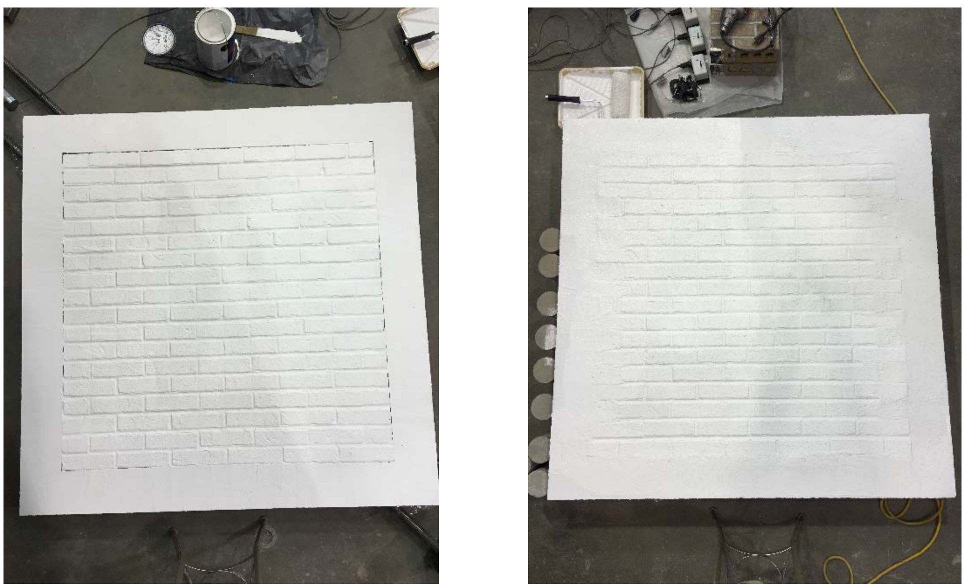

(a) (b)

Figure 28: Digital image correlation data acquisition preparation for (a) the masonry infill, and (b) confined masonry walls

Videos of the tests were taken by a 1080p GoPro at a rate of 30 frames per second. The video taken of each test were separated into thirty, high-resolution pictures for every second during the test. These photos were uploaded into the digital image correlation program, ARAMIS, to calculate the strain along different points of the wall based off of the first picture of the series known as the reference image.

After the masonry infill test, it was found that the top bars of the loading apparatus interfered with the ARAMIS software's ability to process the photo images. For this reason, the bars were covered with white tape for the confined masonry test to minimize the interference. This rids the DIC of the color contrast from the steel bar and makes it less-discernible to the ARAMIS program.

The completed, test-ready masonry infill and confined masonry walls can be seen in Figure 29.

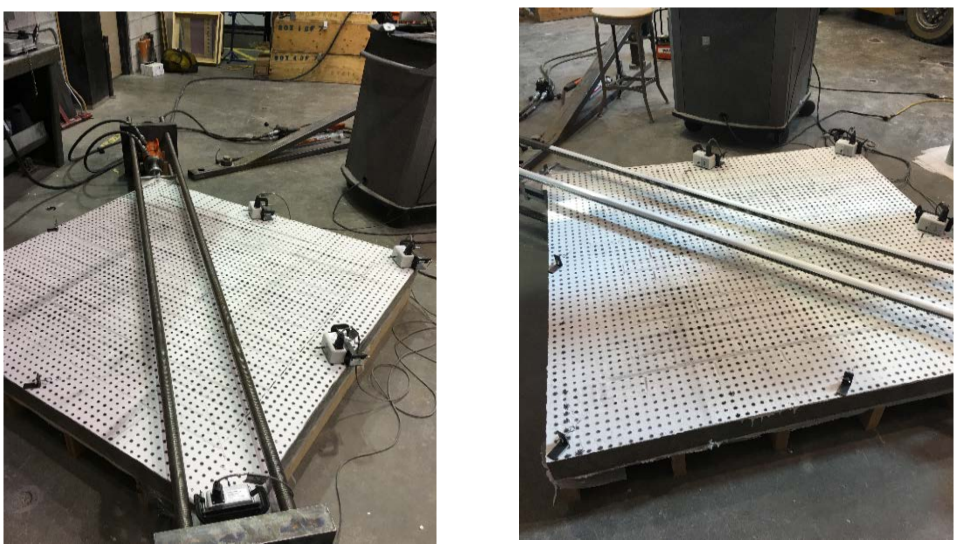

(a) (b)

Figure 29: Ready to test (a) masonry infill and (b) confined masonry walls with completed DIC preparation and potentiometer and loading apparatus

Experimental Procedure

The first specimen tested according to ASTM E519M was the unreinforced wall. The applicable load rate was determined to be 100 psi per second. Because the loading was manually controlled using the pneumatic pump, this target load rate was 1000 psi every ten seconds applied until failure. The same load rate was used for the masonry infill and confined masonry specimens.

After each wall specimen was tested, the corresponding masonry test prism was broken. This was done to find the same-day shear strength that could be taken as approximately the shear strength of the masonry panel within each wall assembly. The results from these tests can be seen in Table 6. After the masonry test prisms, concrete cylinders were also broken to determine the concrete strength on the day of the test. These results can be seen in Table 4.

ANALYSIS AND DISCUSSION

Results

Experimental test results of the plain masonry, masonry infill, and confined masonry wall assemblies are presented and discussed in this section.

Plain Masonry Specimen

The load displacement response of the plain masonry wall is shown in Figure 30 with photographs of the failed specimen. The peak load measured was 39.8 kip which occurred at a longitudinal displacement (displacement parallel to the direction of the applied load) of 0.04 in. Failure of the plain masonry wall was accompanied by an almost instantaneous displacement of 0.33 in. The load carrying capacity of the masonry panel dropped to zero immediately after the peak load was reached. The plateau shown in Figure 30 is an artifact of the sampling rates for the data recorded during the test. Notably, the data acquisition system's collection rates varied between the load cell and the displacement potentiometers.

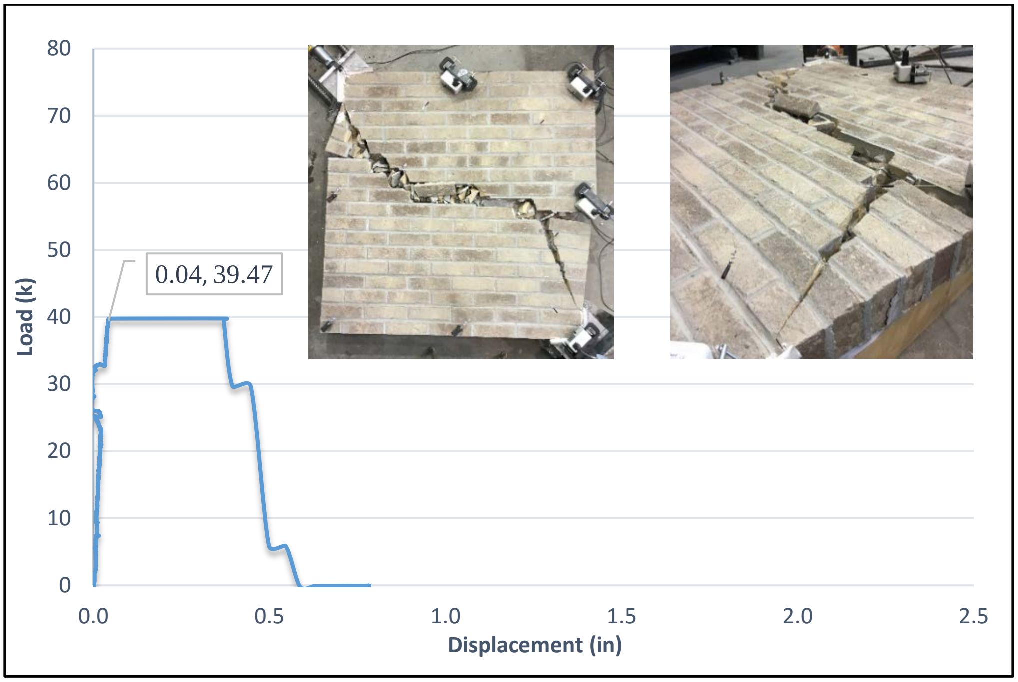

Figure 30: Plain masonry load-displacement response for potentiometer oriented parallel to loading plane accompanied with pictures of the failed specimen

In the transverse direction (perpendicular to the direction of the applied load), the load-displacement response for the three additional potentiometers did not record any discernable displacement until complete failure. After failure, the measured displacements of the masonry panel were 2.2 in., 2.8 in., and 3.2 in. for potentiometers 1, 2, and 3, respectively (Figure 24). The wall suffered a complete shear fracture in the diagonal dimension, parallel with the direction of loading. With no reinforcement present in the plain masonry wall, the load displacement plot indicates an absence of ductile behavior that could retain any load carrying capacity after ultimate load. After failure, the crack widths measured at two locations along the diagonal were approximately 1.5 in. and are shown in Figure 31.

(a) (b)

Figure 31: Shear crack widths observed after testing of the plain masonry specimen (a) along center of masonry panel and (b) along diagonal planes respectively

<u>Masonry Infill Specimen</u>

The peak load reached by the masonry infill specimen was 53.4 kip, and this specimen showed far more energy dissipation capacity than the plain masonry specimen. The load-displacement response of the failed specimen can be seen in Figure 32. After peak load was reached, cracks began to propagate through the masonry, but the reinforced concrete beam and column confinement contributed to a more ductile failure. Cracks were concentrated within the loaded corner, and the width of the cracked zone diminished along the diagonal dimension of the panel. The corner opposite of the hydraulic loading jack had only small hairline fractures present. The crack distribution is shown in Figure 33.

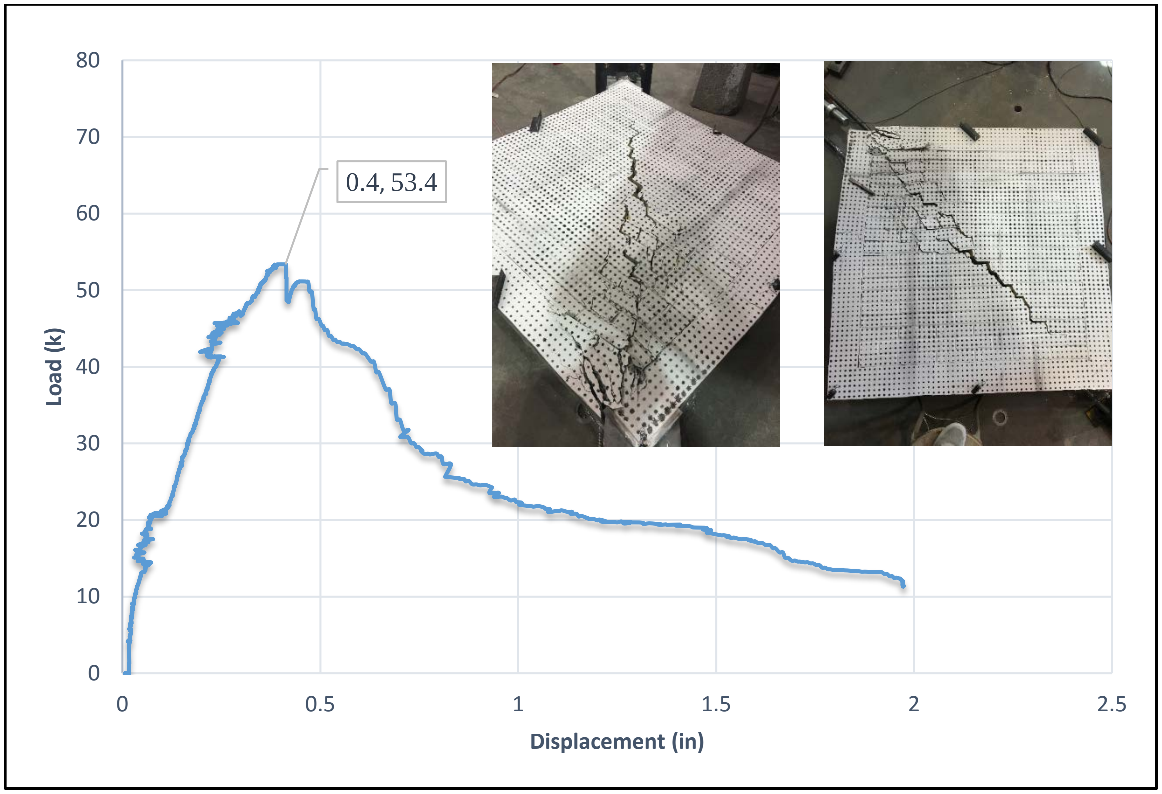

Figure 32: Masonry infill load-displacement response for potentiometer placed parallel to loading plane accompanied with pictures of the failed specimen

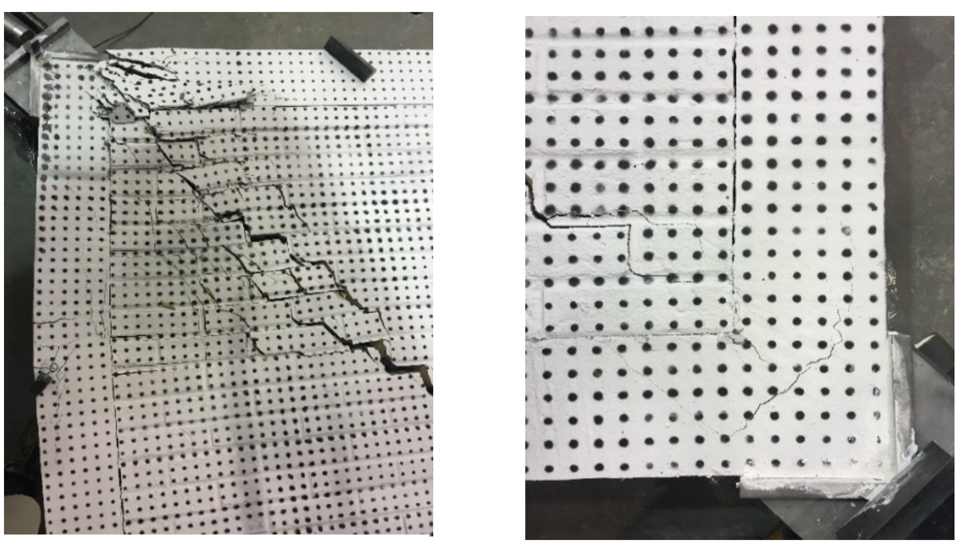

(a) (b)

Figure 33: Crack distribution in masonry infill specimen after failure of the (a) loaded corner and (b) the opposing corner

At the specimen's peak load, the longitudinal displacement was approximately 0.4 in. The displacement capacity of the masonry infill specimen was 0.58 in. This capacity was defined by Priestley (1982) as the displacement corresponding to a 20% loss of peak load carrying capacity. By the end of the test, the wall still carried approximately 20% of the peak load (10.6 kip) after a displacement of nearly two inches.

One reason for the large (0.4 in.) longitudinal displacement of the wall measured at peak load is the presence of small gaps between the masonry panel and the concrete frame. These are a result of the manner in which such walls are constructed. The concrete frame is cast first followed by the placement of the masonry panel after curing is complete. The gaps vary in size around the perimeter of the masonry panel from approximately 0.03 to 0.15 in. and result in immediate displacements of the corners of the concrete confining frame. Examples of the gaps present prior to the testing of this specimen can be seen in Figure 34. Another source of the large displacement measured at peak load is the sliding observed between the brick and concrete, resulting from the lack of bond between the concrete and masonry components.

(a) (b)

Figure 34: Gaps between the masonry panel and concrete frame of the masonry infill wall prior to testing (a) located at the bottom of the frame and (b) the top of the frame

Transverse potentiometers recorded larger displacement closer to the applied load than at the opposing corner of the panel and are shown in Figure 35 and Figure 36. Potentiometer 1, which is closest to the hydraulic jack, shows over three times more displacement than Potentiometer 3 located at the opposing corner. The data in Table 7 reflects the triangular crack propagation throughout the diagonal length of the masonry panel. This triangular failure can be seen in Figure 36.

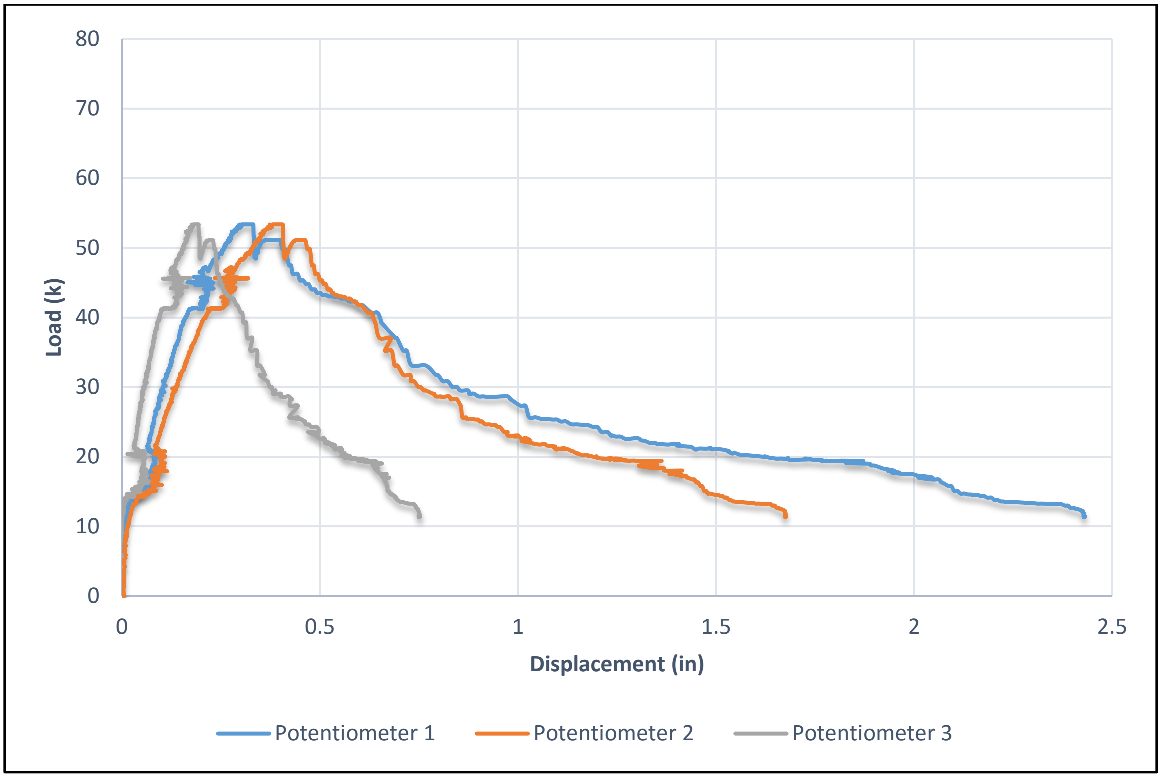

Figure 35: Masonry infill load-displacement response for transverse potentiometers

Table 7: Measured Transverse Displacements for Masonry Infill Specimen

Potentiometer	Displacement at Peak Load (in.)	Displacement at 80% of Peak Load (in.)
P1	0.35	0.57
P2	0.42	0.58
P3	0.17	0.28

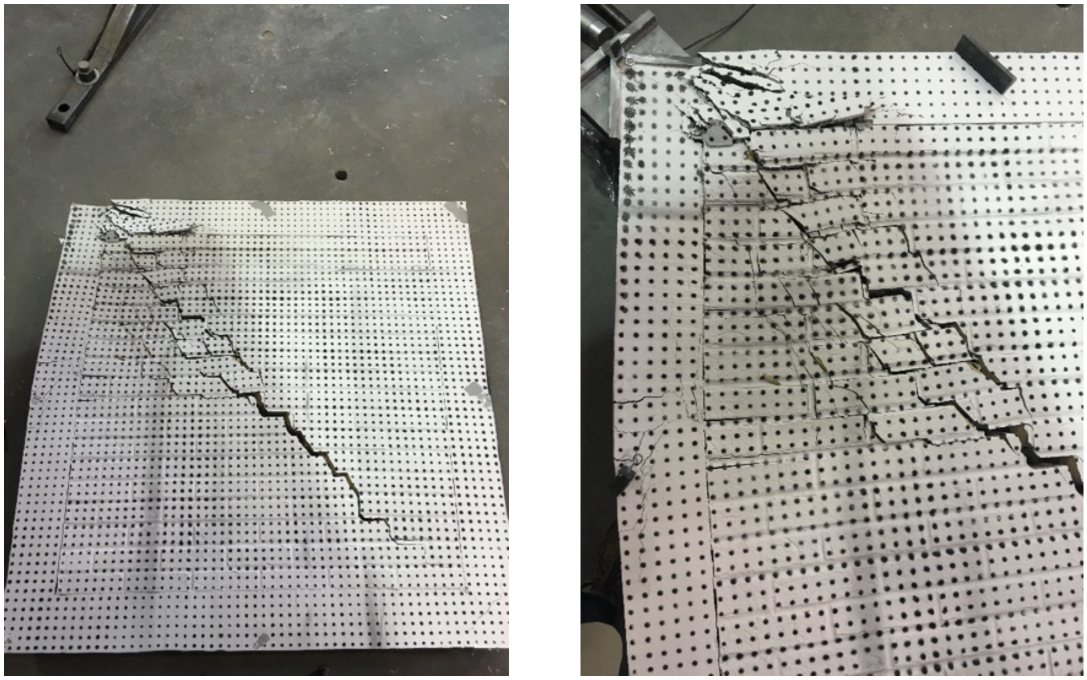

(a) (b)

Figure 36: Triangular crack distribution of effective shear width observed in the failed masonry infill panel from (a) a profile view and (b) focus on the loaded corner

The concrete frame confining the masonry infill wall also suffered damage. The loaded corner experienced shear failure at the joint between the tie-column and tie-beam members in the tie-beam and is shown in Figure 37. This shear failure caused the loading shoe to bear more heavily on top of the adjacent concrete column member and accelerated crushing of the concrete and masonry surrounding the joint. The eccentric axial force also caused increased flexural stresses in the tie-column, evident in the large cracks occurring at its mid span. The opposing corner of the panel only developed small stress cracks at the tie member joint by the end of the test.

(a)

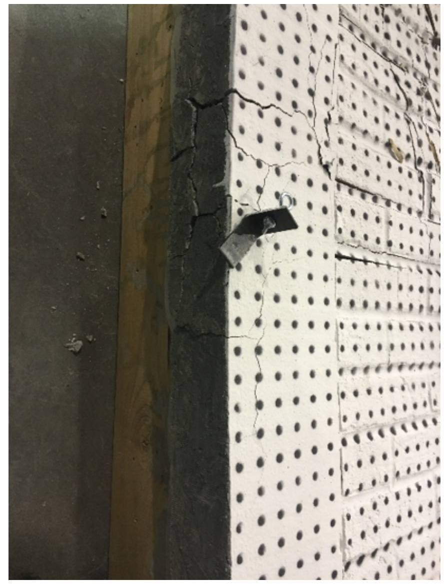

(b)

Figure 37: Damage to the concrete confining frame in the masonry infill panel in the form of (a) shear failure of the tie-beam and crushing resulting from failure in the joint and (b) flexural failure of tie-column confining masonry panel

Confined Masonry Specimen

The peak load reached by the confined masonry specimen was 69.8 kip at a displacement of 0.1 in. Pictures of the failed panel and the load-displacement response is shown in Figure 38. After peak load was reached, cracks began to propagate through the center region of the masonry panel. The cracks within this region developed uniformly throughout the diagonal length of the wall. Cracks were also found within the shear keys located in the concrete tie-columns. The distribution of the cracks are also shown in Figure 40.

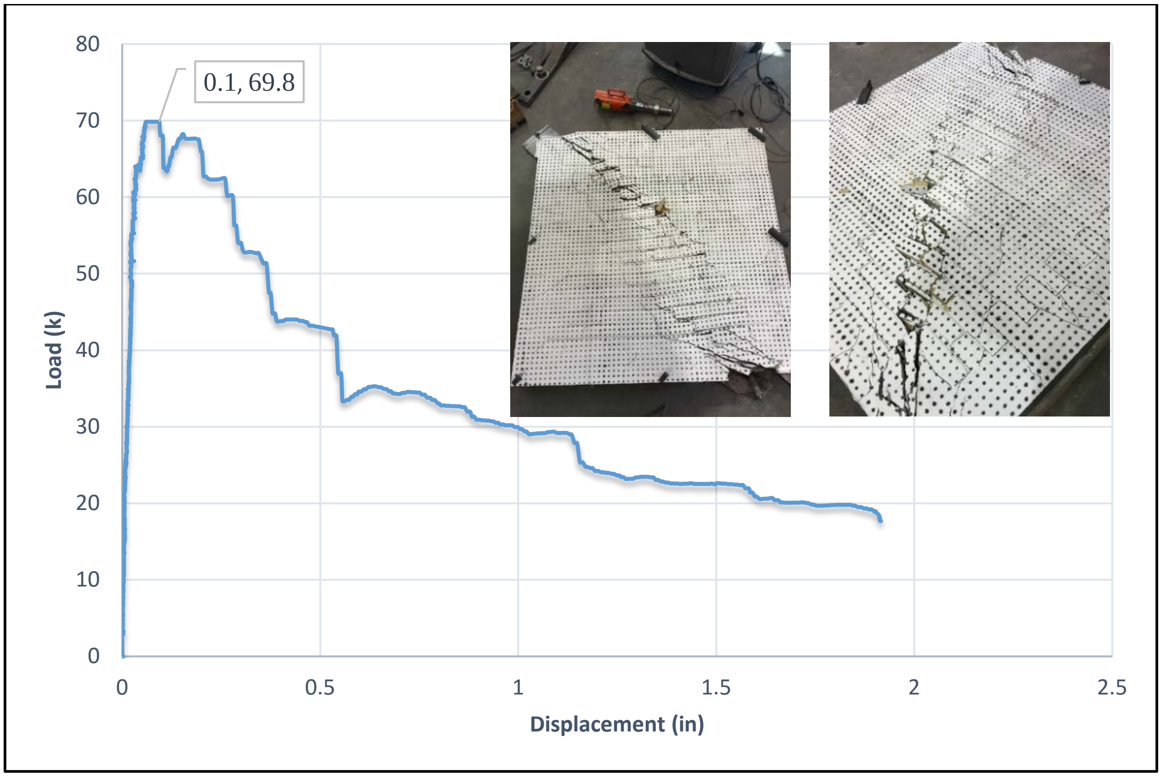

Figure 38: Confined masonry load-displacement response for potentiometer placed parallel to loading plane accompanied with pictures of the failed specimen

At the specimen's peak load, approximately 0.1 in. longitudinal displacement was measured by Potentiometer 4. Although significantly stronger than the masonry infill wall, this displacement represents one-fourth that of the masonry infill wall measured at its peak load. Similar to the masonry infill wall, the specimen was displaced a total of nearly two inches, maintaining approximately 25% of its peak load (17.5 kips) when the test was terminated.

The transverse potentiometers show uniform displacement of the masonry panel along the length of the panel diagonal as failure progressed. That is, all transverse potentiometers display a similar magnitude of displacement with applied load, as shown in Figure 39. This led to a failure that shows a more uniform distribution of shear stresses across the panel than was observed for the masonry infill panel, which mobilized an area more triangular in nature (Figure 36). The uniform effective shear width within the failed confined masonry panel can be seen in Figure 40 and is generally reflected in the displacement values reported in Table 8.

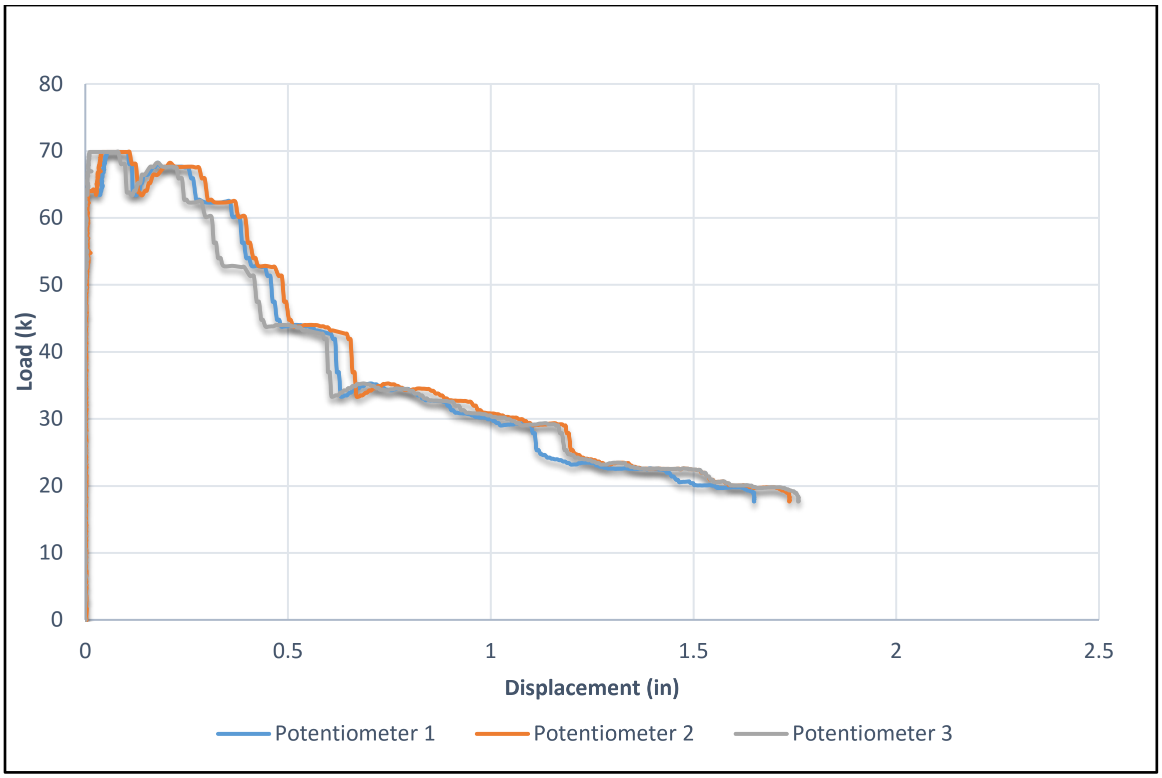

Figure 39: Confined masonry load-displacement response for the three transverse potentiometers

Table 8: Measured Transverse Displacement for Confined Masonry Specimen

Potentiometer	Displacement at Peak Load (in.)	Displacement at 80% of Peak Load (in.)
P1	0.08	0.40
P2	0.08	0.41
P3	0.01	0.32

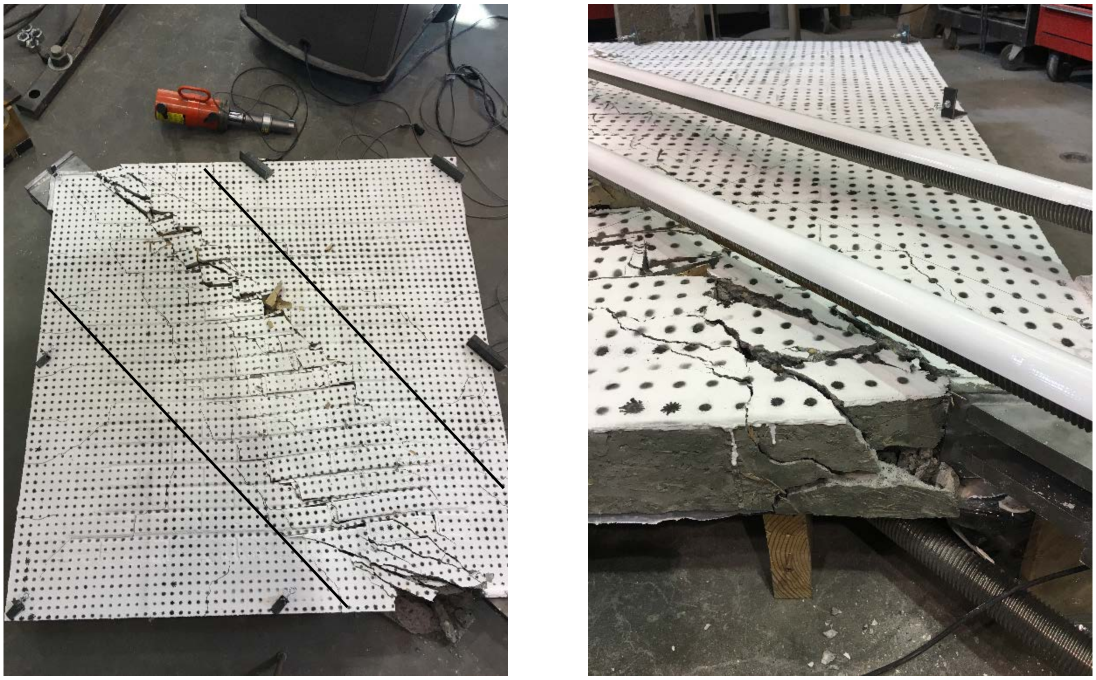

(a) (b)

Figure 40: Uniform effective shear crack within confined masonry wall shown (a) from a profile view and (b) extending through the concrete tie-members

Similar to the masonry infill wall, the tie-joint suffered damage in the form of shear failure and concrete crushing. Large shear fractures were localized on the tie-beam (Figure 41). These shear fractures extended through the depth of the concrete tie-beam section. Unlike the masonry infill specimen, the tie-columns also suffered moderate damage. Cracks were observed at the shear keys which extended through the column thickness. Failure of the concrete confinement and masonry panel can be seen in Figure 41.

Figure 41: Damage observed within (a) in the shear keys located within the tie-columns of the confining concrete, (b) the concrete tie-beam at the loaded corner, (c) and the center of the masonry panel

Discussion

A summary of the results, including peak load and corresponding displacement, and a comparison of the performance of the infill and confined walls relative to the plain masonry specimen, is shown in Table 9.

Table 9: Specimen Comparison

Specimen	Peak Load (k)	Normalized Peak Load (k)	Displacement at Peak Load (in)	Normalized Displacement at Peak Load (in)
Plain Masonry	39.7	1.00	0.04	1.00
Masonry Infill	53.4	1.35	0.41	10.25
Confined Masonry	69.8	1.76	0.10	2.50

The unreinforced plain masonry wall failure was expectedly brittle due to the absence of any confining members or reinforcement. The masonry infill and confined masonry walls behaved more ductile, however, they experienced different crack patterns and load distributions. The behaviors of these specimens when subjected to lateral load is discussed below.

Plain Masonry

Equation 5 was used to calculate the shear stress at failure in the 12 in. x 12 in. masonry prisms constructed to accompany each wall specimen, the results of which are shown in Table 10.

Table 10: Shear Stress of 12 in. x 12 in. Masonry Test Prisms

Specimen	Peak Load (k)	Net Area, A_n (in^2)	Shear Stress, S_s (psi)
Plain Masonry	7.9	43.5	128
Masonry Infill	10.3	43.5	167
Confined Masonry	9.7	43.5	158

The value attained from Equation 5 for the 12 in. x 12 in. prism built for the plain masonry specimen is conservative compared to the test results for the 48 in. x 48 in. wall. The plain masonry test specimen failed at a shear stress of 161 psi, or 39.7 k, which is approximately 26% higher than predicted using the smaller prism tests values.

Masonry Infill

The peak diagonal compression force measured during the testing of the masonry infill specimen was 53.4 kips which was 35% larger than the plain masonry specimen, and the displacement at peak load was over ten times larger than the plain masonry specimen (Table 9). It is important to note that the masonry prism strength for the masonry infill was 30% larger than the plain masonry prism strength and could be the cause of the increased strength of the masonry infill specimen.

The slip between the concrete members and masonry during loading is evident from the pictures obtained from the high-speed video recording, as shown in Figure 42. The large relative displacements between the concrete frame and masonry infill led to a diagonal crack that extended approximately 2/3 the diagonal wall length and was immediately followed by a shear failure in the tie-beam member closest to the applied load. This shear concrete shear failure can be seen in Figure 43.

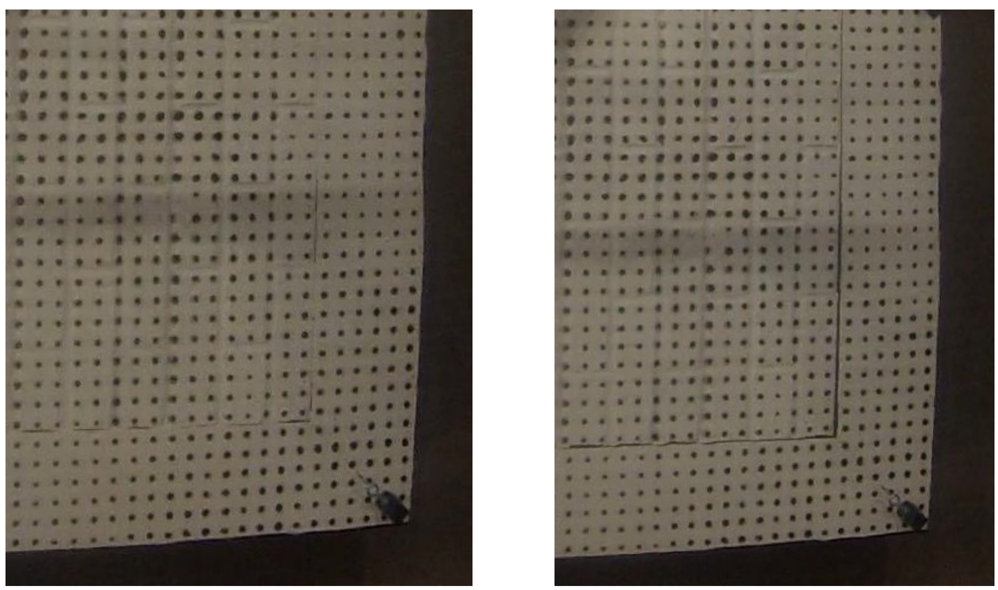

(a) (b)

Figure 42: Separation of concrete and masonry components (a) before loading and (b) after loading

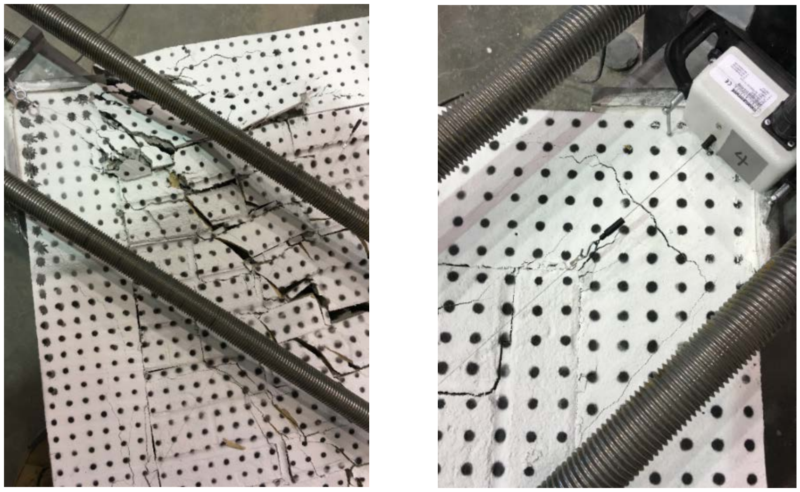

(a) (b)

Figure 43: Concrete confinement shear failures at peak compression load in masonry infill wall at (a) the loaded corner and (b) the opposite corner

To estimate the observed peak load of the masonry infill specimens, independent shear strengths were calculated for the reinforced concrete tie-beam and the infilled masonry wall. The relative displacement that was observed between the reinforced concrete and wall members, indicates the wall behavior was not composite and could be estimated by the sum of the individual shear strengths. The shear strength of the 4 in. wide x 6 in. deep reinforced concrete was estimated using the following equations from ACI 318-14. Variables used in the equations are shown in Table 11.

$$V_c = 2\sqrt{f'_c} b_w d \qquad \text{Equation 7}$$

where:

f'_c = average compressive strength of concrete, psi

b_w = effective width of concrete section, in.

d = effective depth of concrete section, in.

Table 11: Variables Used in Concrete Shear Strength Equations.

Variable	Masonry Infill	Confined Masonry
f'_c	5667	4268
b_w	5.3	5.3
d	4	4

The calculated shear strength of the reinforced concrete tie-beams and columns was 4.5 kips for the masonry infill wall and 4.1 kips for the confined masonry.

To estimate the shear strength of the masonry, the calculated shear stress of 167 psi for the 12-in. x 12-in. prism (Table 10) was distributed over the 48-in. x 48-in. masonry infill. The net masonry wall area used was the diagonal wall dimension multiplied by the brick width (246 in^2). The estimated masonry shear strength was 41.1 kips (167 psi x 246 in^2). Combining the estimated concrete and masonry shear strengths result in a total masonry infill wall strength of 46 kips. The calculated strength is 14% lower than the measured strength and could be the result of the assumed masonry shear strength that was obtained from a single 12 in. x 12 in. masonry prism test. For the plain masonry wall, the calculated strength was 20% lower than the measured strength based on the 12 in. x 12 in. companion prism. In addition, the assumption of non-composite behavior observed between the concrete and masonry at the tie-column mid-height may not be representative near the loaded and supported corners.

To further investigate the method of estimating the shear strength of the masonry wall assemblies described above, it was extended to a larger-scale experimental program that tested masonry infill walls subjected to lateral loading with axial loads. The larger-scale studies were done by Pujol and Fick (2010). Pertinent parameters from each investigation are shown in Table 12. The subsequent calculated shear strengths shown in Table 13 only include the contribution of the masonry, because column and beam failures were not reported by the investigators at the measured peak loads.

Table 12: Masonry Infill Wall Specimen Comparison

Researcher	Masonry Wall Dimensions (in.)	Column Dimensions (in.)	Beam Dimensions (in.)
Pujol & Fick	232 x 113 x 3-5/8	18 x 18	7 in. slab
Present Study	48 x 48 x 3-5/8	4 x 6	4 x 6

Table 13: Calculated Shear Strengths of Masonry Infill Wall Specimens

Researcher	Peak Horizontal Load, V_{test} (k)	Shear Strength of Prisms (psi)	Horizontal Wall Area (in^2)	V_{calc} (k)	Ratio (V_{calc}/V_{test})
Pujol & Fick	153	270	410	110	0.72
Present Study	37.8	167	174	29.1	0.77

Using the determined prism strengths to calculate the shear strength of the wall was found to be conservative for the masonry infill tests performed in this study and the study by Pujol and Fick (2010). The walls broke at 77% and 72% of the observed capacity compared to what was calculated, respectively. This implies that the rest of the strength observed in the physical tests was taken by the concrete frame members.

Confined Masonry

The peak diagonal compressive strength of the confined masonry wall was 69.8 kips which was 75% higher than the plain masonry wall and even 31% (69.8/53.4) higher than the masonry infill wall. The masonry prism strengths for the confined masonry wall were less than the masonry infill wall and indicate that the concrete frame contributed to the increased strength.

The load displacement plots for both confined masonry and masonry infill reveal a significant difference in stiffness. A trend line representing the load displacement data leading up to ultimate load for both specimens reveals that the confined masonry wall is approximately ten times stiffer than the masonry infill wall. The stiffness of both walls leading up to ultimate load is shown in Figure 44. It should be noted that the stiffness shown in Figure 45 does not take into account the different material properties of each specimen.

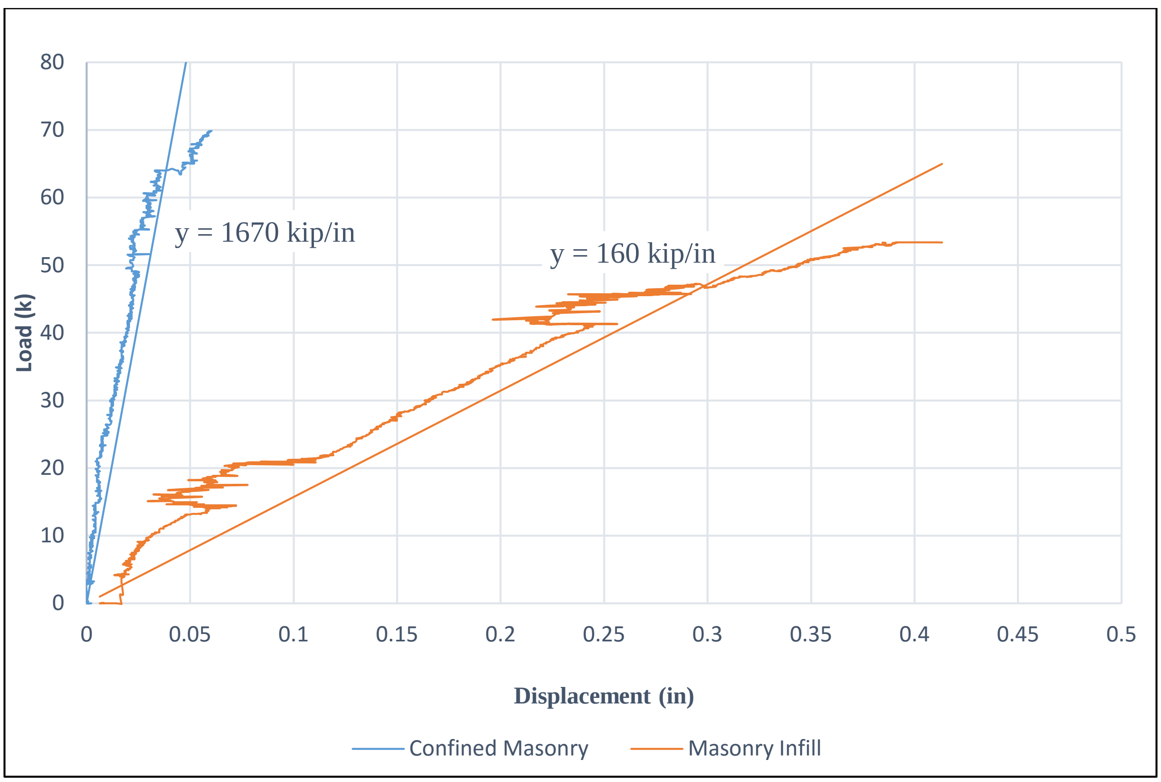

Figure 44: Stiffness comparison of masonry infill and confined masonry specimens

The increased stiffness of the confined masonry wall could result in larger base shears in a building utilizing this type of construction. However, as seen in Figure 44, the confined masonry wall also has much more strength which may be desirable in certain seismic regions.

As shown by the load displacement plot of the transverse potentiometers (Figure 39), the confined masonry wall had a much more evenly distributed failure throughout the masonry panel. Recall that the masonry infill wall showed failure of the masonry panel localized in the loaded corner of the wall (Figure 36). In the case of the confined masonry wall, shear cracks were spread throughout the entire diagonal length of the masonry panel. This indicates that the confined masonry wall engaged a larger area of masonry which contributed to a larger peak load. Similar to the masonry infill wall, the shear strength of the masonry component of the wall was determined using the tested strength of the masonry prisms. It can be seen in Table 14 that the masonry portion of the confined masonry wall only made up 56% of the total strength observed in the wall. This implies that the concrete frame members of the confined masonry wall as well as the shear keys and the bond between materials collectively contribute to the strength of this wall.

Table 14: Calculated Shear Strength of Confined Masonry Wall

Peak Horizontal Load, V_{test} (k)	Shear Strength of Prisms (psi)	Horizontal Wall Area (in^2)	V_{calc} (k)	Ratio (V_{calc}/V_{test})
49.3	158	174	27.5	0.56

Like the masonry infill specimen, failure of the confined masonry was accompanied by shear failures in the reinforced concrete frame. The observed concrete shear failure in the frame of the confined masonry wall can be seen in Figure 45.

(a)

(b)

Figure 45: Shear failure in the concrete frame shown in (a) the bottom corner of the wall with (b) a measurement of the amount of damage observed

<u>Displacement Capacity</u>

One important property associated with the load displacement response of each specimen is their displacement capacity. The displacement capacity is defined as the displacement when the wall's strength drops 20% from the ultimate load value (Priestley 1982). From the load-displacement figures, the displacement capacity and associated failure load for each specimen can be seen in Table 15.

Table 15: Displacement Capacity Associated with Each Specimen

	Masonry Infill	Confined Masonry	Percent Change
Peak Load (k)	53.4	69.8	31%
Failure Load (k)	42.7	55.8	31%
Displacement at Peak Load (in.)	0.41	0.10	-310%
Displacement at Failure (in.)	0.58	0.29	-100%

The behaviors numerically portrayed in Table 15 are shown graphically in Figure 46. The plain masonry's displacement capacity is the same as its peak load because the wall exhibited brittle behavior and lost all load carrying capacity after peak load was reached. The two walls with concrete frames exhibited increased displacement capacity. With respect to strength and displacement capacity, the masonry infill and confined masonry walls are inverse to each other. Where the masonry infill wall exhibits a higher displacement capacity it has less strength than the confined masonry wall.

The damage sustained by each wall at its displacement capacity can be seen in Figure 47. Different levels of damage are evident. The masonry infill wall displaced twice as much as the confined masonry wall at a residual strength of 80% of the peak load carried and has larger, more defined panel cracks as well as increased cracking to the reinforced concrete frame.

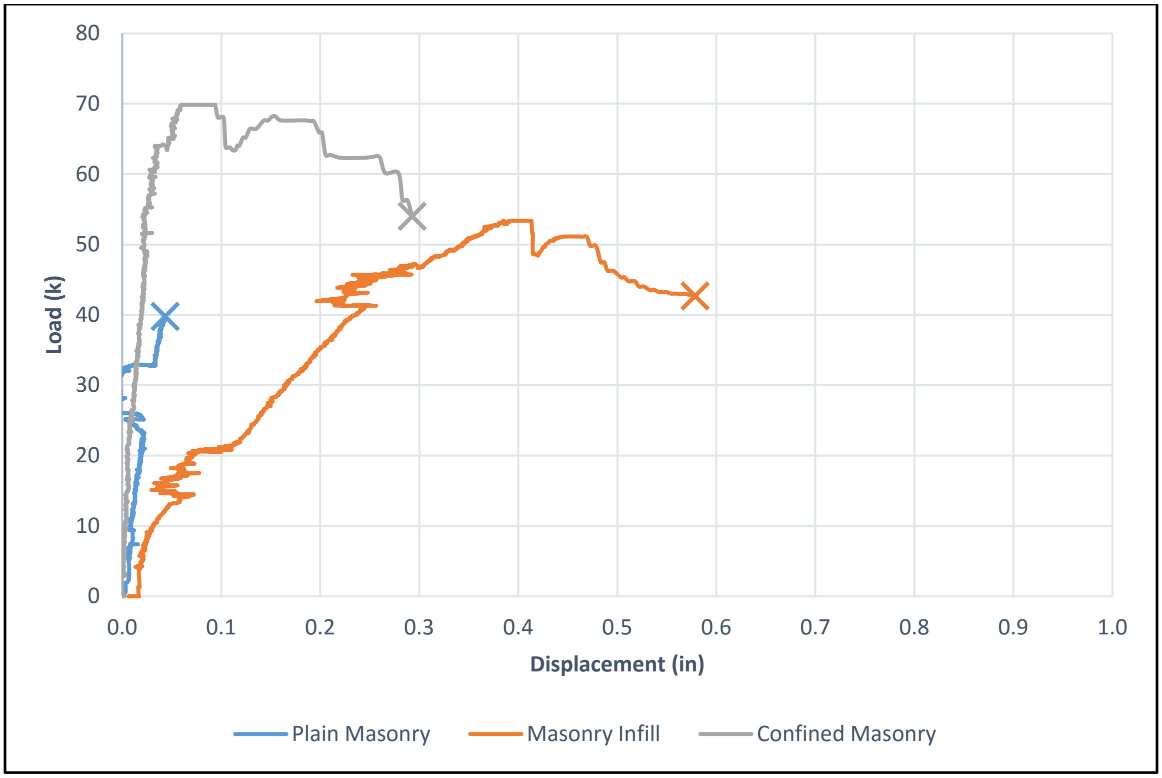

Figure 46: Overlay of load-displacement curves showing the displacement capacity and failure load of each specimen

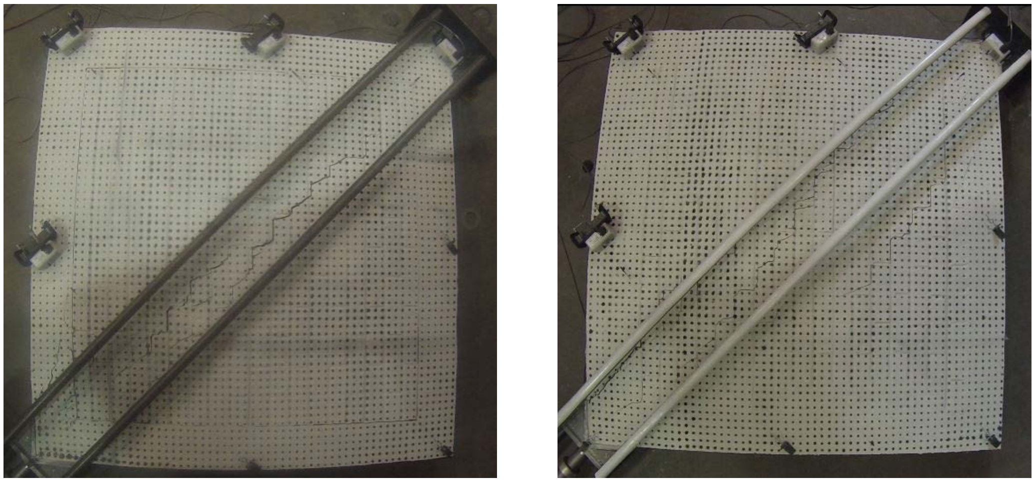

(a) (b)

Figure 47: Damage observed at load associated with displacement capacity in (a) the masonry infill wall and (b) the confined masonry wall

To gain further understanding into the advantages of the different systems, a direct comparison of the strengths and displacements associated with the peak load and 80% of the peak load are considered. Table 15 compares the strengths and displacements of the two systems at peak load and the load associated with displacement capacity. It can be seen through this comparison, that the percentage strength increase of the confined masonry specimen is less than the percentage displacement increase for the masonry infill specimen.

The second comparison, associated with the displacement capacities of the two specimens, is the ability of the specimen to deflect and displace. At peak load the masonry infill wall holds a strong advantage over the confined masonry deflecting approximately four times the amount as its counterpart. Even at failure defined by displacement capacity the masonry infill wall has deflected two times more than the confined masonry wall.

Strain Analysis with Digital Image Correlation

The digital image correlation data gathered from the MI and CM tests was put through the ARAMIS program to analyze strain propagation through the specimens under increasing load. A brief tutorial on the use of ARAMIS as well as the means for running an analysis are included in Appendix B.

Strain was analyzed at both peak load and displacement capacity, with an additional image showing the magnitude of strain before peak load was reached. These images are shown Figure 51 and Figure 53 for the masonry infill and confined masonry walls, respectively. Included is the load-displacement response for the associated specimen with the points identified corresponding to the strain images. These load-displacement responses are shown in Figure 52 and Figure 54. The results shown from the DIC analysis are tensile strains along the diagonal plane of the masonry walls. The red markings on some of the images denote the calibration points set in ARAMIS prior to running the analysis.

Recall, Priestley (1981) noted that cracking and crushing in unconfined plain masonry panels was estimated to occur at strains around 0.15%. Strain in the confined masonry panel seen in Figure 53a is nearly the same, however, it is acting above the diagonal plane at a steeper incline. It seems that with the addition of confining beams and columns, the masonry panels have an increased strain capacity for both the masonry infill and confined masonry walls.

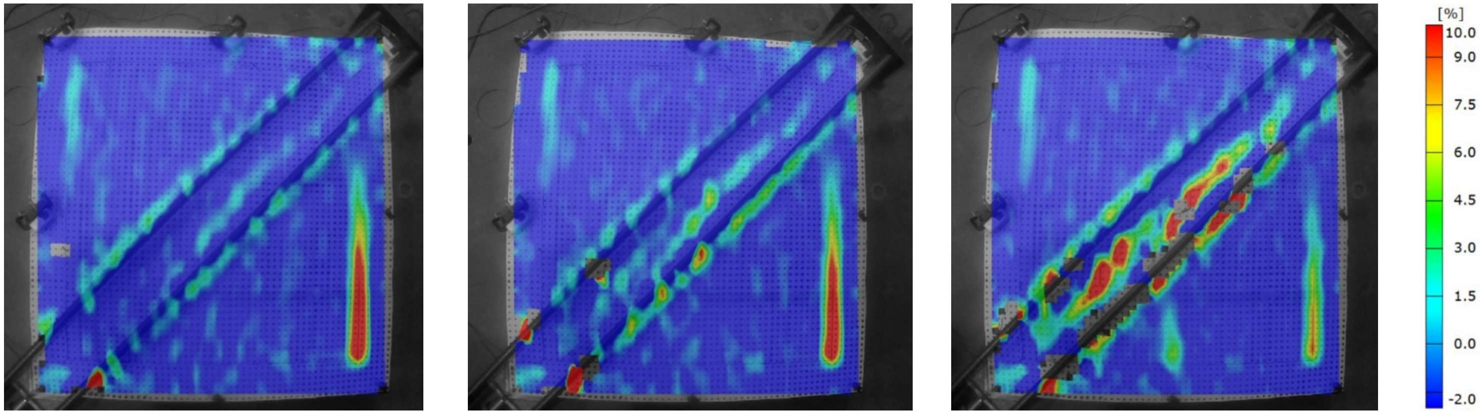

(a) (b) (c)

Figure 49: Strain correlation data for the masonry infill specimen measured (a) prior to peak load, (b) at peak load, and (c) at displacement capacity

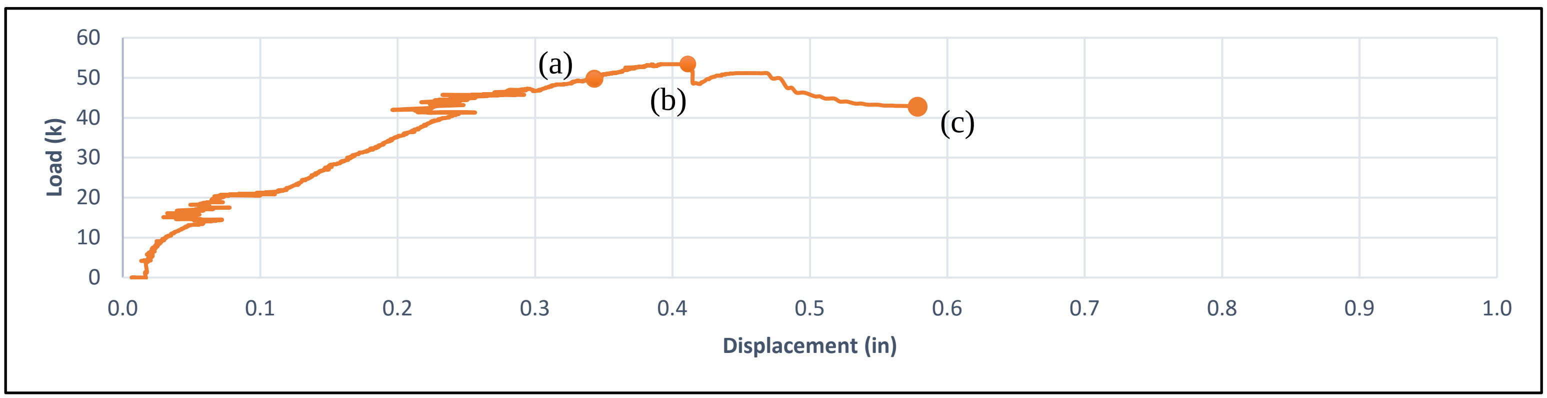

Figure 48: Load-displacement response for the masonry infill wall with markers indicating the location of each data point

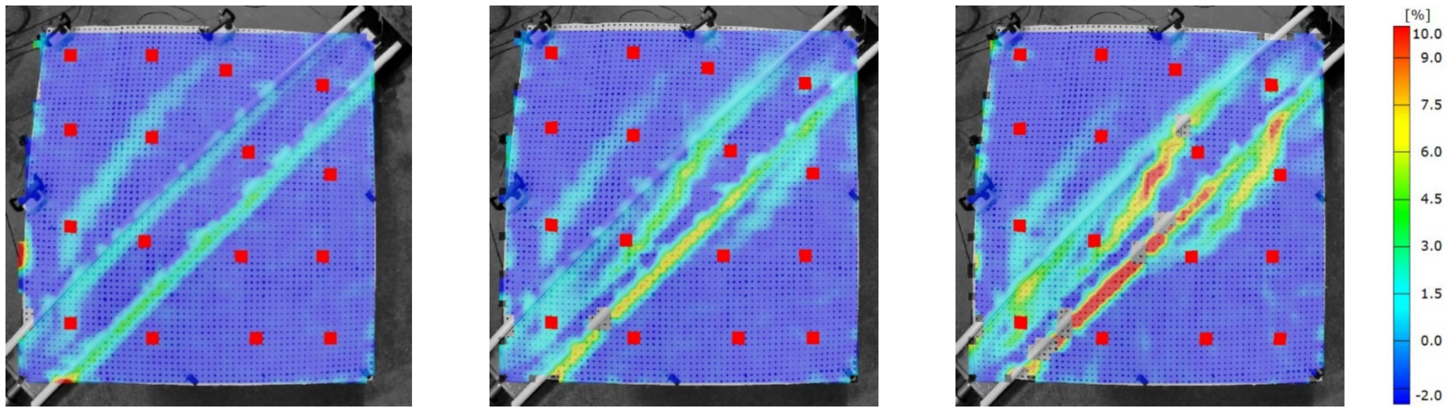

(a) (b) (c)

Figure 50: Strain correlation data for the masonry infill specimen measured (a) prior to peak load, (b) at peak load, and (c) at displacement capacity

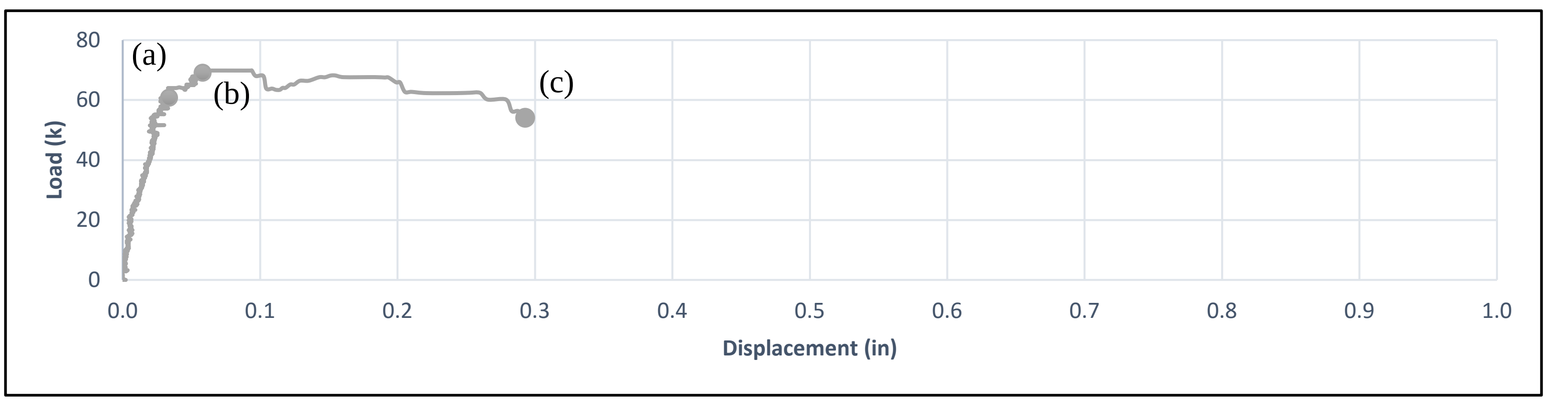

Figure 51: Load-displacement response for the confined masonry wall with markers indicating the location of each data point

Evaluating strains at peak load, both walls show strain concentrated around the diagonal plane of the masonry panel. These strains are concentrated along the diagonal plane for the masonry infill. However, in the confined masonry wall strain is not only developing in the diagonal plane but in more of an effective area surrounding the diagonal. This indicates a wider, more evenly distributed concentration of the strain in the panel as peak load is reached. This is likely the reason for the more uniform crack generation seen in the tested confined masonry specimen.

Finally, each specimen at displacement capacity were analyzed; the corresponding strains at displacement capacity can be seen in Figure 51c and Figure 50c.The portions of the masonry panel that are already cracked are either shown in red or did not get read by the ARAMIS program. At this point in the test, the masonry infill wall still has cracking confined to the diagonal plane of the masonry panel. However, it can be seen that at displacement capacity, the confined masonry wall has the beginnings of cracking on the outside of the diagonal plane.

Compressive Strut

The main load carrying member in the masonry wall assemblies tested is a compression strut that spans diagonally across the panel. The width of this compressive strut can be calculated using FEMA 273 (1997) equations reproduced in the literature review of this paper (see Equation 2). Compressive strut widths were calculated for both the masonry infill and confined masonry specimens. The values used for these calculations can be seen in Table 16. The calculated compressive strut width, w, is 6.1 in. for both the masonry infill and confined masonry walls. The experimentally determined strut widths estimated from the cracking in the masonry panels were 11 and 14 inches for the masonry infill and confined masonry specimens, respectively.

Table 16: Values Used for Calculation of Compressive Strut Using FEMA 273

	Masonry Infill	Confined Masonry	
E_m	900000	900000	psi
t_{inf}	3.625	3.625	in
f'_c	5667	4268	psi
E_{fe}	4290930	3723806	psi
I_{col}	72	72	in^4
H_m	48	48	in
L_m	48	48	in
H	60	60	in
D	67.9	67.9	in
θ	0.785	0.785	rad

The difference between the width of the approximate compressive strut measured in the tested specimens and the estimations given by the FEMA equations is less for the masonry infill wall than for the confined masonry wall (see Table 17). This could be due to the fact the FEMA approach assumes a uniform width throughout the compressive strut which was seen in the confined masonry specimen but not in the masonry infill. Recall, the masonry infill specimen showed a triangular crack distribution through the masonry panel as the strut developed.

Table 17: Actual Versus Calculated Compressive Strut Results

	Masonry Infill	Confined Masonry	
Observed Strut Width	11	14	in.
Calculated Strut Width	6.1	6.1	in.
Difference	45%	56%	

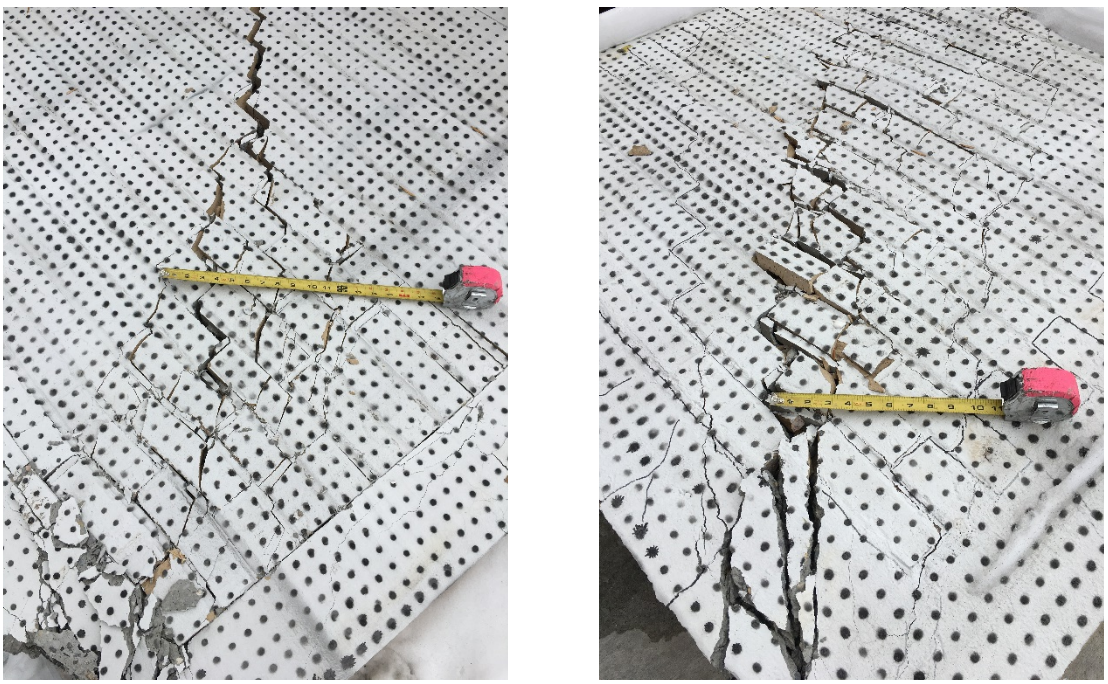

(a) (b)

Figure 52: Compressive strut formation in (a) the masonry infill specimen and (b) the confined masonry specimen

A PROJECTION TO THE EARTHQUAKE ENVIRONMENT

Analytical Modeling

Application of the measured properties of the masonry infill and confined masonry walls in assessing their performance in seismic events was investigated using analytical models. The experimentally observed load and displacement response was reproduced in finite element models of each specimen. The calibrated models were then used to estimate the response of a full-scale building using seismic records recorded during the 2015, 7.8 Mw Nepal earthquake. Building damage surveys performed after the earthquake were used to compare predicted damage from the analytical model with relevant damage pictures and building floor plans.

2D Frame Members

The masonry walls were modeled as 2D frames with pinned supports and a diagonal steel member using SAP2000 as seen in Figure 53. Reinforced concrete frame members were used for the tie-beam and tie-column members with dimensions and reinforcement matching that of the specimens constructed. The geometry, concrete strengths, and reinforcement used in the tie-members for each frame are shown in Table 18.

Table 18: Properties of Tie-Members Used in Analytical Model

Model	f'c (psi)	Member Depth (in)	Member Width (in)	Longitudinal Reinforcement	Transverse Reinforcement
Masonry Infill	5667	6	4	4-#3 Bars	1/4" Ties @ 6" o.c.
Confined Masonry	4268				

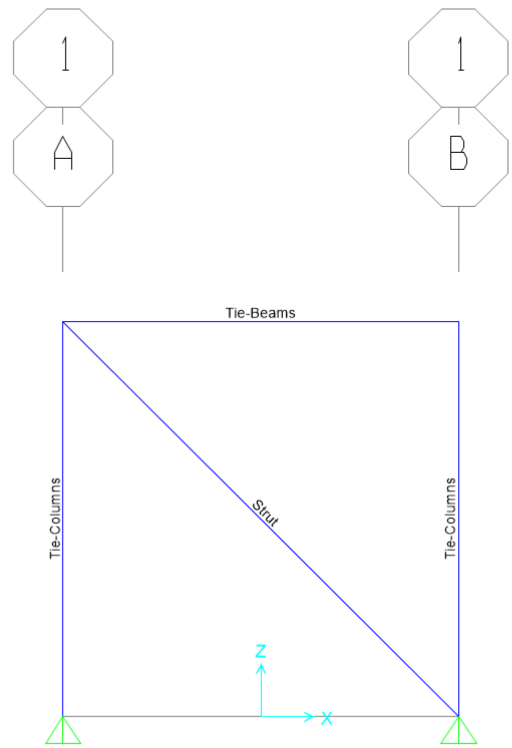

Figure 53: 2D frame model configuration used for both masonry infill and confined masonry walls

The compressive strut was modeled as a square tube member with a yield strength of 50 ksi and alternatively as a masonry element. In the former case, the cross sectional area of the steel was selected so that the yield strength (f_y*A_{steel}) matched the peak load observed in the masonry infill and confined specimen tests. The area of steel strut used was 1.07 and 1.40 in.^{2} for the masonry infill and confined masonry models, respectively. The strut members were assigned a modulus of elasticity that produced the initial axial stiffness measured during the tests of the physical specimens. The target stiffness was 160 kips/in and 1670 kips/in (Figure 44) for the masonry infill and confined masonry walls, respectively. This resulted in moduli of elasticity of 12,800 ksi and 71,600 ksi for the MI and CM specimens respectively.

A second approach for estimating appropriate stiffness of the analytical model used the material properties of the masonry wall assemblies and an effective masonry strut area. The modulus of elasticity for the masonry strut was estimated as 900 f'_m. Effective strut widths calculated by FEMA 273 (Table 17), were used with the brick thickness of 3-5/8 in. to calculate the area of the masonry strut.

Following this approach, the effective strut width calculated by FEMA 273 underestimates the contribution of the tie beams and columns to the overall frame stiffness. If the effective strut widths are increased by 2.5 and 3.5 times the brick thickness for the masonry infill and confined masonry models, a more representative stiffness is obtained.

Hinges

Two plastic hinges were used in SAP2000 to represent the nonlinear behavior of the masonry wall and reinforced concrete tie beam observed after the peak load. Axial compression-only hinges were modeled in the steel diagonal struts and were defined by four different loads and displacements as shown in Table 19. The displacements shown in this table are the values that were observed post peak load in the actual specimens.

Table 19: Masonry Strut Hinge Properties Used in SAP2000

Masonry Infill		Confined Masonry	
Fraction of Peak Load	Displacement Past Peak Load	Fraction of Peak Load	Displacement Past Peak Load
100%	0	100%	0
95%	0.07	95%	0.19
85%	0.10	85%	0.27
80%	0.18	80%	0.30

A shear hinge in the reinforced concrete tie-beam was used to represent the sudden shear failure that was observed in the masonry infill specimens. The concrete shear strengths of the tie-beam members calculated using the measured concrete strengths were used as the peak hinge strength. These values were 5.1 kips and 4.2 kips for the masonry infill and confined masonry specimens, respectively. This hinge did not include any post-yielding strength and represents the sudden shear failure that was observed. The shear hinges were located five inches from the face of the tie column to match the location of the observed shear failure.

A step-by-step pushover analysis was performed by increasing the lateral load on the model until hinges formed, thus capturing the post-peak behavior of the wall. Examples of the deflected shape with hinge formation and an axial load diagram of the analyzed model is presented in Figure 54.

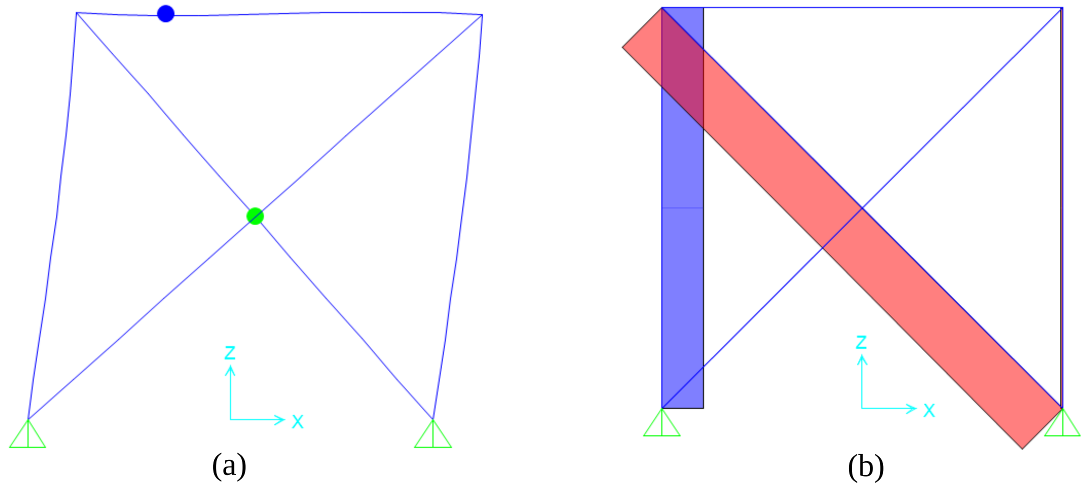

Figure 54: SAP analysis showing (a) hinge formation in model specimens and (b) axial load present in members

The non-linear load-displacement response for both the masonry infill and confined masonry models are shown in Figure 55 and Figure 56. Response up to peak load was accurate for both specimens and the load at displacement capacity is within a 20% margin of error.

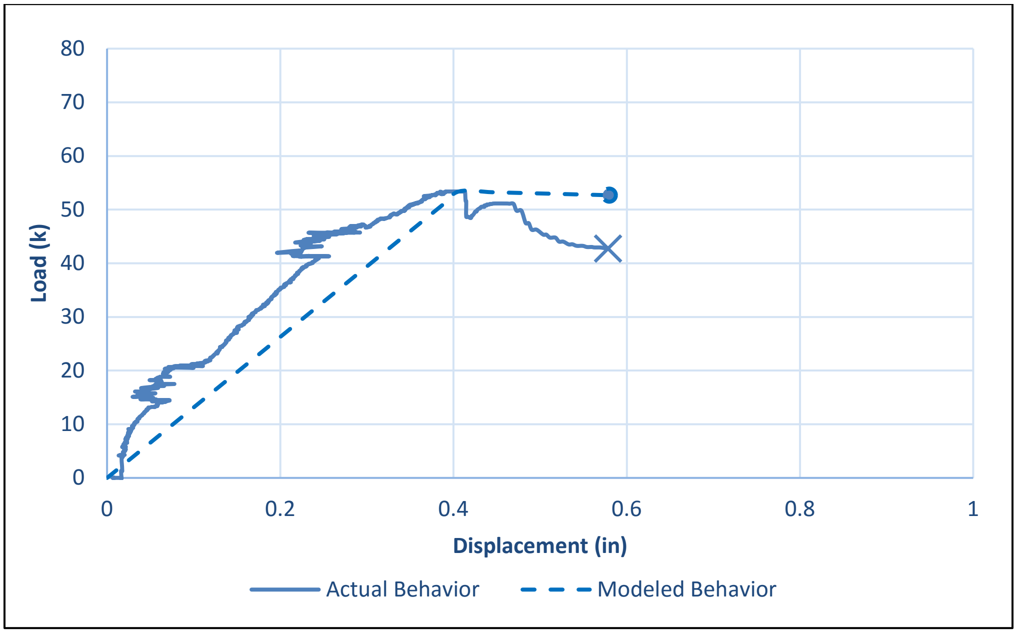

Figure 55: Actual versus modeled load-displacement behavior of masonry infill specimen

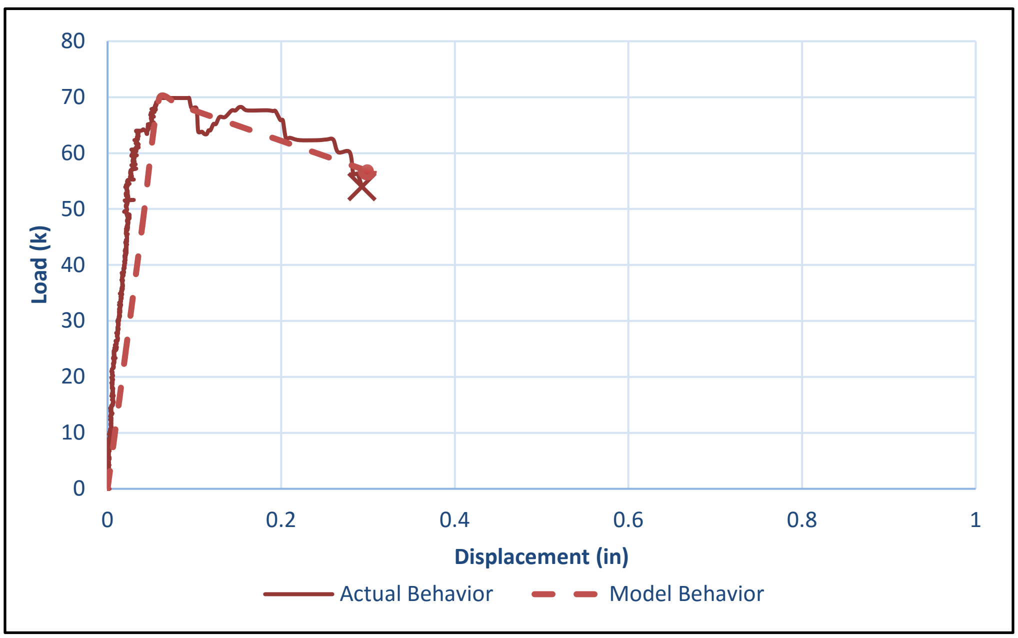

Figure 56: Actual versus modeled load-displacement behavior of confined masonry

Modeling a Structure Damaged by Strong Ground Motions

The objective of this part of the research effort was to model a multi-story building surveyed by the EERI reconnaissance team following the 2015 Nepal earthquake. This was done using the models developed for both masonry infill and confined masonry lateral resisting elements. A step-by-step pushover analysis was performed to compare calculated story drifts using both MI and CM models. The reported priority index for the building was evaluated for both lateral resisting systems and the applicability of priority index damage thresholds is discussed.

2015 Nepal Earthquake

In response to the 2015, 7.8 Mw Nepal earthquake, a team of engineers from the United States traveled to the area to assess the damage to the structures in the region. Data collected included the damage levels to various structural elements, a layout of the lateral force resisting elements, and accompanying photographs. Engineers also collected column and wall dimensions, which were used to calculate the priority index of each structure (see Appendix A).

The damage levels and reported priority indices shown in Figure 57 for the Nepal earthquake match the priority index trends shown in Erzincan and Haiti. As previously commented in the literature review, at the lowest values of priority index, percentage of severe damage for both reinforced concrete and masonry elements exceeded 70%. Structures with priority indices over 0.4% suffered no severe damage to reinforced concrete elements and only one in seven buildings had masonry elements classified as severely damaged.

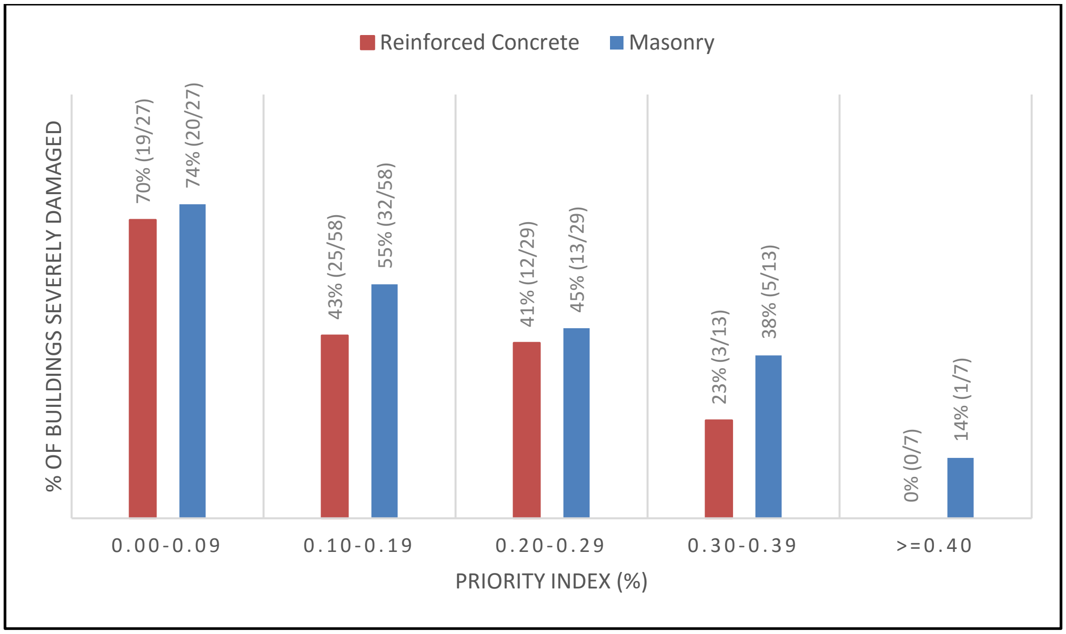

Figure 57: Priority index versus percentage of buildings severely damaged in 135 sampled structures from the 2015, 7.8 Mw Nepal earthquake

Building of Interest

The building analyzed is a four-story building located in Kathmandu, Nepal and referred to as Gongabu Bus Park Building 2A. A 2D model representing the interior wall of the building was analyzed using the geometry of the floor plan shown in Figure 58 scaled by a factor of approximately 1/3 to match the dimensions of the wall panels tested as part of this study. Original and scaled column, beam, and panel dimensions are shown in Table 20.

Table 20: Wall Dimensions Observed in Building Versus Model Dimensions

	Column Dimensions (in.)	Beam Dimensions (in.)	Masonry Panel Dimensions (in.)	Story Height (ft)
Actual	9 x 12	9 x 12	132 x 150	12
Scaled	4 x 6	4 x 6	48 x 48	5

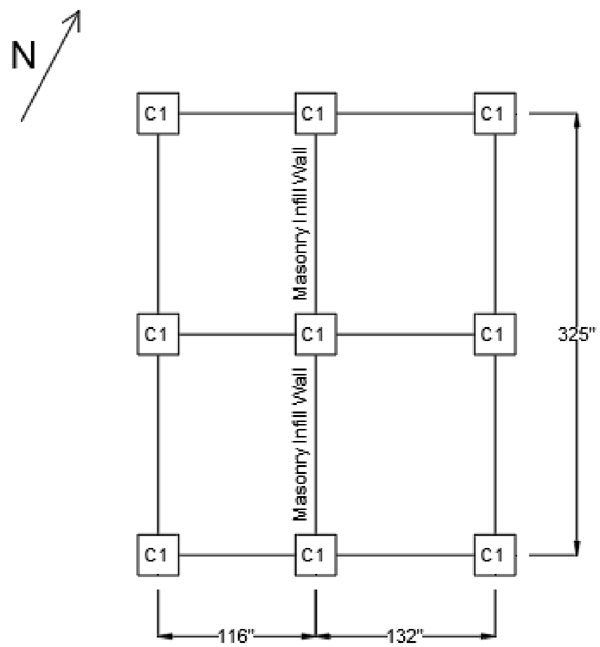

Figure 58: Gongabu Bus Park Building 2A floor plan showing lateral resisting elements on the eastern wall of interest

Reported damage levels for the Gongabu Bus Park Building 2A were ‘moderate’ masonry wall damage and ‘light’ damage to the reinforced concrete members. This building had a column index of 0.13% and a wall index in the North-South direction of 0.08% resulting in a priority index of 0.21%. Recalling the findings of O’Brien, Eberhard et al. (2011), a priority index of less than 0.4% would classify the building as at-risk for seismic damage. The data from 2015 Nepal earthquake, seen in Figure 57, shows that 41% of masonry elements and 45% of concrete elements suffered severe damage with buildings having priority indices ranging from 0.20-0.29%.

Because the 1/3-scaled Gongabu Bus Park Building was approximately equal to the size of the MI and CM wall specimens, the same analytical models were used. The four-story SAP2000 model is shown in Figure 59a. Effective moments of inertia of 35%

and 70% of the gross cross section were used for the beams and columns, respectively. Properties of the diagonal compression strut were the same as those developed for the masonry infill and confined masonry tests specimens. A linear distribution of load as a function of story height (1P, 2P, 3P, 4P) was used for the step-by-step pushover analysis. The pushover analysis terminated when the bottom two diagonal struts formed hinges, as shown in Figure 59b and Figure 59c for the masonry infill and the confined masonry models, respectively. Roof and story drift ratios, in addition to the total base shear at failure are shown in Table 21.

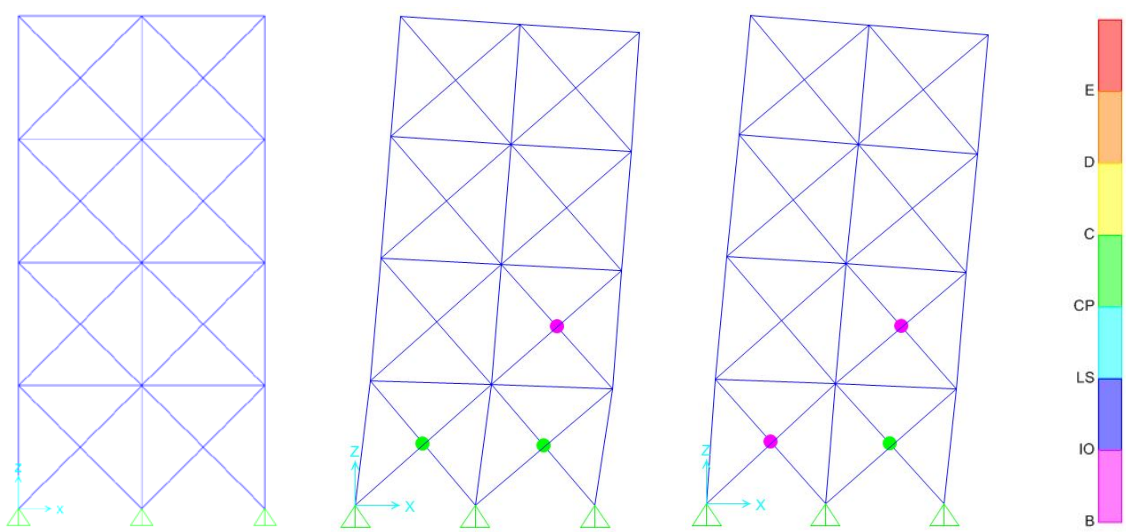

(a) (b) (c)

Figure 59: Four-story building SAP2000 model results showing (a) undeformed model, (b) hinge formation in masonry infill model, and (c) hinge formation in confined masonry model

Table 21: Nepalese Building Model Results

Specimen	Base Shear at Failure (k)	Roof Drift Ratio (%)	Level 1 Story Drift Ratio (%)	Level 2 Story Drift Ratio (%)
Masonry Infill	75.4	0.31	0.46	0.26
Confined Masonry	95.5	0.31	0.28	0.31

Damage to the masonry and reinforced concrete elements in the building of interest can be seen in Figure 60 and Figure 61, respectively. Similar crack patterns were observed in masonry infill walls of a full-scale reinforced concrete flat plate structure at roof drift ratios of 0.25% (Pujol & Fick, 2010) and are shown in Figure 62.

Figure 60: Masonry damage observed on the eastern wall of the Gongabu Bus Park Building 2A

(a) (b)

Figure 61: Damage to reinforced concrete elements confined the masonry on the eastern wall of the Gongabu Bus Park Building

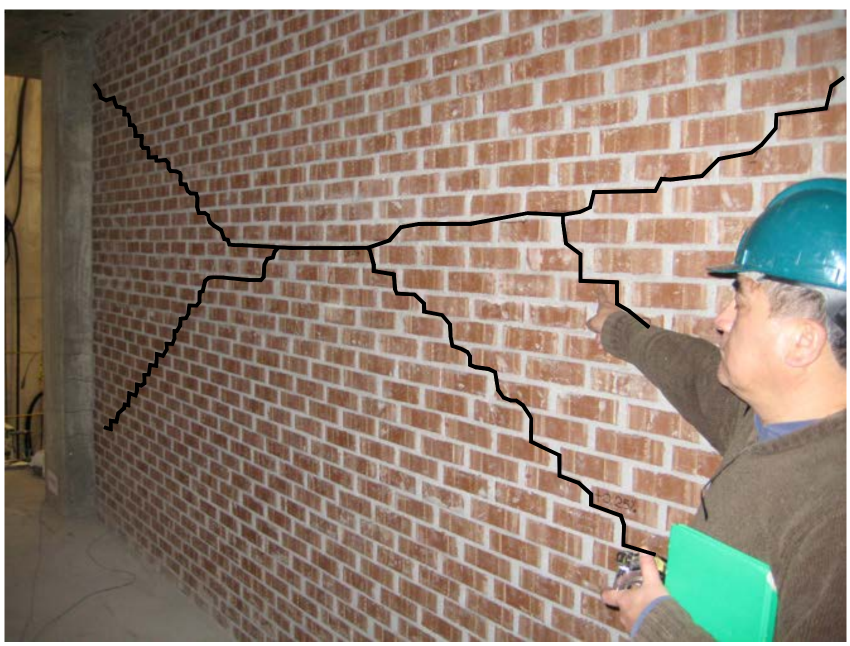

Figure 62: Masonry infill cracks in a full-scale building test showing crack formation at a 0.25% drift ratio

The moderate cracking observed by Pujol and Fick (2010) at a drift ratio of 0.25% suggests the calculated first story drift ratio of 0.46% for the masonry infill model is too large. The hinge locations in the infill model (Figure 59) did, however, occur in the same regions of the cracks observed in the building shown, as they are shown in Figure 60.

Relative comparisons between the two models suggest that seismic base shears causing failure in the first-story walls in buildings with similar proportions to the Gongabu Bus Park Building could be approximately 27% larger in the confined masonry system than that of a masonry infill system. The larger story drift ratio (0.46 versus 0.28%) of the masonry infill building is a result of the reduced stiffness of these lateral resisting systems.

The confined masonry model showed less severe first story drift ratios as compared to the masonry infill model. This suggests a higher threshold for severe damage for confined masonry structures than the 0.4% used for masonry infill structures.

SUMMARY AND CONCLUSIONS

The main concern with masonry walls used as a lateral force resisting system is their tendency for brittle failure. The use of concrete confinement in the form of reinforced concrete columns and beams surrounding the wall has been shown in previous studies to increase strength and ductility of these wall assemblies. In this thesis, three specimens (e.g. plain masonry, masonry infill, and confined masonry) were tested to study the strength and ductility in direct shear. The results of these tests were used to create analytical models to further investigate the ultimate strength of real buildings constructed with these wall assemblies. Based on this investigation, the following conclusions can be made.

1. When compared to a plain masonry wall, both the masonry infill and confined masonry walls provide increased shear strength. The masonry infill wall exhibited the ability to deflect 10 times more at peak load than the plain masonry specimen. The confined masonry wall had 2.5 times deflection at peak load when compared to the plain masonry wall. It was also noted that the confined masonry assembly had a higher strength capacity than the plain masonry wall.
2. The contribution of the masonry panel to the ultimate strength of the wall assembly was approximately 75% of the peak load for the masonry infill wall. The confined masonry wall contributed only approximately 55% of the wall’s lateral strength. This indicates that the confined masonry wall engages additional strength from the shear keys and the bond between the brick and concrete materials.

3. The confined masonry wall carried 30% more load than the masonry infill wall at their displacement capacities; however, the masonry infill was able to deflect twice as much than the confined masonry at this capacity. It should also be noted that at these displacement capacities, the masonry infill exhibited more damage to the masonry panel than the confined masonry specimen.
4. Strain was concentrated along the diagonal direction of the masonry infill. However, in the confined masonry specimen the strain concentrations were distributed over a wider effective strut.
5. The compressive strut width that forms in the masonry infill wall panel was underestimated by the equations provided by FEMA 273. Instead, values of 2.5 and 3.5 times the brick thickness for the masonry infill and confined masonry, respectively, provided for a more accurate representation of the width of the observed compressive strut and the resultant panel stiffness.
6. The calculated base shear that initiated two plastic hinges in the diagonal struts was 27% larger (95.5 k/75.4 k) for the confined masonry specimen. Roof drift ratios were approximately the same (0.31%) for both models at these base shears. The story drift ratio at the first level, however, was 64% larger (0.46%/0.28%) for the masonry infill building.

Future research should include investigations into the out-of-plane behavior of both walls, and development of a screening tool similar to the priority index for assessing the seismic vulnerability of buildings constructed with confined masonry walls. Additional building geometries and strong ground motions should also be considered.

Future test specimens should apply lateral and gravity loads to compare with the results found in this thesis. Including walls of various aspect ratios would provide additional insight to the masonry panel behavior of longer walls.

REFERENCES CITED

Atkinson, R., et al. (1989). "Response of masonry bed joints in direct shear." Journal of Structural Engineering **115**(9): 2276-2296.

Brzev, S., et al. (2010). "Performance of confined masonry buildings in the February 27, 2010 Chile earthquake." Earthquake Engineering Research Institute, Oakland, California (www. confinedmasonry. org).

Council, B. S. S. (1997). "NEHRP guidelines for the seismic rehabilitation of buildings." FEMA-273, Federal Emergency Management Agency, Washington, DC.

Council, B. S. S., et al. (1997). NEHRP guidelines for the seismic rehabilitation of buildings, Federal Emergency Management Agency.

DataHub (2015). "Database of low-rise reinforced concrete buildings with earthquake damage." from https://datacenterhub.org/resources/123.

DataHub (2016). "Public Datasets." from https://datacenterhub.org/dv_dibbs/view/eng_experiments%3Adibbs/case_information/.

Dolšek, M. and P. Fajfar (2001). "Soft storey effects in uniformly infilled reinforced concrete frames." Journal of Earthquake Engineering **5**(1): 1-12.

Donmez, C. and S. Pujol (2005). "Spatial distribution of damage caused by the 1999 earthquakes in Turkey." Earthquake Spectra **21**(1): 53-69.

Farshidnia, P. (2009). "Behavior and analysis of masonry-infilled reinforced concrete frames subjected to lateral load." Earthquake Resistant Engineering Structures VII **104**: 13.

FEMA-306 (1998). "Evaluation of Earthquake Damaged Concrete and Masonry Wall Buildings–Basic Procedures Manual." FEMA, Washington, DC.

Fierro, E., et al. (2007). "The Pisco, Peru, Earthquake of August 15, 2007." EERI Special Earthquake Report.

Gulkan, P., et al. (2003). "Preliminary Observations on the May 1, 2003 Bingol, Turkey, Earthquake." EERI Special Earthquake Report.

Gur, T., et al. (2009). "Performance of school buildings in Turkey during the 1999 Düzce and the 2003 Bingöl earthquakes." Earthquake Spectra **25**(2): 239-256.

Hashemi, S. A. (2007). Seismic evaluation of reinforced concrete buildings including effects of masonry infill walls, University of California, Berkeley.

Hassan, A. F. and M. A. Sozen (1997). "Seismic vulnerability assessment of low-rise buildings in regions with infrequent earthquakes." ACI Structural Journal **94**(1): 31-39.

Lizundia, B., et al. (2016). "M7.8 Gorkha, Nepal Earthquake on April 25, 2015 and its Aftershocks." Earthquake Engineering Research Institute.

Mainstone, R. J. (1971). "SUMMARY OF PAPER 7360. ON THE STIFFNESS AND STRENGTHS OF INFILLED FRAMES." Proceedings of the Institution of Civil Engineers **49**(2): 230.

Matošević, Đ., et al. (2015). "Cyclic testing of single bay confined masonry walls with various connection details." Bulletin of earthquake engineering **13**(2): 565-586.

Meli, R., et al. (2011). "Seismic design guide for low-rise confined masonry buildings."

Murty, C., et al. (2006). "At risk: the seismic performance of reinforced concrete frame buildings with masonry infill walls." Earthquake Engineering Research Institute, Publication No. WHE-2006-03 **70**.

O'Brien, P., et al. (2011). "Measures of the seismic vulnerability of reinforced concrete buildings in Haiti." Earthquake Spectra **27**(S1): S373-S386.

Priestley, M. (1981). "Ductility of Unconfined Masonry Shear Walls." Bulletin, NZNSEE **14**(1): 12-20.

Priestley, M. (1982). "Ductility of Confined Concrete Masonry Shear Walls." Bulletin of the New Zealand National Society for Earthquake Engineering **15**(1): 22-26.

Priestley, M. and D. Elder (1983). Stress-strain curves for unconfined and confined concrete masonry. Journal Proceedings.

Pujol, S. and D. Fick (2010). "The test of a full-scale three-story RC structure with masonry infill walls." Engineering Structures **32**(10): 3112-3121.

Sezen, H., et al. (2003). "Performance of reinforced concrete buildings during the August 17, 1999 Kocaeli, Turkey earthquake, and seismic design and construction practise in Turkey." Engineering Structures **25**(1): 103-114.

Singhal, V. and D. Rai (2014). Seismic behavior of confined masonry walls when subjected to in-plane and out-of-plane loading. Tenth US National Conference on Earthqueake Engineering Frontiers of Earthquake EnCanadian Masgineering, Anchorage, Alaska.

Singhal, V. and D. C. Rai (2014). "Role of toothing on in-plane and out-of-plane behavior of confined masonry walls." Journal of Structural Engineering **140**(9): 04014053.

Zhou, W., et al. (2013). "Seismic vulnerability of reinforced concrete structures affected by the 2008 wenchuan earthquake." Bulletin of earthquake engineering **11**(6): 2079-2104.

APPENDICES

APPENDIX A

DAMAGE INDICES CONTINUED

Introduction

Recent building surveys performed after earthquakes have generated a large dataset of information related to damage levels and building performance. Priority indices have been reported for over 700 buildings and compared with damage levels from seven different earthquakes from 1992-2015 (DataHub 2016). To determine if the priority index could be used as a reliable screening tool in the assessment of the vulnerability of low-rise reinforced concrete buildings in future earthquakes, O’Brien et al. (2011) compared damage levels reported from the 1999 Duzce earthquake with the 2010 Haiti earthquake. Results of their study revealed frequency of damage was higher in Haiti than Turkey. The study showed that 90% of the buildings in Haiti would have been classified as vulnerable using the priority index. A similar study was performed by Zhou et al. (2013) after the 2008 Wenchuan, China Earthquake and provided additional evidence that the priority index can be an effective way to prioritize resources for building strengthening. This investigation expands on the comparison of damage levels observed in other countries by evaluating a comprehensive dataset of 759 buildings surveyed after seven earthquakes. Included in this data set are recent surveys performed after the 2015 earthquakes in Nepal and Peru. Characteristics of earthquakes and construction methods where the priority index is less applicable are discussed. For the components and equations involved in calculating the priority index reference the confined masonry section of the literature review.

Previous Studies

1992 Erzincan Earthquake

To test the sensitivity of the priority index, the condition of 46 institutional buildings damaged by the 1992, 6.7 Mw Erzincan earthquake were documented (Hassan and Sozen 1997). Most of the buildings assessed were reinforced concrete frames with masonry infill walls made of either stone, brick, or tile masonry. Each building surveyed was assigned two damage ratings, one for reinforced concrete and one for masonry ranging from "light", to "moderate", to "severe". Damage levels and corresponding physical conditions observed are shown in Table 22.

Table 22: Damage Levels used in Surveying

Structural Element	Damage Level	Observed Condition
Reinforced Concrete	Light	Flexural cracks in the columns and beams
	Moderate	Formation of shear cracks accompanied with spalling
	Severe	Inclined cracks associated with shear failure or failure of any structural element
Masonry Infill	Light	Hairline cracks present
	Moderate	Larger cracks and large sections of plaster has spalled off
	Severe	Element collapse, masonry crushed, or cracks wide enough to see through wall

Priority indices were calculated for each of the 46 buildings. The sample was organized to plot priority index values and percent of buildings in that range suffering severe damage, as shown in Figure 63. Out of the sample considered, 17 of the 46 buildings surveyed had indices lower than 0.4%. Of the 17 structures, five sustained severe damage, representing approximately 30% of at-risk buildings. For the 1992 Erzincan earthquake, the priority index established a method to estimate damage levels caused by earthquakes without needing to account for material properties or reinforcement detailing.

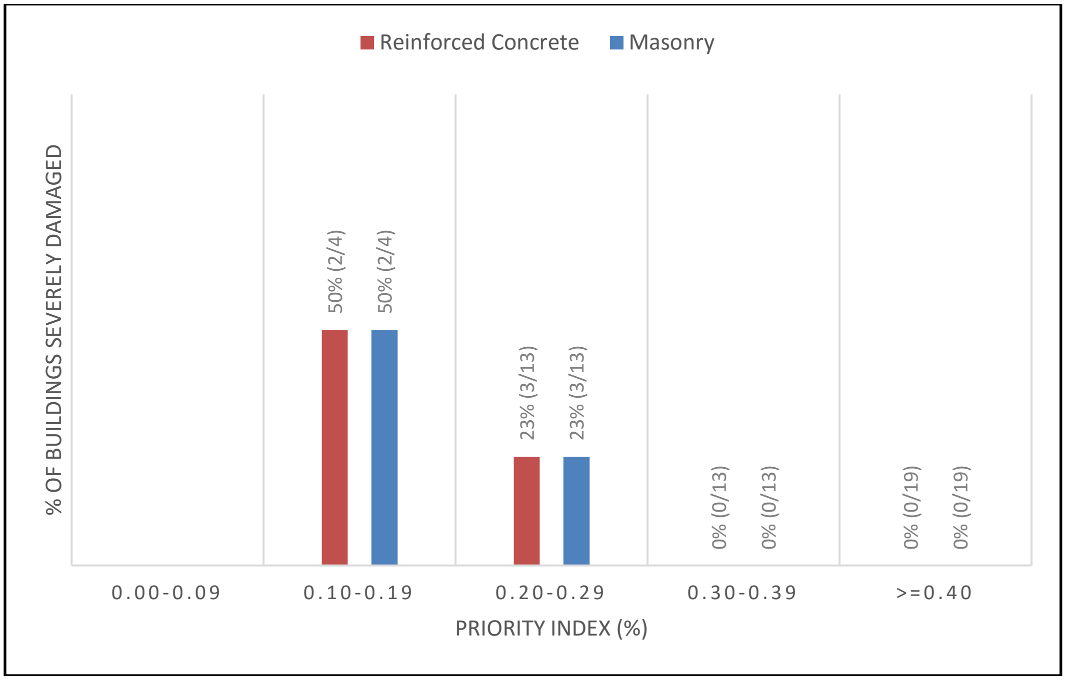

Figure 63: Priority index versus percentage of buildings severely damaged in 46 structures surveyed from the 1992, 6.7 Mw Erzincan earthquake (DataHub 2015)

1999 and 2003 Earthquakes in Turkey

Two earthquakes occurred in northwest Turkey in 1999 within a four-month period. The August 17, 7.4 Mw Marmara earthquake and the November 12, 7.2 Mw Duzce earthquake were located approximately 70 miles apart. Donmez and Pujol (2005) reported priority indices for 181 buildings that were surveyed after both earthquakes and observed similar trends reported after the 1992 Erzincan earthquake (Hassan and Sozen 1997). As would be expected, the percentage of buildings that suffered severe damage decreased as the priority index increased as shown in

Figure 64. It was also noted that higher storied buildings were associated with lower priority indices. Data for masonry wall damage was not collected.

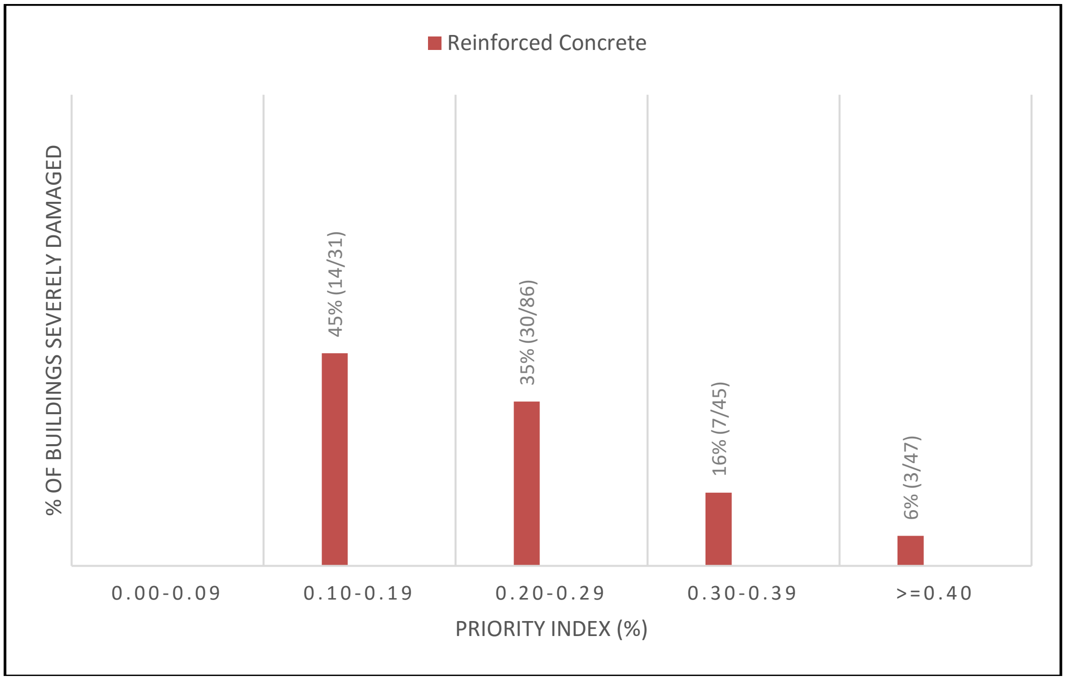

Figure 64: Priority index value versus percentage of buildings severely damaged in 181 structures sampled from the 1999, 7.4 Mw Maramara, and 7.2 Mw Duzce earthquakes (Donmez and Pujol 2005)

A similar building and damage level survey was performed after the 2003, 6.4 Mw Bingol earthquake. The combined data set for the three earthquakes included 21 school buildings with identical floor plans and different lateral force resisting systems. Research by Gur et al. (2009) used the priority index to compare reinforced concrete moment frames found in 16 buildings with 5 buildings containing structural concrete walls combined with the moment frames (dual system). Damage levels observed in buildings with dual systems were significantly less than those for the moment-resisting frame only. It was observed that only one of the five buildings was severely damaged.

For the reinforced concrete frame buildings, 10 of the 16 buildings were severely damaged. This is shown in Figure 65. The improved performance was attributed to the additional wall density provided by the structural walls.

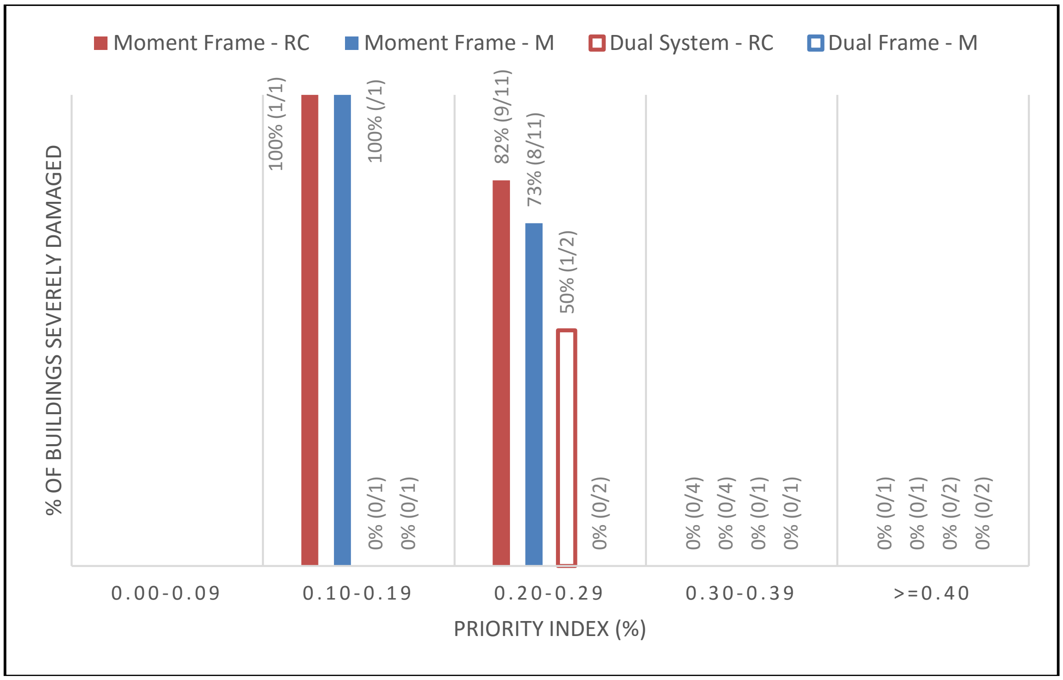

Figure 65: Priority index versus percentage of buildings severely damaged for 21 structures having identical floor plans but different lateral force resisting systems in the 1999, 7.2 Mw Duzce, 7.4 Mw Marma, and 2003 6.4 Mw Bingol (adapted from Gur et al. (2009)).

<u>2008 Wenchuan Earthquake</u>

Research by Zhou et al. (2013) further investigated the use of the priority index as a simple tool for prioritizing resources based on damage levels observed after the 2008, 8.0 Mw Wenchuan earthquake. The priority index was calibrated to screen structures that do not meet building code requirements in areas of high seismic risk to identify the most vulnerable structures that could be prioritized for repair and retrofits. Priority indices and percent severe damage in the Wenchuan earthquake for 116 school structures is shown in

Figure 66. It should be noted that the data collected from this seismic event does not match the downward linear trend in percent of severely damaged structures as priority index increases as seen in the other studies.

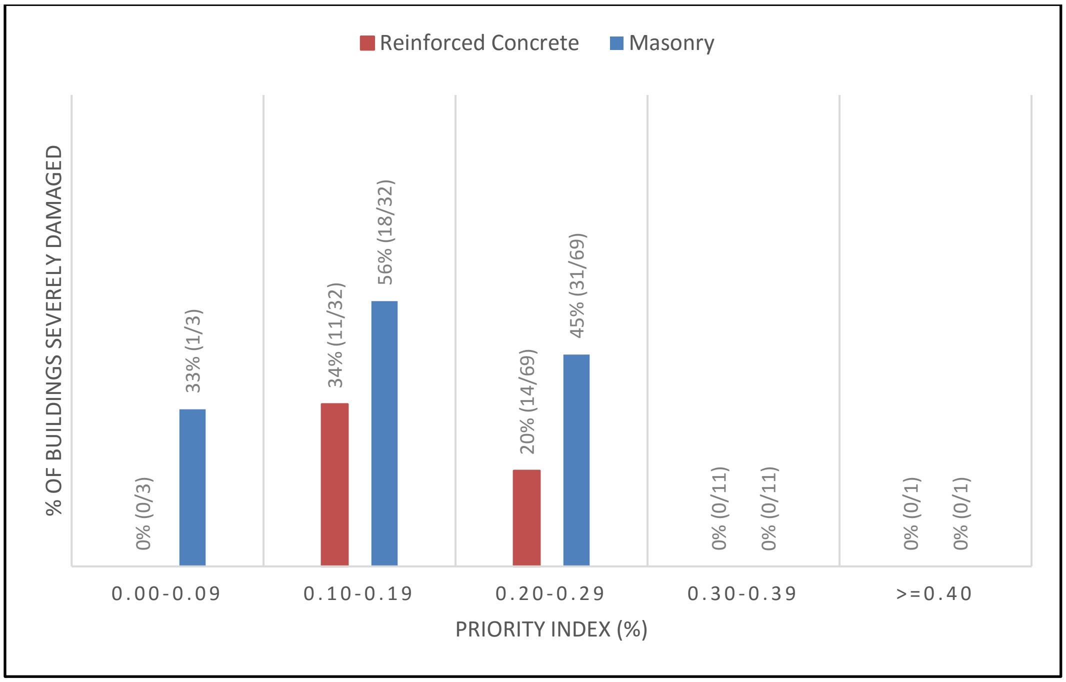

Figure 66: Priority index versus percentage of buildings severely damaged in 116 sampled structures from the 2008, 8.0 Mw Wenchuan, Sichuan earthquake. (Data adapted from Zhou et al. (2013)).

2010 Haiti Earthquake

A study completed by O'Brien et al. (2011) made a comparison of priority indices and damage levels reported during the 2010 Haiti and 1999 Duzce earthquakes. Their results showed that approximately 90% of the structures surveyed in Haiti would have been classified as vulnerable with priority indices less than 0.4%. The number of buildings with severe damage in Haiti was 50% larger than in Duzce and suggests the buildings in Haiti were more vulnerable. Figure 67 shows the downward trend of higher priority indices being associated with a lower percentage of severely damaged structures.

The building surveys and priority indices reported for the 1992 Erzincan, 1999 Duzce, 1999 Marmara, 2003 Bingol, 2008 Wenchuan, and 2010 Haiti earthquakes provide convincing evidence that buildings with priority indices less than 0.4% result in over 30% of buildings with severe damage as shown in Table 23.

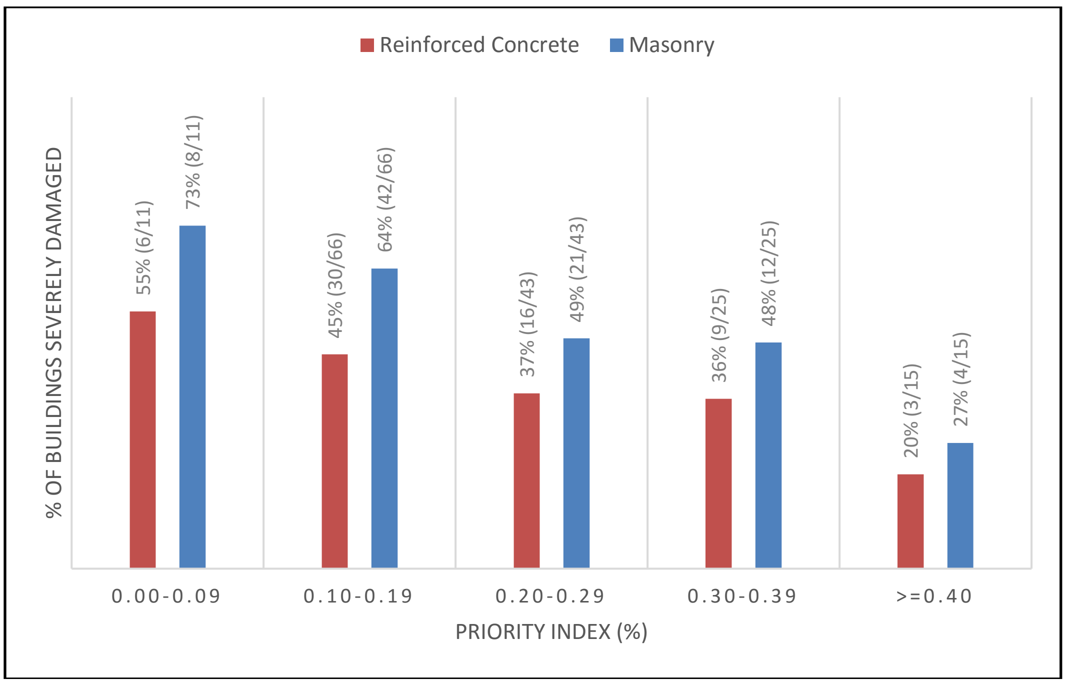

Figure 67: Priority index versus percentage of buildings severely damaged in 160 structures sampled from the 2010, 7.0 Mw Haiti earthquake (O'Brien, Eberhard et al. 2011)

The objective of this investigation is to review reported damage levels and priority indices from a comprehensive dataset that includes the 591 buildings surveyed and shown in Table 23, including an additional 161 buildings surveyed after the earthquakes in Peru and Nepal. The sensitivity of the priority indices to local construction practices, materials, and earthquake characteristics will also discussed.

Comprehensive Dataset

The number of buildings and damage levels reported for the vertical concrete walls and columns and masonry walls for 752 buildings and seven earthquakes are shown in Table 24. As was done for the previous building surveys for the earthquakes shown in Table 23, the damage levels included for the Nepal and Peru earthquakes will focus on the percentage of buildings with severe damage and priority indices less than 0.4%.

Table 23: Severe Damage and Priority Indices Less than 0.4%

Earthquake	No. of Buildings Surveyed	No. of RC Buildings with PI<0.4	No. of Masonry Buildings with PI<0.4	% of RC Structures with PI<0.4 with Severe Damage	% of Masonry Structures with PI<0.4 with Severe Damage
1992 Erzincan, 6.7 Mw	30	5	5	17%	17%
1999 Duzce 7.2 Mw	162	51	0	31%	0%
2003 Bingol, 6.4 Mw	57	27	26	47%	46%
2008 Wenchuan, 8.0 Mw	115	25	50	22%	43%
2010 Haiti, 7.0 Mw	145	61	83	42%	57%
			Average % Damage	**32%**	**33%**

2008 Peru Earthquake

The 2008, 8.0 Mw Pisco Peru earthquake showed a slightly different trend in severe damage as a function of priority index than data from previous earthquakes, as shown in Figure 69. No obvious trend is shown by the data for priority indices from 0.1% to 0.39%, with buildings in this category having similar amounts of severe damage. It is important to note that there was a the sharp drop in severe damage in buildings that had a priority index over 0.4%, with no reinforced concrete structures exhibiting severe damage and less than 20% (1/6) of the masonry damage structures experiencing severe damage. The information shown in Figure 68 could be a result of the relatively low sample size of 27 structures. The data in this graph still confirms the observation that structures having a priority index under 0.4% are overall more vulnerable to severe damage in the event of an earthquake.

Table 24: Damage Rating and Priority Index from Earthquakes Surveyed

	Damage to Vertical Reinforced Concrete Structural Elements				Damage to Masonry Walls			
Priority Index (%)	Total	Light Damage	Moderate Damage	Severe Damage	Total	Light Damage	Moderate Damage	Severe Damage
1992 Erzincan Earthquake								
0.00-0.09	*	*	*	*	*	*	*	*
0.10-0.19	4	0	2	2	4	0	2	2
0.20-0.29	13	5	5	3	13	5	5	3
0.30-0.39	13	7	6	0	13	7	6	0
>=0.40	19	15	4	0	19	15	4	0
Total	49	27	17	5	49	27	17	5
1999 Duzce Earthquake								
0.00-0.09	*	*	*	*	*	*	*	*
0.10-0.19	31	8	9	14	*	*	*	*
0.20-0.29	86	44	12	30	*	*	*	*
0.30-0.39	45	26	12	7	*	*	*	*
>=0.40	47	39	5	3	*	*	*	*
Total	209	117	38	54	*	*	*	*
2003 Bingol Earthquake								
0.00-0.09	*	*	*	*	*	*	*	*
0.10-0.19	14	6	1	7	14	2	4	8
0.20-0.29	24	4	2	18	24	1	6	17
0.30-0.39	11	1	8	2	11	2	8	1
>=0.40	8	5	2	3	8	3	5	0
Total	57	16	13	30	57	8	23	26
2008 Wenchuan Earthquake								
0.00-0.09	3	2	1	0	3	0	2	1
0.10-0.19	32	10	11	11	32	6	8	18
0.20-0.29	69	42	13	14	69	0	38	31
0.30-0.39	11	10	1	0	11	11	0	0
>=0.40	1	1	0	0	1	1	0	0
Total	116	65	26	25	116	18	48	50
2010 Haiti Earthquake								
0.00-0.09	11	5	0	6	11	1	2	8
0.10-0.19	66	28	8	30	66	18	5	42
0.20-0.29	43	19	8	16	43	13	9	21
0.30-0.39	25	13	3	9	25	11	2	12
>=0.40	15	6	6	3	15	6	5	4
Total	160	71	25	64	160	49	23	87
2007 Pisco Peru Earthquake								
0.00-0.09	*	*	*	*	*	*	*	*
0.10-0.19	4	1	0	3	4	1	0	3
0.20-0.29	12	5	2	5	12	7	0	5
0.30-0.39	5	1	0	4	5	2	0	3
>=0.40	6	5	1	0	6	4	1	1
Total	27	12	3	12	27	14	1	12
2015 Nepal Earthquake								
0.00-0.09	27	6	2	19	27	3	4	20
0.10-0.19	58	27	6	25	58	16	10	32
0.20-0.29	29	15	2	12	29	11	5	13
0.30-0.39	13	8	2	3	13	5	3	5
>=0.40	7	7	0	0	7	6	0	1
Total	134	63	12	59	134	41	22	71

* Indicates no collection of data

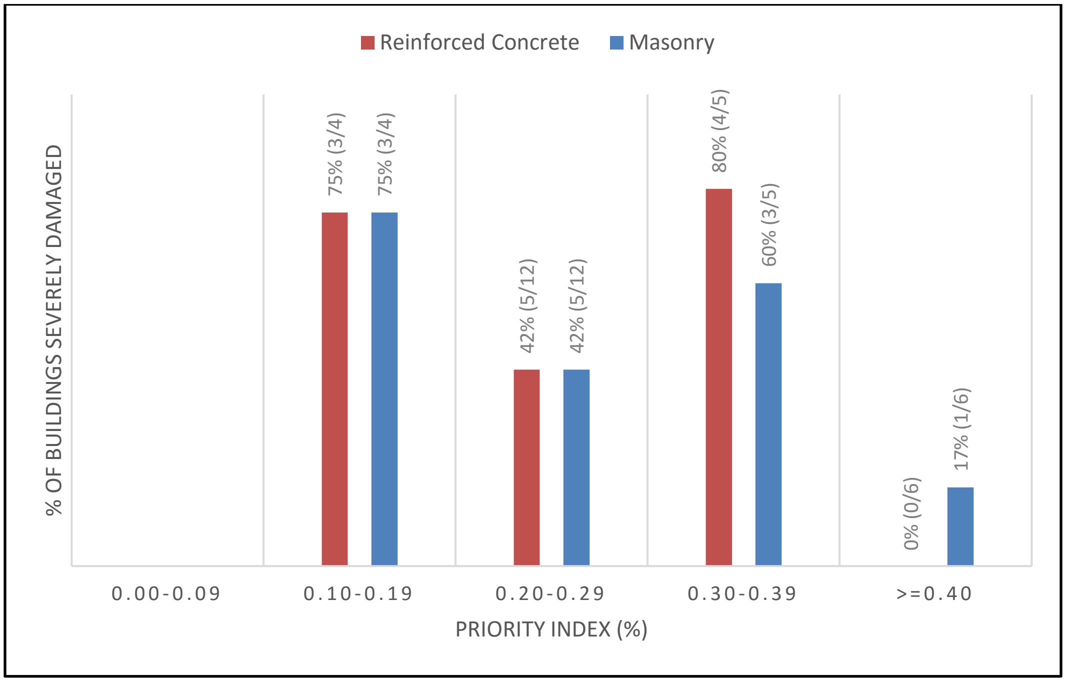

Figure 68: Priority index versus percentage of buildings severely damaged in 27 sampled structures from the 2007, 8.0 Mw Pisco Peru earthquake

<u>2003 Bingol Earthquake</u>

The data from the 2003, 6.4 Mw earthquake that struck Bingol, Turkey also shows little indication of the priority index trends seen in the previous surveyed earthquakes. This data, shown in Figure 69, indicates that buildings with priority indices within the range of 0.20-0.29% are most at risk to seismic loads. When looking at the number of buildings within each 0.1%, range it is seen that the 0.20-0.29% range had over double the amount of buildings surveyed than any of the other ranges. With only 57 buildings surveyed after the earthquake, the Bingol earthquake has significantly less data points than many of the earthquakes discussed in this paper (with the exception of Peru and Erzincan). Based on the number of structures collected within each priority index grouping, the conclusion can still be drawn that structures having indices less than 0.4% are at higher risk.

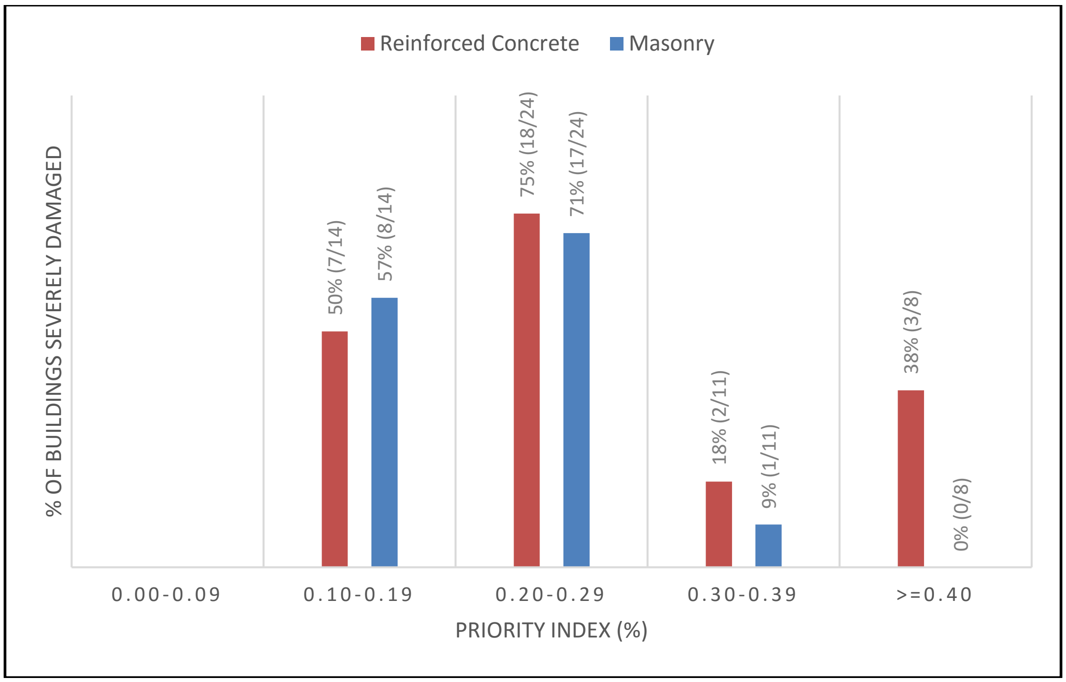

Figure 69: Priority index versus percentage of buildings severely damaged in 57 sampled structures from the 2003, 6.7 Mw Bingol earthquake

Average Priority Indices Associated with Multiple Stories

Through organization of the data given in Data Center Hub (2015) the average priority index for structures of varying stories from each of the seven earthquakes was found and are plotted as a function of story height in Figure 71. Referring to Figure 70, higher storied structures are clearly associated with lower priority indices and therefore more at risk to seismic damage. The average priority indices of each earthquake do not consistently dip below 0.4% until buildings reach three-stories in height. This information can be useful in screening for at-risk structures for one-storied structures become less of a priority for retrofits as structures three-stories or above.

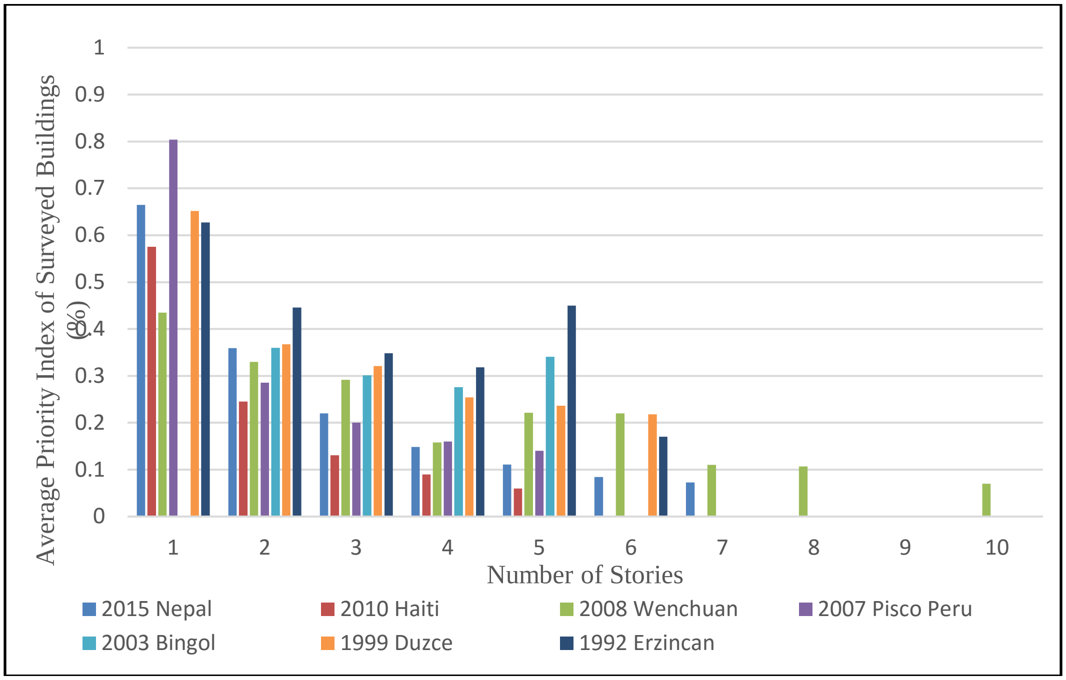

Figure 70: Average priority index associated with each story for each of the seven surveyed earthquakes (DataHub 2015)

Earthquake Characteristics

The challenge in the organization of these trends comes from discerning comparable data from seven very different seismic events. Many of the earthquakes occur in different areas, with each likely having their own materials and building practices. Therefore, in addition to simply plotting the surveyed damage levels against the priority index values, consideration must be given to several different factors that may have an influence on their relationship. Each earthquake is accompanied with a compiled report from reconnaissance trips following the seismic event which may provide the necessary information.

Fundamental characteristics of the seven seismic events, including peak ground acceleration, peak ground velocity and duration can be seen in Table 25.

Table 25: Seismic Properties from Each Earthquake

Year	Earthquake	Buildings Investigated	Magnitude (Mw)	Intensity (MMI)	Duration (s)	PGA (g)	PGV (cm/s)	Reference
2015	Nepal	135	7.8	IX	55	0.24	100	(Lizundia, Shrestha et al. 2016)
2010	Haiti	160	7.0	X	30	1.0	120	(Eberhard, Baldridge et al. 2010)
2008	Wenchuan	116	8.0	XI	60	0.97	133	(Wang, Dai et al. 2008)
2007	Pisco Peru	27	8.0	X	100	0.50	62.2	(Fierro, Blondet et al. 2007)
2003	Bingol	57	6.4	IX	17	0.55	40	(Gulkan, Akkar et al. 2003)
1999	Duzce	210	7.2	IX	10.5	0.50	90	(Ghasemi, Cooper et al. 1999)
1992	Erzincan	49	6.7	VIII	9.1	0.49	78.1	(Williams, Pomonis et al. 1992)

Nepal Earthquake

The 2015, 7.8 Mw Nepal earthquake, with a Mercalli Intensity of IX (Violent), killed as many as 8,000 people, injured over 20,000 with many more than that being displaced from their homes. After the earthquake, members of EERI visited the country to perform reconnaissance and remediation work. Upon inspection, it was found that a majority of buildings effected by the quake were not properly engineered, with over 80% being built by owner (Lizundia, Shrestha et al. 2016). It was also noted that poor detailing and geometric irregularities were the main reason for failure in severely damaged buildings in the area. Reinforcement was present but observed as being less than the

Nepalese code required in most instances of failure. Failures caused by poor detailing are shown in Figure 71.

Upon researching the strong ground motion and subsequent effects on the area, it was found that many pertinent seismic characteristics of the event relative to structural vulnerability were less severe than expected. It was found that that average period of the earthquake was approximately 4.5 seconds. Most masonry infill structures have a natural period of under 1 second and therefore did not experience peak spectral demands from the seismic event (Lizundia, Shrestha et al. 2016). The highest peak ground acceleration felt by a recording station during the earthquake's approximately 55 second duration was 0.24 g. EERI noted that this acceleration was relatively low was a seismic event of this magnitude (Lizundia, Shrestha et al. 2016).

(a) (b)

Figure 71: Severe failure caused by poor detailing. (a) insufficient joint reinforcement at beam-column connections, (b) poor quality concrete in structural elements (Lizundia, Shrestha et al. 2016)

After investigation, epicentral regions were found to have felt high amplitudes and high frequencies while regions further away from the epicenter experienced high amplitudes and low frequencies. Members of EERI noted Kathmandu, where many of the buildings in this data set were located, rests on a sediment basin that can amplify ground motions at low frequencies; however, when subjected to strong ground motion, soil can respond non-linearly leading to de-amplification at high frequencies (Lizundia, Shrestha et al. 2016). With Kathmandu approximately 135 km from the epicenter it can be assumed that the sediment basin contributed to some de-amplification of the earthquake.

The main source of failure observed in the Ghorka Valley can then be assumed to be poor detailing and construction. Buildings with lower priority indices therefore suffered more severe damage than similarly constructed buildings with higher priority indices.

Peru Earthquake

The 2007, 8.0 Mw earthquake in Peru was similarly destructive. Classified by a Maximum Mercelli Intensity of X (Extreme), peak ground accelerations during the quake reached 0.5 g. Members of EERI responded to the disaster by sending reconnaissance teams to provide relief and study the buildings affected.

Researchers found the average duration of the earthquake to be approximately 100 seconds, which was noted as being significantly longer than earthquakes of similar magnitude. EERI reported that shallow crusted earthquakes of 8.0 Mw or higher have a median duration of 48 seconds (Fierro, Blondet et al. 2007). In addition to the initial earthquake, 12 aftershocks having a magnitude greater than or equal to 5.0 Mw were recorded. The repeated strong ground motions that the buildings in this sample were subjected to and the fact that the data shown in Figure 68 does not trend similarly to other earthquakes suggests these structures may have performed with brittle behavior. Therefore, even if all structures did have priority indices greater than 0.4%, they may have still been at risk due to an inability to inability to dissipate the seismic energy through ductile behavior. Severe damage resulting from the initial 8.0 Mw earthquake is shown in Figure 72 and Figure 73.

Figure 72: Severely damaged masonry infill building in Peru following the 8.0 Mw earthquake (DataHub 2015)

(a) (b)

Figure 73: Severely damaged structural elements found in the building; (a) Masonry infill panels that have been crushed or have fallen out completely, (b) Severely damaged concrete captive column (DataHub 2015)

Using the methods outlined by Hassan and Sozen (1997) priority indices and damage levels associated with 27 buildings were recorded. As compared to the data of the other seven earthquakes, Peru has the smallest sample of buildings inspected in relation to the priority index. Peru is also one the the two earthquakes that do not conform to the expected trend shown by the other five earthquakes. The data for the sampled buildings in Peru only contains approximately six structures for each tenth increment of the priority index as compared to nearly 50 structures for the same increment taken for the Duzce earthquake. Therefore, the priority index is likely still valid for buildings in Peru, however, for a more accurate representation of the seismic vulnerability of the area, more structures would have to be analyzed.

Bingol Earthquake

Similar to data from the Peru earthquake, the 6.4 Mw Bingol earthquake provided data that did not fit the expected priority index trend shown by the other earthquakes being studied. The earthquake had a Maximum Mercelli Intensity characterized as IX (Violent), peak ground accelerations up to 0.55 g, and shook the area for an average duration of approximately 17 seconds.

Through the reconnaissance of engineers responding to the disaster, it was noted that several of the buildings were built using stock designs. This implies that the structures could have been inadequate in their ability to resist the seismic loads of the area. With this in mind, inspectors observed several instances of poor detailing including inappropriately sized and unwashed aggregate in concrete and inadequate reinforcement detailing in beams, columns, and joint regions (Gulkan, Akkar et al. 2003). Upon testing concrete from a few of the sampled structures it was found that, at times, strength was as low as one third the intended value (Gulkan, Akkar et al. 2003). The Bingol Region has been described as one of the poorest regions in Turkey, which could have implications to the overall quality of their construction. Therefore, non-conformance of the data for the priority index could possibly be drawn from insufficient design and materials of the structures located in the region.

Examples of severely damaged structural members which led to the collapse of the school building located in Bingol can be seen in Figure 74 and Figure 75. Poor detailing of reinforcement can be seen in the columns in addition to masonry infill crushing as a result of the displacement of the reinforced concrete frames.

Similar to Peru, the sample size of structures analyzed with respect to the priority index was relatively low, at 57. For a more accurate representation of the vulnerability of the area in need of remediation a larger sample of structures may be needed.

Figure 74: School building in Bingol, Turkey that suffered collapse in the 6.4 Mw earthquake (DataHub 2015)

(a) (b)

Figure 75: Severely damaged structural elements found in the collapsed school building; (a) masonry exhibiting large shear cracks and crushing, (b) concrete beam-column connection failure as a result of poor detailing (DataHub 2015)

Conclusions

Data from seven different earthquakes was organized by Hassan and Sozen’s (1997) priority index and the associated level of severely damaged buildings. Largely, the data conformed to a trend of a negative linear regression as the value of the priority index became larger.

Through organization of the collected data it was found that earthquakes in Nepal, Haiti, Wenchuan, Duzce, and Erzincan fit the expected trend. Lower priority indices were associated with a higher percent of severe damage. The majority of buildings with priority indices higher than 0.4% suffered only light damage confirming this as a reasonable value to consider for prioritation of seismic retrofits. Priority indices also showed a trend of decreasing with increasing amount of stories meaning higher storied structures are more vulnerable to seismic damage. With the data conforming to the expected trend, representing approximately 90% (670/754 structures) of the data, these observation gives strong evidence that the priority index is a reliable screening tool for assessing seismic vulnerability. Seismically vulnerable areas could begin to train local inspectors to assess the structures located in their area. Given these valuable skills, areas could begin preparation to prevent catastrophic damage by the time of the next high ground motion event.

However, it is just as important to take note of factors and characteristics in which the priority index may not be the best suited technique for large scale screening. Two of the seven surveyed earthquakes did not match the trend displayed by the other five. While there was a strong correlation between structures having a priority index under 0.4% and severe failure it did not exhibit the same consistency in linear regression. The non-conformance of the data has been attributed to brittle behavior of the sampled structures due to poor design, detailing, and construction. It could also be a factor of not having enough data points to accurately represent the expected regression. It should also be noted that the investigation of the Erzincan earthquake only contained a sample size of 49 structures and that the conformance of the priority index data to the expected trend may have been coincidental. Future investigations into the seismic vulnerability of an area should include larger sample sizes of structures to accurately and efficiently prioritize the need of remediation for the area.

APPENDIX B

ARAMIS TUTORIAL

The following section will help to outline the necessary steps to run a digital image correlation analysis using the program ARAMIS. This section will also include tips for most efficiently acquiring strain data.

1. Open the current version of ARAMIS that is available. Within the open program, click on the File tab and select New Project.

2. You will be prompted to pick an active directory for which ARAMIS can save the collected data. Make sure that the directory chosen has enough space to accommodate all the data. Depending on the size of the image set being analyzed, new image and movie files can take up a large amount of space. In the space marked 'Dimensions' pick the field that is most appropriate for your data. Use the 2D option if only one camera was used to collect the data during the test. If two cameras were used to collect data during the test, the 3D option would be appropriate.

3. Next you will be required to designate a facet size and a facet step. These numbers represent a few of the project parameters that will have to be set before the analysis can occur. The facet size represents the size, in pixels, in which ARAMIS will collect strain data from. When choosing the facet size, the amount of data points inside the facet must be considered. For the most accurate data, the facet size should be large enough to contain several data points. The next parameter to designate is the facet step. This represents the length, in pixels, in which the facet will overlap with the previous facet in its propagation over the complete area of your test surface. The overlay must also contain several data points within for accurate data. Start with a 2:1 or 2.5:1 ratio of size to step until the adequate results are attained. This may take a few iterations.

4. After facet dimensions are chosen, your collected data can be uploaded into the program. To do this, click on the Stage tab and select New Stage > From Data Series. Select the folder in your directory that contains the image set and it will begin to upload them into ARAMIS. The newly uploaded stage data will appear on the left hand side of the window in sequential order. Make sure that the first image of the test is set as the Reference Image for the analysis.

5. The next project parameter that has to be set is the mask. The mask defines the area of interest for the test. For example, if the object being tested does not fill the entire frame the mask can tell the program not to analyze the area outside of the object's area. You can define your mask by masking the whole image and then unmasking the area of interest. This can be done using geometric commands provided within the program or it can be drawn manually. When defining your mask, leave some space on the outside of your area of interest. This provides for better data. When the mask is drawn to an acceptable standard click the escape button and ARAMIS will begin to apply the mask all the images in the image series.

6. The next, and most important project parameter, is the defining of the start points. Start points mark the location from which your facets will propagate and collect data. To do this click on Define Start Point. The command 'Auto Start Point' can be chosen from here but I prefer to add my start points manually. When manually adding start points hold control and left click the location in which you want your start point to be placed. When satisfied with the location, check the box that says apply to all stages and click next. The program will now go through all the images in the series to see if it has enough accuracy

for the start point to be effective. Depending on the size of your image series this can take time. The amount of start points chosen for your project is dependent on the object and the expected failure. For example, facets cannot span across fractures so start points must be placed on each side of any expected fractures.

7. When start points are defined the test can be analyzed. Click on Compute Project and let ARAMIS run through all the images in the series. This portion of the process will take the longest amount of time. It is recommended to leave the program overnight while it runs.

8. After the project has been analyzed various forms of strains can be viewed by changing the strain preference underneath the tool bar. Through this you can view epsilon x, epsilon y, epsilon xy, etc. Each stage will have a different range of strains at first. Spend time looking through all stages and find a range that encapsulates the strain changes throughout the test. Double click the top and bottom values on the strain scale and change the values to the determined range. This change will be applied to all stages of the test.

9. On the bottom image, you can change the way the analyzed stage is viewed. Right click the bottom image and click on “Visualization”. From this command, several different views can be chosen from including strain data being superimposed on top of the original image.

10. A picture files and movies can be created from the data using the “ImageSeries” tab in the tool bar. From there click on Create Image Series and choose the image set for which you want the series to be created. After the image series is created, go back to the same tab and choose Export Image Series. This will make the data into viewable jpeg or

png files. Another option from the Image Series tab is to export the images in the form of a movie. Choose the command and designate a frame rate.